

File ID 67123  
Filename Thesis

---

SOURCE (OR PART OF THE FOLLOWING SOURCE):

Type Dissertation  
Title Alice electrodynamics, On the Gauging of charge conjugation symmetry  
Author J. Striet  
Faculty Faculty of Science  
Year 2003  
Pages 132

FULL BIBLIOGRAPHIC DETAILS:

<http://dare.uva.nl/record/142361>

---

*Copyright*

*It is not permitted to download or to forward/distribute the text or part of it without the consent of the author(s) and/or copyright holder(s), other than for strictly personal, individual use.*

---

# ALICE ELECTRODYNAMICS

On the Gauging of Charge Conjugation Symmetry



Jelper Striet

# ALICE ELECTRODYNAMICS

On the Gauging of Charge Conjugation Symmetry

ACADEMISCH PROEFSCHRIFT

ter verkrijging van de graad van doctor  
aan de Universiteit van Amsterdam  
op gezag van de Rector Magnificus  
prof. mr. P.F. van der Heijden

ten overstaan van een door het college voor promoties ingestelde  
commissie in het openbaar te verdedigen in de Aula der Universiteit  
op dinsdag 14 oktober 2003 te 14.00 uur.

door

**Jelper Striet**

geboren te Den Helder

**Promotiecommissie:**

Promotor: prof. dr. ir. F.A. Bais

Overige leden: prof. dr. A. Achúcarro  
prof. dr. P.J. van Baal  
prof. dr. J. de Boer  
prof. dr. G. 't Hooft  
prof. dr. C.J.M. Schoutens  
prof. dr. J. Smit  
prof. dr. E.P. Verlinde

Faculteit der Natuurwetenschappen. Wiskunde en Informatica

*Als de juffrouw thee drinkt,  
drink ik water.*

...

Paranimfen: Marloes Sont  
Sander Dalhuisen

This thesis is based on the following papers:

- J. Striet and F. A. Bais.  
Simple models with Alice fluxes.  
Phys. Lett., B497:172–180, 2000. [hep-th/0010236](#)
- F. A. Bais and J. Striet.  
On a core instability of 't Hooft Polyakov type monopoles.  
Phys. Lett., B540:319–323, 2002. [hep-th/0205152](#)
- J. Striet and F. A. Bais.  
Simulations of Alice electrodynamics on a lattice.  
Nucl. Phys., B647:215–234, 2002. [hep-lat/0210009](#)
- J. Striet and F. A. Bais.  
Dynamical vacuum selection in field theories with flat directions in their potential.  
JHEP, 01:032, 2003. [hep-th/0211265](#)
- F. A. Bais and J. Striet.  
Charge instabilities due to local charge conjugation symmetry in (2+1)-dimensions.  
Nucl. Phys., B666:243–268, 2003. [hep-th/0304186](#)
- J. Striet and F. A. Bais.  
More on core instabilities of magnetic monopoles.  
JHEP, 06:022, 2003. [hep-th/0304189](#)

# Contents

<b>1 Alice physics: an introduction and survey</b>	<b>9</b>
1.1 Alice theories . . . . .	9
1.2 Alice phenomena in Alice electrodynamics . . . . .	11
1.2.1 The structure of AED . . . . .	11
1.2.2 Some specific realizations of Alice electrodynamics . . . . .	17
1.2.3 Instabilities and topological defects . . . . .	24
<b>2 <math>U(1) \times \mathbb{Z}_2</math> models</b>	<b>33</b>
2.1 Alice electrodynamics . . . . .	33
2.1.1 The Alice flux solution . . . . .	34
2.2 Alternative Alice models . . . . .	37
2.2.1 Alice flux solutions . . . . .	37
2.2.2 First order equations . . . . .	40
2.3 Conclusions . . . . .	44
<b>3 Lattice Alice electrodynamics</b>	<b>45</b>
3.1 A brief introduction to lattice gauge theory . . . . .	45
3.2 Lattice Alice electrodynamics . . . . .	48
3.2.1 The action . . . . .	48
3.2.2 The problem of locating monopoles (or instantons) . . . . .	49
3.2.3 Implementation of the model . . . . .	53
3.3 The phase diagram in three and four dimensions . . . . .	54
3.4 Analytic and other approximations . . . . .	57
3.4.1 The average action of unpierced plaquettes . . . . .	57
3.4.2 The condensation lines of the Alice fluxes . . . . .	59
3.4.3 Contours of constant flux density . . . . .	61
3.4.4 The monopole/instanton density . . . . .	62

## Contents

---

3.4.5	Discussion . . . . .	63
3.5	Conclusions and outlook . . . . .	65
<b>4</b>	<b>Dynamical vacuum selection</b>	<b>67</b>
4.1	Introduction . . . . .	67
4.2	DVS in 1 dimension . . . . .	68
4.2.1	The model . . . . .	68
4.2.2	Static kinks . . . . .	69
4.2.3	Kinks in finite space . . . . .	70
4.2.4	Non static kink configurations . . . . .	73
4.3	DVS in 2 dimensions . . . . .	73
4.4	No DVS in 3 dimensions . . . . .	74
4.5	Conclusions and outlook . . . . .	76
<b>5</b>	<b>A monopole core instability</b>	<b>77</b>
5.1	Introduction . . . . .	77
5.2	The core instability . . . . .	78
5.3	The Alice model . . . . .	79
5.4	Numerical simulations . . . . .	81
5.4.1	The variational ansatz . . . . .	81
5.4.2	Some numerical details . . . . .	82
5.4.3	A typical set of experiments . . . . .	86
5.5	The results . . . . .	88
5.6	Conclusions and outlook . . . . .	90
<b>6</b>	<b>Charge instabilities in (2+1)-dimensions</b>	<b>93</b>
6.1	Introduction . . . . .	93
6.2	Alice fluxes in the presence of a charge . . . . .	94
6.2.1	The induced Cheshire dipole . . . . .	95
6.2.2	The field configuration . . . . .	99
6.2.3	The energy gain . . . . .	102
6.3	The charge instability . . . . .	104
6.3.1	The life time of charge . . . . .	105
6.3.2	Charge decay due to creation of an Alice flux pair . . . . .	107
6.3.3	Charge decay time due to creation of point charges . . . . .	110
6.3.4	Comparing the decay channels . . . . .	113
6.4	Conclusions and outlook . . . . .	115

6.5 Cheshire current and confinement . . . . .	117
6.5.1 The Cheshire current . . . . .	117
6.5.2 Confinement in a two dimensional picture . . . . .	118
<b>Epilogue</b>	<b>121</b>
<b>Bibliography</b>	<b>123</b>
<b>Samenvatting</b>	<b>129</b>
<b>Dankwoord</b>	<b>133</b>

## Contents

---

# Chapter 1

## Alice physics: an introduction and survey

*Nothing shocks me!  
I'm a scientist.*

Indiana Jones

In this first chapter we will present an overview of different aspects of Alice physics. First we explain what Alice physics is and present some examples. Then we turn to Alice electrodynamics, the theory we will explore thoroughly in this thesis. In section 2 we preview the main results that will subsequently be described extensively in the following chapters.

### 1.1 Alice theories

The term “Alice physics”<sup>1</sup> refers to a certain type of topological interactions, which may for example occur in spontaneously broken gauge theories where a larger non-abelian gauge group  $G$  is broken to a smaller, the unbroken, gauge group  $H$  which itself is still non-abelian. This occurs if one of the scalar fields in the theory gets a vacuum expectation value which is not invariant under the whole gauge group  $G$ , but only under the unbroken part of the gauge group  $H$ . This implies that the classical ground state is degenerate and the vacuum manifold is isomorphic to the coset space  $G/H$ , the orbit of the order parameter under the group  $G$ . Broken symmetries manifest themselves by the appearance of massless scalar modes if the broken symmetries are global, and massive gauge particles if they are local. The broken generators generate translations in the vacuum manifold. Another, equally important

---

<sup>1</sup>The subject has no relation to the physics studied with the ALICE detector at CERN. The name Alice in Alice physics rather refers to the book “Alice in Wonderland”. This connection will become clear later on.

manifestation of broken symmetries is the possible appearance of topological defects in the broken phase. Their nature is intimately linked to the topological properties of the vacuum manifold. A topological defect is a spatially extended field configuration where the order parameter satisfies nontrivial boundary conditions characterized by some topological invariant. This boundary condition implies that the order parameter field cannot stay within the vacuum manifold everywhere in the bulk. Well known examples are monopoles, flux tubes and domain walls.

To point out what is characteristic of Alice theories it is illuminating to look at the case of (magnetic) flux tubes. To every flux a specific element  $h$  of the unbroken gauge group  $H$  can be associated, defined by the untraced closed Wilson loop around the flux, given by:

$$h = P e^{\oint A_\mu(x) dx^\mu} . \quad (1.1)$$

with  $P$  denoting path ordering along the loop  $\gamma$ , and  $A_\mu(x)$  the gauge field. The element  $h$  can in principle be any element of the residual gauge group, but the flux is topologically stable if it is an element of a disconnected part of the unbroken gauge group  $H_d$ <sup>2</sup>. If the element  $h$  is not part of the center of the unbroken group, i.e. does not commute with all of  $H$  [1], then it is called an Alice flux. Note that this is a priori not a topological statement, but it is essential that the unbroken group is non-abelian. The important thing is that, as  $h$  does not commute with the unbroken gauge group  $H$ , it is not possible to give a single valued definition for all the generators/charges of  $H$  in the presence of such an Alice flux. Apparently in these models there is an intricate interplay between possible topological sectors (i.e.. topological quantum numbers) and the allowed gauge charges in those sectors. The consequences of having defects, which form an obstruction to defining charges globally, can be quite drastic and lead to a number of remarkable physical phenomena, which forms the main subject of this thesis.

### Topological Alice models

Alice phenomena may show up in many different guises. An obvious class of models where Alice phenomena appear, are the models where the topological non-triviality of a flux implies the Alice behavior of the flux. Examples of these types of models are non-abelian discrete gauge theories [2, 3] where a continuous group is broken to some discrete non-abelian subgroup and Alice electrodynamics [1, 4, 5] where a non-abelian group is broken to a residual  $H = U(1) \ltimes \mathbb{Z}_2 \sim O(2)$ . Theories with non-abelian discrete gauge groups have been extensively analyzed and have in particular been linked with the notion of (spontaneously broken) Hopf symmetry [6, 7, 8, 9]. These theories have gained some interest because they provide ideal models for topological quantum computing. The Hopf symmetries in turn are connected to the general link between Chern-Simons theories and quantum symmetries [10, 11, 12] as for example in (2+1)-dimensional gravity [13, 14].

---

<sup>2</sup>Here we assume  $\Pi_2(G) = \Pi_1(G) = \Pi_0(G) = 0$ .

### Dynamical Alice models

Another interesting class of models consists of models where the Alice behavior of the topologically stable flux is present for dynamical reasons. In these models, where typically the flux itself is topologically stable, not all topologically equivalent fluxes are Alice fluxes. However an Alice flux in this topological non-trivial sector can be the lowest energy solution. Examples from this class of models are the  $SO(6) \rightarrow SO(3) \times SO(3) \times \mathbb{Z}_2$  model [5] and the  $Spin(10) \rightarrow SU(5) \times \mathbb{Z}_2$  model [15, 16, 17]. In [18, 19] a topological definition of Alice models is given, which works if there are also magnetic monopoles present in the theory. In that case the Alice behavior can already be encoded in the topology of the theory as Alice fluxes influence magnetic monopoles and electric charges in a similar way.

### Wonderland in physics

Although we will concentrate on a specific model containing Alice physics, we would like to remark that Alice features show up in various parts of physics. It has been used as a baryogenesis mechanism in for example [20, 21]. Alice effects appear in topologically non-trivial universes [22, 23], in two dimensional gravity [24, 25, 26, 13], they pop up in the study of confinement [27, 28], in string theory the Alice effect connects parallel branes [29] and it provides a possible solution to the strong CP-problem by gauging the CP-symmetry [30, 31]. Alice effects also appear in different condensed matter systems, such as in the study of certain Bose-Einstein condensates in optical lattices [32, 33, 34], rotating Helium III [35, 36], superconductors [37, 38, 39] and in nematic liquid crystals, where the uniaxial version has the same symmetry structure as Alice electrodynamics (see for example [40, 41, 42]).

## 1.2 Alice phenomena in Alice electrodynamics

In this section we introduce Alice ElectroDynamics (AED) and preview some of the main results obtained in the coming chapters. We start with a description of the topological structure of AED and introduce the notions of Alice flux and Cheshire charge. Then we discuss some explicit continuum and lattice models and finally we briefly report some remarkable physical consequences of the subtle interplay of topological features leading to a variety of instabilities in the theory.

### 1.2.1 The structure of AED

Alice electrodynamics (AED) is a theory of electrodynamics in which charge conjugation is a local gauge symmetry. To be specific, AED is a gauge theory with gauge group  $H = U(1) \times \mathbb{Z}_2 \sim O(2)$ , so, in a certain sense it is the minimally non-abelian extension of ordinary electrodynamics. The nontrivial  $\mathbb{Z}_2$  transformation reverses the

direction of the electric and magnetic fields and the sign of the charges.

$$XQX^{-1} = -Q \quad , \quad (1.2)$$

with  $X$  the nontrivial element of  $\mathbb{Z}_2$  and  $Q$  the generator of the  $U(1)$ .

The generator of  $U(1)$  and the nontrivial element of the  $\mathbb{Z}_2$  do not commute with each other, in fact they anti-commute. This means that the  $\mathbb{Z}_2$  part of the gauge group acts as a charge conjugation on the  $U(1)$  part of the gauge group and that is what is meant by the phrase “AED is electrodynamics in which charge conjugation symmetry is gauged”.

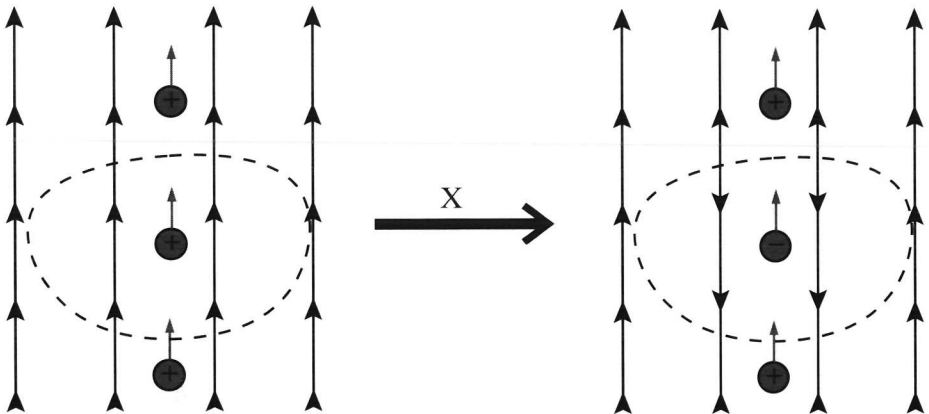


Figure 1.1: A local charge conjugation transformation does not change the force on a charged particle in an electric field in electrodynamics.

One might envisage a local discrete symmetry by defining arbitrary patches and having nontrivial gauge transformations between them. The transition functions can become topologically nontrivial as we will see. A topologically trivial patch is depicted in figure 1.1, where inside the contour the direction of the electric and magnetic fields and charges is reversed, so that indeed the resulting physics is not affected. Charged particles move across the boundary without “noticing” it. So it appears that in a typical situation of ordinary electrodynamics nothing dramatically changes if charge conjugation symmetry is gauged. However there are profound differences between ED and AED, which we will discuss in this chapter and the coming chapters. It is important to realize that, as the non-abelian extension with respect to ordinary electrodynamics is discrete, it only affects electrodynamics through certain global (topological) features, involving nontrivial  $\mathbb{Z}_2$  bundles.

In figure 1.2 we schematically indicate the structure of the gauge group,  $U(1) \times \mathbb{Z}_2$ , of (compact) AED. It consists of two copies of  $U(1)$  connected by the nontrivial element  $X$  of the  $\mathbb{Z}_2$  part of the gauge group.

From the structure of the (residual) gauge group in figure 1.2 it is clear what the

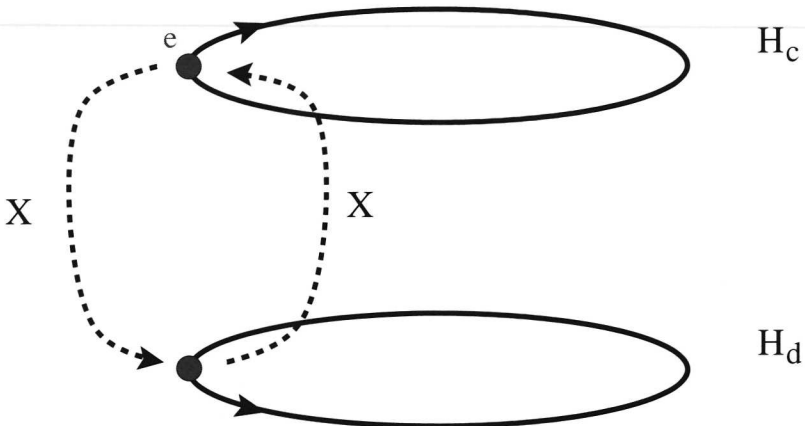


Figure 1.2: A schematic picture of the gauge group of AED. It shows the action of  $X$ , the connected and the disconnected part of the gauge group and the sign difference between the two branches.

possible topological defects in AED are<sup>3</sup>. As  $\Pi_0(U(1) \times \mathbb{Z}_2) = \mathbb{Z}_2$  there will be a topological  $\mathbb{Z}_2$  flux, denoted as Alice flux, and furthermore as  $\Pi_1(U(1) \times \mathbb{Z}_2) = \mathbb{Z}$  there are also magnetic monopoles in this theory (like in compact ED). The element of the unbroken gauge group associated with the Alice flux contains the nontrivial element of the  $\mathbb{Z}_2$  part of the gauge group,  $X$ . This means that if a charge is moved around an Alice flux it gets charge conjugated. At first this might not be a very interesting observation as charge conjugation is part of the local gauge symmetry of the model. However there is the notion of a relative sign, which is path dependent in the presence of Alice fluxes. This means that if one starts with two equal charges (repulsion) and moves one of the charges around an Alice flux one ends up with two charges of the opposite sign (attraction), due to the non-commutativity of  $X$  and  $Q$ . In the presence of an Alice flux the generator of the  $U(1)$  is not single valued and therefore there is a topological obstruction to a global definition of electric charge. However if there are no Alice fluxes present it is possible to globally define the  $U(1)$ . But note that also in the trivial sector of the theory a pair of Alice fluxes or a closed Alice loop can be created out of the vacuum. What happens in that case to the definition of  $U(1)$  charge? As the creation of such a topologically trivial configuration is a local process the overall charge should not be affected, changes in the definition of the  $U(1)$  should occur only locally. A way to understand what happens is to cut out a region of space which is such that the closed Alice ring lies on its boundary. Now the  $U(1)$  can still be globally defined in the rest of the space. But physically one can of course not just exclude this region and problems do indeed arise when a charged particle moves through this region. The closed loop of Alice flux will bound a so called Dirac or  $\mathbb{Z}_2$ -sheet and if a particle crosses this sheet it gets charge conjugated.

<sup>3</sup>Here one has to envisage that AED is realized by breaking a larger gauge symmetry with the help of a Higgs mechanism and that this larger gauge group,  $G$ , has:  $\Pi_2(G) = \Pi_1(G) = \Pi_0(G) = 0$ .

It looks rather artificial, but in fact it is just a convenient singular gauge choice. In this gauge a charge which moves around an Alice flux, gets charge conjugated at a very specific point where its trajectory goes through the sheet which is bounded by the Alice loop. Clearly the location of this  $\mathbb{Z}_2$ -sheet is gauge dependent while the location of its boundary is the gauge independent Alice ring. In this sense there is an analogy between the sheet and the Dirac-string of a magnetic monopole.

In a situation where it is possible to define a global  $U(1)$  charge the total charge should be conserved. Then the question arises what will happen to this conservation of charge if a particle gets charge conjugated when moved through an Alice ring as this appears to violate the conservation of charge. To resolve this paradox it is illuminating to perform some simple thought experiments. Let us start with a pair of oppositely charged particles and then create an Alice ring out of the vacuum. Then we take one of the charges through the Alice ring. We end up with two like charges next to each other, say both positive. As the total charge cannot change by local processes, i.e., the creation of an Alice ring and moving one of the charged particles, the total charge should still be zero. This tells us that the missing charge must be hiding in the excluded spatial volume, i.e., it must be carried by the Alice ring configuration.

There are several ways to understand how the missing charge in AED is carried by the Alice ring configuration. First we discuss a symmetric configuration in which it is very easy to understand how the missing charge is carried. Then we will do a thought experiment from which it should become clear that the configuration we found for the symmetric configuration is essentially generic.

First consider a symmetric configuration, where we put the Alice ring in the horizontal plane and assume there to be an up-down symmetry with respect to this plane (the famous “Alice mirror”). We choose the  $\mathbb{Z}_2$ -sheet to also lie in this plane. The nice thing of this symmetric configuration is that the electric field lines have to be perpendicular to the  $\mathbb{Z}_2$ -sheet as the sign needs to change once they pass the  $\mathbb{Z}_2$ -sheet and due to the up-down symmetry. This means that in this symmetric configuration the boundary conditions for the electric field on the  $\mathbb{Z}_2$ -sheet are the same as those for a charged conducting plate. Now we maneuvered ourselves into a position where the answer to the question of the missing charge is very simple. From the perspective of the space which is not excluded the Alice ring bounds a conducting plate<sup>4</sup>. Obviously the missing charge is carried (ignoring for the moment the boundary effects the Alice ring may have) by this “would be” conducting plate and the resulting field line pattern is clear, see figure 1.3(d). Now it is important to note that although the direction of the field lines depends on the location of the  $\mathbb{Z}_2$ -sheet the field line pattern itself is gauge invariant. Although the field line pattern is gauge invariant the conducting plate boundary condition of the field lines on the  $\mathbb{Z}_2$ -sheet is clearly not. They only hold in the symmetric gauge we started with.

A most remarkable feature of these charged Alice ring configurations is that the source of the charge cannot be localized. Suppose we have a small test charge which we want to use to locate the source of the charge. The test charge will follow a specific field

---

<sup>4</sup>At least the excluded space has the same boundary conditions as a conducting plate.

line and expects to end up at a charge. However, there are no sources for the field lines. As the test charge moves through the Alice ring - the sheet that is - its sign changes exactly where the field lines change direction and the charge will just move on. So, from far away a definite charge is carried by the Alice ring configuration, but as one comes closer one finds there is no source of that charge. This elusive type of charge is called a Cheshire charge after the grinning cat in *Alice in Wonderland* who disappears but leaves his grin behind [43, 44].

A second way of understanding how a Cheshire charge appears in AED, does not involve any symmetry arguments. We reexamine the thought experiment where we move a charge through an Alice ring. To understand the appearance of Cheshire charge in this setting we make use of the fact that due to charge conservation and/or quantization electric field lines can not pass an Alice flux<sup>5</sup>. We start with a single charge and create in its vicinity an Alice ring out of the vacuum. As the electric field lines cannot pass through the Alice flux they are pushed away by the Alice ring, see figure 1.3(b). Next we pull the charge through the Alice ring, see figure 1.3(c). If we then move the charge to infinity it is clear what the resulting Cheshire charge configuration looks like, see figure 1.3(d). This thought experiment demonstrates the generic nature of the Cheshire phenomenon.

In the appendix of chapter 6 we will encounter the so called Cheshire current, see figure 6.11. This object typically only lives in two dimensions, while a Cheshire charge can appear in two and three dimensions. A Cheshire current appears if one takes a charge around two Alice fluxes. In that case the charge can be annihilated with the anti-charge that stayed behind. Due to the fact that the electric field lines can not close around a single Alice flux, the pair of fluxes will carry a Cheshire current. We refer to the appendix of chapter 6 for more details on the Cheshire current configuration and its relation with Cheshire charge.

As  $\Pi_1(U(1) \ltimes \mathbb{Z}_2) = \mathbb{Z}$  there are also magnetic monopoles in compact AED (as in compact ED). Already at this point there is a subtle interplay between the fluxes and the monopoles in AED [45]. Exactly this point is used in [18] to define topological Alice models. In the presence of an Alice flux the sign of a magnetic charge is no longer uniquely defined, i.e., in AED the monopole and the anti-monopole belong to the same topological sector. To understand this feature of AED we will investigate a configuration where a monopole and an Alice flux are coexisting, see figure 1.4.

Often the so called base point in homotopy theory is not important. However if  $\Pi_0(H) \neq 0$  the position of this base point can become relevant. This is the case in AED and results in the topological equivalence of the monopole and the anti-monopole. A monopole charge is determined with the help of a closed surface enclosing the monopole, see figure 1.4(a). If there are no Alice loops or fluxes present the base point of this surface,  $x_0$ , is irrelevant. However if there is an Alice loop present the

---

<sup>5</sup>Indeed the fact that electric and also magnetic field lines cannot penetrate an Alice flux is reminiscent of the Meissner effect, where magnetic fields are expelled from an electric superconductor. In that case magnetic flux is quantized and can be trapped in a superconducting ring. The paradoxical situation in our model is that the Alice flux appears to be both electrically and magnetically superconducting yet strictly neutral: in other words the analogy appears to break down at this point.

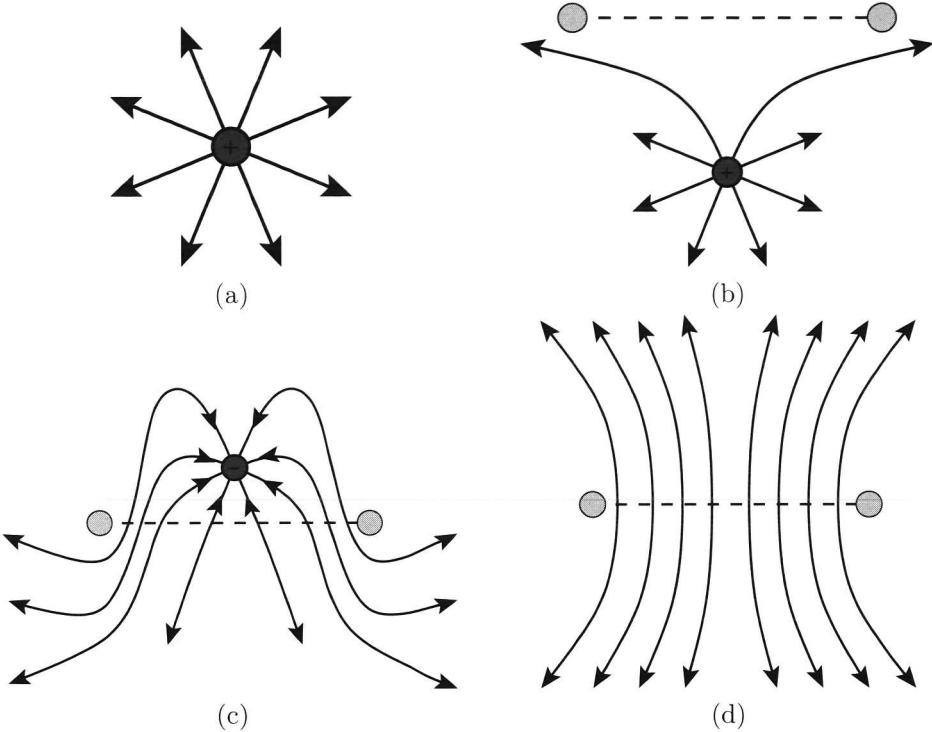


Figure 1.3: This sequence of pictures makes clear that the Cheshire phenomena is a generic phenomenon in AED and does not depend on the symmetry of the configuration. Using the fact that due to charge conservation and/or quantization electric field lines cannot cross an Alice flux one is lead to the notion of Cheshire charge.

base point of this surface does become relevant. As the fundamental homotopy group of AED is  $\mathbb{Z}_2$ , there are two different ways by which one can enclose the monopole with the closed surface starting from the base point. In one, see figure 1.4(b), the surface does not go through the Alice loop, in the other, see figure 1.4(c), the surface does go through the Alice loop. These two possibilities are equally well suited to define the charge of the magnetic monopole, but differ in outcome. To understand the difference in outcome we deform the latter surface, see figure 1.4(d). We see that the two surfaces differ by a transformation around the Alice flux,  $\beta$ . As the nontrivial element  $X$  of  $\mathbb{Z}_2$  does not commute with the generator  $Q$  of  $U(1)$  in AED there is distinct difference between the two definitions of the magnetic charge. This difference is caused by the presence of the Alice flux and is called *the influence of  $\Pi_0(H)$  on  $\Pi_1(H)$* . Obviously there is a sign difference between the outcomes of the two definitions of the magnetic charge. This means that there is no topological distinction between positive and negative magnetic monopoles in the presence of an Alice flux. This may not be too surprising for a theory where charge conjugation is part of the local gauge symmetry. However, we note that there is still the notion of the relative sign between magnetic

charges, which is path dependent as we explained in the context of electrical charges. We seem to be confronted with a puzzling arbitrariness in talking about charges in this simple model.

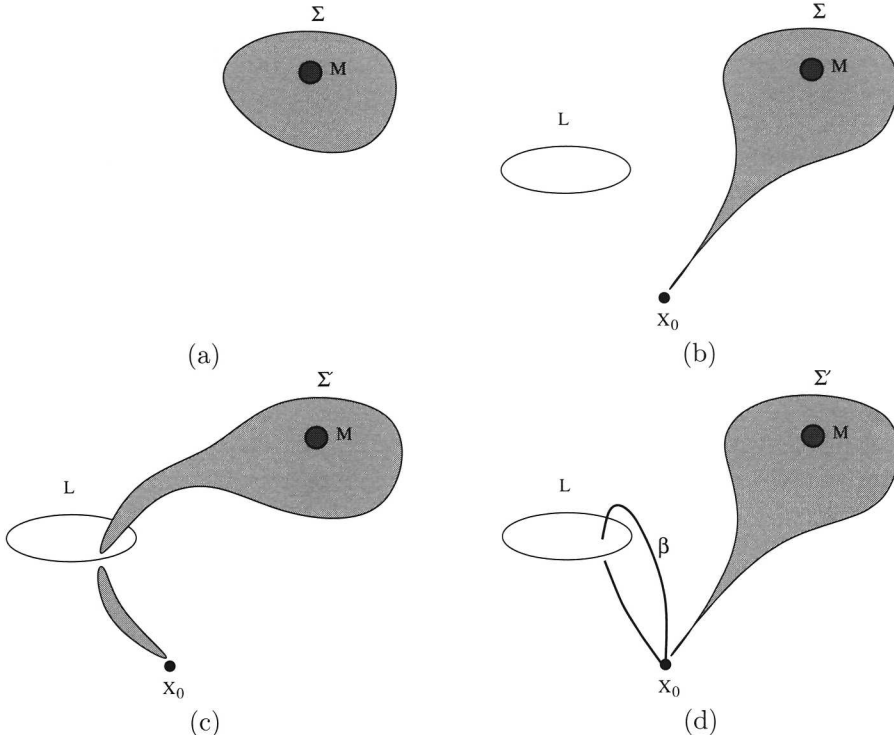


Figure 1.4: These figures show that in the presence of a loop of Alice flux,  $L$ , the sign of the (monopole) charge is not uniquely defined. The two surfaces  $\Sigma$  and  $\Sigma'$  are equally well suited to measure the (monopole) charge, but differ by the path  $\beta$ , which shows that they are charge conjugated with respect to each other.

### 1.2.2 Some specific realizations of Alice electrodynamics

In this subsection we will introduce and briefly discuss some specific AED models. First we will look at continuum models where AED is realized after spontaneous symmetry breaking through some suitable Higgs mechanism. Subsequently we look at a lattice model of AED. Both types of models will allow the formation of magnetic monopoles and Alice fluxes. In the continuum models they appear as solitons due to the symmetry breaking, but in the lattice model they appear because of the lattice structure.

### The continuum models

The continuum models of AED are the main subject of chapter 2 and we refer to this chapter for more details. Let us think of a spontaneously broken gauge theory where the order parameter in the broken phase, the Alice phase, can be represented by a director field. We may think of this order parameter as a line segment or a bidirectional arrow. Thus it fixes an orientation but not a direction. Just like a normal vector field, such an order parameter is invariant under rotations around its axis, which represents the  $U(1)$  gauge degree of freedom. But the bidirectional arrow has an additional symmetry, the reflection symmetry, i.e., the invariance under rotations of an angle of  $\pi$  around an axis perpendicular to its own orientation. This invariance represents the charge conjugation symmetry of AED. These two symmetry operations do not commute with each other, they anti-commute. So we find that the director field is an appropriate order parameter for AED.

The original model [4] of AED uses the five dimensional symmetric tensor representation of  $SU(2)$  (for this representation one can just as well use  $SO(3)$ ). The action of this model is given by:

$$S = \int d^4x \left\{ \frac{1}{4}F^{a,\mu\nu}F_{\mu\nu}^a + \frac{1}{4}\text{Tr}(D^\mu\Phi D_\mu\Phi) - V(\Phi) \right\} , \quad (1.3)$$

where the Higgs field  $\Phi = \Phi^{ab}$  is a real symmetric traceless  $3 \times 3$  matrix. The potential is given by:

$$V = -\frac{1}{2}\mu^2\text{Tr}(\Phi^2) - \frac{1}{3}\gamma\text{Tr}(\Phi^3) + \frac{1}{4}\lambda(\text{Tr}(\Phi^2))^2 . \quad (1.4)$$

By a suitable choice of parameters the Higgs field will acquire a vacuum expectation value,  $\Phi_0$ . In the gauge where  $\Phi_0$  is diagonal it takes the form  $\Phi_0 = \text{diag}(-f, -f, 2f)$ . As an aside we mention a field in physics where the same order parameter has shown up: the theory of nematic liquid crystals. Here the symmetry is realized as a global symmetry whereas in AED the  $U(1) \times \mathbb{Z}_2$  symmetry is local. A typical model used to describe these systems is the Landau-de Gennes free energy model [46, 47, 48, 49], given by:

$$\mathcal{F} = \int (f_{el} + f_v) dV \quad (1.5)$$

$$f_{el} = \frac{L_1}{2}\partial_\gamma Q_{\alpha\beta}\partial_\gamma Q_{\alpha\beta} + \frac{L_2}{2}\partial_\beta Q_{\alpha\beta}\partial_\gamma Q_{\alpha\gamma} + \frac{L_3}{2}\partial_\gamma Q_{\alpha\beta}\partial_\beta Q_{\alpha\gamma} \quad (1.6)$$

$$f_v = \frac{a}{2}\text{Tr}(Q^2) - \frac{b}{3}\text{Tr}(Q^3) + \frac{c}{4}(\text{Tr}(Q^2))^2 \quad (1.7)$$

Although the two models are quite different they can be mapped onto each other for a limited region of the parameter spaces. In the limit of vanishing gauge coupling of the AED model and for static solutions of the equations of motion the original AED model can be mapped onto the Landau-de Gennes model with  $L_2 = L_3 = 0$ . This

correspondence will be used in the analysis of the monopole core instability in chapter 5.

The vacuum manifold after symmetry breaking corresponds to the gauge orbit of the order parameter and therefore becomes equal to the real projective space  $\mathbb{RP}^2$ , i.e., the sphere,  $S^2$ , with opposite points identified. The topologically non-trivial structure of this manifold is quite well known and its first and second homotopy groups are given by:

$$\Pi_1(\mathbb{RP}^2) = \mathbb{Z}_2 \quad \text{and} \quad \Pi_2(\mathbb{RP}^2) = \mathbb{Z} \quad (1.8)$$

The nontrivial  $\Pi_2(\mathbb{RP}^2)$  results in the appearance of magnetic monopoles in AED. This does not make specific use of the head-tail symmetry of the order parameter and is for example also present in a theory with a vector order parameter field, such as the Georgi-Glasgow model [50]. The fact that  $\Pi_1(\mathbb{RP}^2) = \mathbb{Z}_2$  means that there are also topologically non-trivial  $\mathbb{Z}_2$  (Alice) fluxes present in the theory. The appearance of Alice fluxes is due to the head-tail symmetry of the order parameter. Indeed, the fact that opposite points on the sphere are identified with each other, which is a direct consequence of the head-tail symmetry of the order parameter, allows these Alice fluxes, see figure 1.5(a). As we explained in the previous subsection the subtle interplay between the monopole and the flux content of the theory gives that monopoles of opposite charge belong to the same topological sector.

One of the key features of the Alice flux is the fact that the order parameter, the Higgs field, only rotates over  $\pi$  around an Alice flux. That this is allowed is due to the head-tail symmetry of the Higgs field. Now it is also clear that the charges with respect to the unbroken  $U(1)$  change sign when they go around an Alice flux, as the generator of the unbroken  $U(1)$ , i.e., a pointed arrow, also only rotates over  $\pi$  when transported around an Alice flux and thus picks up a minus sign, see figure 1.5(b).

As we now have an explicit model we can try to find explicit solutions of the magnetic monopole and the Alice flux. Appropriate ansätze were given in [4]. We will discuss the monopole ansatz later on, but for the moment we mention that it is very similar to the spherically symmetric 't Hooft-Polyakov magnetic monopole ansatz. The ansatz for the Alice flux is more interesting. Locally one can always gauge the Higgs field such that it is in a diagonal form. However it need not always have the one parameter structure  $\Phi = \text{diag}(-a, -a, 2a)$  mentioned before. The spherically symmetric magnetic monopole does have this form, but for the Alice flux it can be shown that this does not allow for a static solution to the equations of motion. So for the Alice flux one needs the more general form  $\Phi = \text{diag}(-a, -b, a + b)$ , implying that the ansatz requires more than a single function for the scalar field.

In figure 2.1 we show a numerical Alice flux solution to the equations of motion, for specific values of the parameters of the model, based on the following ansatz:

$$A_\theta = \frac{\alpha(r)}{2er} T_1 \quad , \quad (1.9)$$

$$\Phi(r, \theta) = e^{\frac{\theta T_1}{2}} \Phi(r) e^{-\frac{\theta T_1}{2}} \quad , \quad (1.10)$$

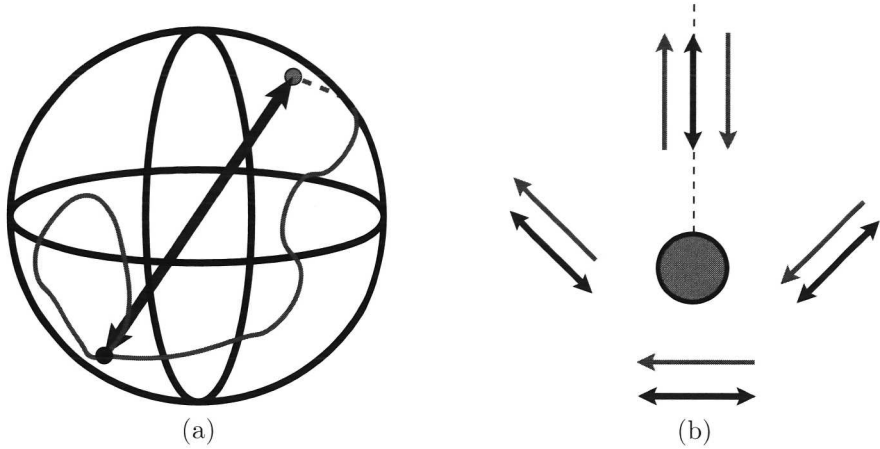


Figure 1.5: Figure (a) shows the possibility to have topologically non-trivial closed loops due to the head-tail symmetry of the Higgs field. Figure (b) shows that the Higgs field is single valued if it only rotates over an angle  $\pi$  after going around the Alice flux and that the generator of the unbroken  $U(1)$  is actually double valued in the presence of an Alice flux.

where the tensor  $\Phi(r)$  is conveniently parameterized as,

$$\Phi(r) = m(r) \begin{pmatrix} 1 & 0 & 0 \\ 0 & -\frac{1}{2} & 0 \\ 0 & 0 & -\frac{1}{2} \end{pmatrix} + q(r) \begin{pmatrix} 0 & 0 & 0 \\ 0 & \frac{3}{2} & 0 \\ 0 & 0 & -\frac{3}{2} \end{pmatrix} . \quad (1.11)$$

and  $T_i$  the generators of  $SO(3)$ .

At spatial infinity the boundary conditions are:  $q = m$  and  $\alpha = 1$  and at the core of the defect the boundary conditions are:  $\alpha = q = 0$ .

An interesting feature of the solution is that the gauge symmetry is not restored at the center of the defect, i.e., the Higgs field does not become zero. The symmetry at the core of the defect is again that of AED only now with a  $U(1)$ -isospace direction different from the unbroken symmetry at spatial infinity. The fact that the Higgs field deviates from the form  $diag(-f, -f, 2f)$  means that it can no longer be represented by a single direction everywhere. This behavior is sometimes referred to as an escape in the biaxial direction.

In equation 2.4 we see that the Higgs field can be represented as a sort of symmetric product of two vector fields. The only information of the two vectors that survives in the translation to the Higgs field is the product of the lengths,  $h$ , and half the relative angle,  $\psi$ . Expressed in these variables the Higgs field is given by:

$$\Phi = \frac{2}{3}h \begin{pmatrix} -(\sin^2 \psi + 1) & 0 & 0 \\ 0 & \sin^2 \psi - \cos^2 \psi & 0 \\ 0 & 0 & \cos^2 \psi + 1 \end{pmatrix} . \quad (1.12)$$

For the present discussion this parameterization is more convenient than the one we

use to find a numerical solution, equation 1.11. As the Higgs field at  $r = 0$  should be single valued it has to commute with  $T_1$ . This means that  $\psi = \pi/2$  or  $h = 0$  at  $r = 0$ . Thus the Higgs field can do two things. Either it can vanish in size or it has to “rotate” to  $\psi = \pi/2$ . Investigating the potential in terms of  $h$  and  $\psi$  shows that rotating and not vanishing of  $h$  realizes a lower potential energy. Thus it is natural that the Alice flux makes use of the possibility to escape in the biaxial direction. Although the Higgs field in the center of the flux is again invariant under an AED part of the gauge group, it is typically in the wrong broken vacuum<sup>6</sup>. Meaning that the Higgs field has the wrong sign, i.e., it is not in (or close to) the global minimum but in (or close to) another minimum of the potential, see figure 1.6.

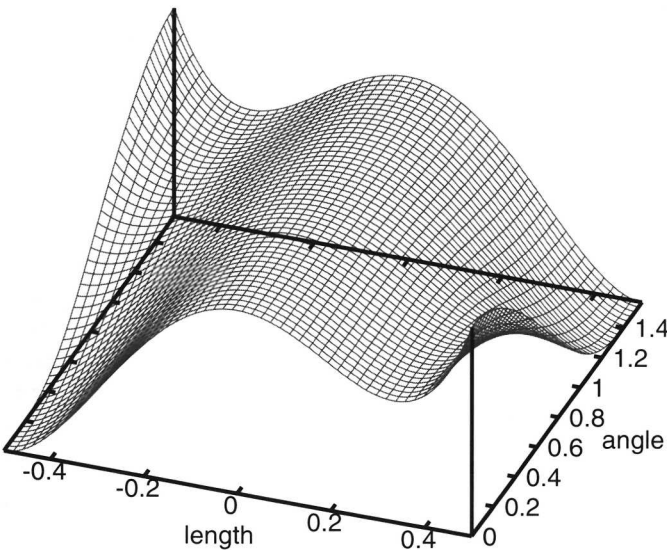


Figure 1.6: This figure shows the typical form of the potential as a function of the length  $h$  and the angle  $\psi$ . Here we plotted it for  $\mu^2 = 1$ ,  $\gamma = -1$  and  $\lambda = 1$ . It makes clear that it is natural for the Alice flux solution to escape into the biaxial direction.

Already at this point one might wonder whether for a magnetic monopole solution there is also the possibility to escape in such a biaxial direction. We return to this issue later on in this chapter when we investigate a core instability of the spherically symmetric magnetic monopole, which is further explored in chapter 5.

We wish to mention two alternative continuum Alice models. These two Alice models have a similar symmetry structure as the original model, but the Higgs sector consists of a pair  $(X, Y)$  of adjoint representations. The head-tail symmetry alluded to before in these models comes about by putting the Higgs field on an orbifold, i.e., imposing

<sup>6</sup>Typically there are two minima of the potential which have the same unbroken AED subgroup. However only one of them is the true global vacuum, while the other is just a local minimum of the potential.

special boundary conditions on the Higgs fields. More specifically in one model the Higgs field,  $X$ , is put on a  $\mathbb{Z}_2$  orbifold which identifies  $X$  with  $-X$ . In the other model the two Higgs fields are put on a  $S_2$  orbifold which identifies the point  $(X, Y)$  with  $(Y, X)$ . The action for both models is given by:

$$S = \int d^4x \left\{ \text{Tr} \left( \frac{1}{4} F^{\mu\nu} F_{\mu\nu} + \frac{1}{2} D^\mu X D_\mu X + \frac{1}{2} D^\mu Y D_\mu Y - \frac{\hat{\lambda}}{2} [X, Y]^2 \right) - \frac{\hat{\lambda}}{4} (\text{Tr}(X^2 + Y^2) - f^2)^2 \right\} . \quad (1.13)$$

There is a gain by introducing this rather intricate Higgs sector, notably that these two models have monopole solutions which can be mapped one to one to the 't Hooft-Polyakov monopoles while the Alice flux solutions correspond precisely to Nielsen-Olesen flux solutions with winding number one-half. Much is known about these solutions and for particular parameter values even a Bogomolny limit exists.

### The lattice model

Let us now introduce a lattice version of compact AED (LAED). In chapter 3 we will study this model quite extensively. Here we limit ourselves to a preview of the main results. We refrain from giving an introduction to lattice gauge theory, for this we refer to the beginning of chapter 3 or for a more thorough introduction to [51, 52]. Our interest in a lattice formulation of the theory is evident for two reasons: (i) it allows us to study the phase diagram and in particular what type of condensates may form, and (ii) it may allow us to study certain nonperturbative quantum properties. The gauge degrees of freedom in a lattice gauge theory are the link variables. These are related to the gauge potentials and for the model at hand given by:

$$U_\nu(x) = e^{iA_\nu(x)\tau_3} \tau_1^{a_\nu(x)} , \quad (1.14)$$

with  $a_\nu(x) \in \{0, 1\}$  and  $A_\nu(x) \in \langle -\pi, \pi \rangle$ .

Here  $a_\nu$  represents the  $\mathbb{Z}_2$  gauge variable and  $A_\nu$  the compact  $U(1)$  gauge variable of the theory. If  $a_\nu(x) = 1$  that implies that a  $\mathbb{Z}_2$ -sheet in  $D = 3$ , or a  $\mathbb{Z}_2$ -volume in  $D = 4$ , crosses the link. These  $\mathbb{Z}_2$ -sheets can of course be moved around by local  $\mathbb{Z}_2$  gauge transformations, but their boundaries, the Alice loops, can not. The action of the lattice model of compact AED we will use is given by:

$$S = \frac{1}{g^2} \sum_p \left\{ -(1 - P_f) \cos \tilde{F} + m_f P_f \right\}_p . \quad (1.15)$$

where  $P_f$  is one if an Alice flux crosses a plaquette and zero if not,  $\tilde{F}$  is the  $F$  of  $U(1)$  after the  $\mathbb{Z}_2$  fields have been gauge transformed away from the plaquette, which is always possible if  $P_f = 0$ . We will use a (hyper-)cubic lattice and the plaquettes are the two dimensional sides of the (hyper-)cubes.

## 1.2. Alice phenomena in Alice electrodynamics

The first term in the action is the well known Wilson action [53] for compact  $U(1)$  lattice gauge theory, if there are no Alice fluxes present. The second term introduces an extra bare mass for the Alice fluxes. As we explained before the difference between ED and AED only arises if there are Alice fluxes present. Even if we do allow local charge conjugation symmetry transformations none of the physics will change. So the tilde in the first term of the action is not important if there are no Alice fluxes present.

In the limit of  $m_f \rightarrow \infty$  and  $g$  finite the Alice fluxes in the theory are excluded and our LAED model becomes equal to the Wilson model. In the limit of  $g \rightarrow \infty$ , but keeping  $m_f/g^2$  finite our LAED model becomes equal to the also well known  $\mathbb{Z}_2$  lattice gauge theory. This is a very nice feature of the model as it allows one in some regions of the parameter space to check the results with well known results from these models and we will also use their results as input for the estimates we make.

This LAED model contains both Alice fluxes and monopoles as lattice artifacts. They disappear in the naive continuum limit. However our introduction of the extra bare Alice flux mass might prevent this if a suitable limit of this extra mass term is taken simultaneously. We could just as well also have introduced an extra bare mass term for the magnetic monopoles present in the model. However, this is computationally a much more involved procedure and it turns out that it is not needed in the sense that the four different phases of the model can be realized without it. The four phases are represented by the different defects that are or are not condensed.

With the help of numerical simulations we determined the regions in parameter space where the different phases in this model occur, for both the three and the four (space-time) dimensional model. The results are shown in figure 1.7.

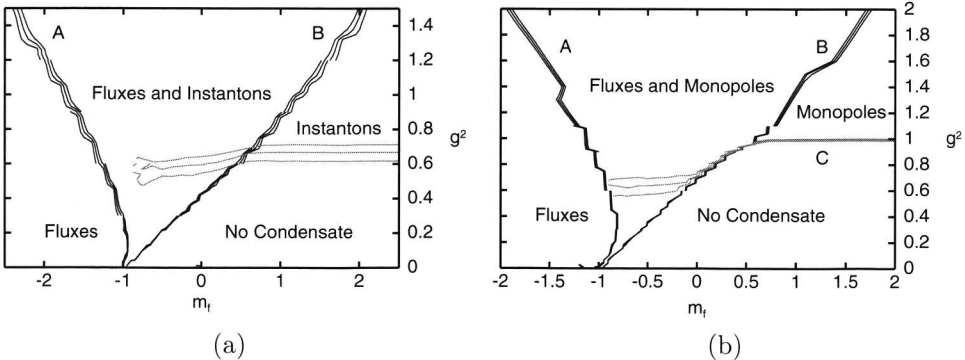


Figure 1.7: In both figures we plotted some specific height lines of the monopole/instanton and Alice flux density, which represent the location of the different phase transitions. Figure (a) contains the result of the three dimensional model, where figure (b) contains the results of the four dimensional model.

The lines in figure 1.7(a) and 1.7(b) are some typical height lines which represent the location of the different phase transitions. As one may see, not all phases are

separated by a phase transition. For example the transition between no condensed instantons and condensed instantons in 3D is a crossover (as is very well known). We see that the transition between condensed fluxes and condensed fluxes plus condensed monopoles/instantons is also a crossover.

The location of the phase transition lines and the values of certain measurable quantities can be very well determined for this model. This is mainly because the parameter space of the model can be divided up into several regions which almost fill out the whole phase space and which can be relatively easily understood as the physics is rather well approximated by some dominant aspects, see section 3.4.

The region where the Alice fluxes are not condensed can be approximated by having no Alice fluxes around at all, i.e., ignoring the effect which the few present Alice fluxes have. As we argued before this is the same as the Wilson model of compact ED. When the Alice fluxes do condense many plaquettes are pierced by a flux. In this region the behavior of the  $U(1)$  degrees of freedom is also well understood. If a plaquette gets pierced by a flux the values of the  $U(1)$  degrees of freedom of that link become irrelevant, see equation 1.15. To lowest order, ignoring the  $\mathbb{Z}_2$ -sheets, this means that pieces of space are cut out by the Alice rings. As the unpierced plaquettes become more and more isolated their behavior can obviously be estimated by the behavior of single plaquettes. Here we note that actually there is no need for the unpierced plaquettes to become fully isolated. It is well known from lattice ED that already two dimensional lattice ED is described by the behavior of a single plaquette. To lowest order also the interaction between the pierced and the unpierced plaquettes is well known, as they exclude each other. The interaction of the fluxes among themselves is the same as it would be for  $\mathbb{Z}_2$  gauge theory. Using these estimates and using the results from  $\mathbb{Z}_2$  and compact  $U(1)$  lattice gauge theory as known results, one can estimate the different features of our LAED model. We estimate quite successfully the location of the different phase transition lines, the average value of  $\cos \tilde{F}$  for the unpierced plaquettes, the flux density and the monopole/instanton density. For more results and more details on the LAED model we refer to chapter 3.

### 1.2.3 Instabilities and topological defects

In this subsection we will briefly discuss situations in which topological defects may develop instabilities of various sorts. To wet the appetite we first look at a simple example which is representative for a generic feature of a rather large class of field theories. We show that a topologically stable kink can reduce the vacuum degeneracy of a model with flat directions. Then we return to AED and study a core instability of the spherically symmetric 't Hooft-Polyakov type magnetic monopole. In particular we will find that the monopole can decay into a Cheshire charged Alice ring. In the last part we will discuss a charge instability that occurs in AED in (2+1)-dimensions. We will find that a static charge is unstable to the creation of a pair of Alice fluxes.

### Dynamical vacuum selection

In the following we will examine a specific field theory with a flat direction in the potential. We want to clarify a general idea and only choose this model for its simplicity, for more details on this subject we refer to chapter 4. The model we will use is a (1+1)-dimensional model and allows for topologically stable kink configurations. The action of the model is given by:

$$S = \int d^2x \left\{ \frac{1}{2} (\partial_\mu \phi_1)^2 + \frac{1}{2} (\partial_\mu \phi_2)^2 - \frac{\lambda}{4} (\phi_1^2 - \phi_2^2 - f^2)^2 \right\} . \quad (1.16)$$

with  $\phi_1$  and  $\phi_2$  two real scalar fields. The field  $\phi_2$  is present to create a flat direction in the potential.

One of the nice features of this particular model is that it is easy to show that only the topologically non-trivial boundary conditions with  $\phi_2$  equal to zero at both plus and minus infinity allow for a truly static kink solution. This is just the standard kink solution for a theory with a single scalar field. Actually, if real space is finite then all topologically nontrivial boundary conditions allow for a static kink solution. In the limit where the boundary values of the  $\phi_2$  field do not deviate too much from zero, the static kink solution can be very well described by a superposition of two independent parts. One corresponds to the special kink solution with  $\phi_2(x) = 0$  and outside the core of this kink there is another part where the Higgs fields only vary within the vacuum manifold of the model, i.e., they satisfy  $\phi_1^2 - \phi_2^2 = f^2$ . This second part, referred to as the “tail”, is easily described by a special combination of the Higgs fields which lives on the vacuum manifold and is therefore called a moduli field. This moduli field is obviously a massless field. The construction is thus as follows: we take the special kink to take us from one part of the vacuum manifold to the other, disconnected part of the vacuum manifold. Then, outside the core of the kink, the moduli field takes over and ensures that the specific boundary conditions are met. The fact that this works in the limit of a large space - large with respect to the deviation of the boundary conditions of  $\phi_2$  from zero - can be understood as follows. In the limit of an infinite space the only static kink solution is the kink solution with  $\phi_2(x) = 0$ . The energy in the tails scales as  $1/R_\infty$ , with  $R_\infty$  the radius of the space. So in the limit of a large but finite space the energy comes close to the energy of the special kink and it is therefore an obvious candidate for the static kink solution as  $R_\infty$  becomes large.

Now we can try to understand what happens in an infinite space if the boundary conditions of the  $\phi_2$  field are not zero and we are in the topologically non-trivial sector. Because the configuration cannot be a static configuration we need to choose some initial conditions. In figure 1.8 we see snapshots of configurations, which started out at rest. In figure 1.8(b) we used a kink in a finite space as initial condition, where in figure 1.8(a) we used a constant  $\phi_2$  and for  $\phi_1$  used a rescaled kink as initial condition.

It is clear that the configurations again consist of two parts. There is the (possibly excited) special kink with  $\phi_2 = 0$  and there is the moduli field. The equations of

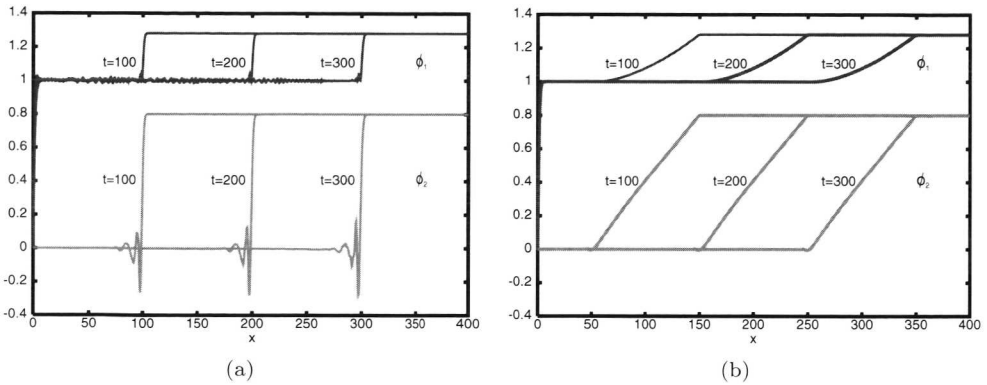


Figure 1.8: These figures show snapshots of non-static configurations. The values of the fields for negative values of  $x$  follow from the antisymmetry of the configuration and are not plotted.

motion for both parts are extremely simple. The special kink is just static and the moduli field, being massless, moves (away) with the speed of light leaving the “special” vacuum, with  $\phi_2(x) = 0$ , behind, see figures 1.8(a) and (b). This is what we refer to as dynamical vacuum selection (DVS). One could wonder if other initial conditions would lead to a different picture. Including dissipation of energy through coupling to other fields it is clear that the Higgs fields will inevitably relax to a configuration containing a special kink together with some moduli field. The energy of such a configuration can come arbitrary close to that of the special kink. In other words dynamical vacuum selection just selects the lowest energy state in a given topologically non-trivial sector, which only depends on the topological information of the boundary conditions and not on the particular location in the flat direction.

It should be clear that the key ingredient in this process is the scaling of the energy of the tails. It is only because these scale to zero as the region over which the moduli field changes becomes larger that DVS works. This shows that DVS is a common feature for all one dimensional field theories which have flat directions in their potential and allow for topologically non-trivial boundary conditions. In fact it has been noted before that such a mechanism is also operative in two dimensions [54, 55, 56], in a situation with topologically stable fluxes with flat directions, where the energy of the tail scales as  $1/\log R_\infty$ . In three or more dimensions, a similar energy argument can be used to show that DVS will no longer occur. We conclude that in one and two dimensions only the topology of the boundary conditions is important, while in higher dimensions also the non-topological information of the boundary conditions is important for the physics in the bulk of the system.

The process we described can be interpreted in two ways. One is the dynamical vacuum selection as we emphasized, on the other hand it can be viewed as an instability of a certain class of topologically non-trivial kinks and fluxes. The latter interpretation is more in line with the discussion of a monopole core instability we turn to next.

## A monopole core instability

We have mentioned that AED features 't Hooft-Polyakov type monopoles. Now we want to examine the core structure of such a magnetic monopole. We discussed that in the Alice flux solution the Higgs field can not be represented by a director field everywhere. Representing the symmetric tensor field by two independent isovectors, see equation 2.4, these will no longer be (anti)parallel in the intermediate region of the space,  $0 < r < \infty$ . The Higgs field escapes in the biaxial direction. For the monopole this is not necessarily the case, but one may wonder if allowing for more general Higgs configurations in the same topological sector, the energy of the monopole solution can be lowered. Here we examine such a possibility. For more details on this investigation we refer to chapter 5.

There is a second reason to expect a monopole core instability of the spherically symmetric magnetic monopole. In section 1.2.1 we encountered an object called the Cheshire charged Alice ring. There we mainly focussed on an electrically Cheshire charged Alice ring, but similarly there is in principle also the possibility of the magnetically Cheshire charged Alice ring. The Alice flux is not an ordinary magnetic flux, it is in some sense orthogonal to the electromagnetic  $U(1)$  direction in the gauge group and does therefore not distinguish between magnetic and electric fields. Bearing this in mind it is a natural question to ask whether such a magnetic Cheshire configuration may have lower energy.

First we will show with the help of some topological deformation considerations that a closed Alice ring really can carry a magnetic charge. Then we will qualitatively argue that this configuration could indeed be stable and finally we show some numerical results establishing a core instability of the spherically symmetric magnetic monopole in part of the parameter space of the model.

The element of the gauge group associated with an Alice flux lies in the disconnected part of the gauge group,  $H_d$ . If one has an Alice ring there is no reason for this element to be the same for all planes intersecting the Alice ring. Parameterizing the Alice ring with an angle this element should be a periodic function of this angle, see figure 1.9(b). This continuous set of elements of the gauge group therefore has to sweep out a closed path in the disconnected part of the unbroken gauge group. From figure 1.2 it is clear that also this path can have an non-trivial topology, i.e., a winding number. Thus the Alice ring, besides carrying a topological charge related to the Alice flux, can also carry another topological charge which is labeled by a winding number.

The description we just gave is very closely related to the topological definition of magnetic charge in the pioneering work of Lubkin [57]. To classify magnetic charge he used a continuous set of closed paths sweeping out the surface of a sphere, see figure 1.9(a). Let us denote these paths as  $C_\phi$ , with  $\phi$  running from zero to  $2\pi$  and  $C_{\phi=0} = C_{\phi=2\pi}$ . This continuous set of paths defines through parallel transport a closed path in the connected part of the gauge group,  $H_c$ , and can be labeled by a winding number. Lubkin then showed that this winding number is the topological magnetic charge inside the sphere. Now let us label the continuum set of paths we

used to describe the Alice ring by  $\bar{C}_\phi$ . The main difference between the two sets of paths is that one describes a closed path in  $H_c$  while the other does so in  $H_d$ . However multiplying the elements of the  $\bar{C}_\phi$  with a specific element of  $H_d$  maps the elements from  $H_d$  to  $H_c$  in an injective way. This one to one map from  $H_d$  into  $H_c$  also maps closed paths in  $H_d$  to closed paths in  $H_c$ <sup>7</sup>. More pictorially one can easily see that the closed paths  $\bar{C}_{\phi=\phi_0}^{-1} \bar{C}_\phi$  are equivalent to the closed paths  $C_\phi$  used by Lubkin. Thus we find that an Alice ring can also carry a magnetic charge which should, following the same arguments as for the electric charge, be carried as a Cheshire charge.

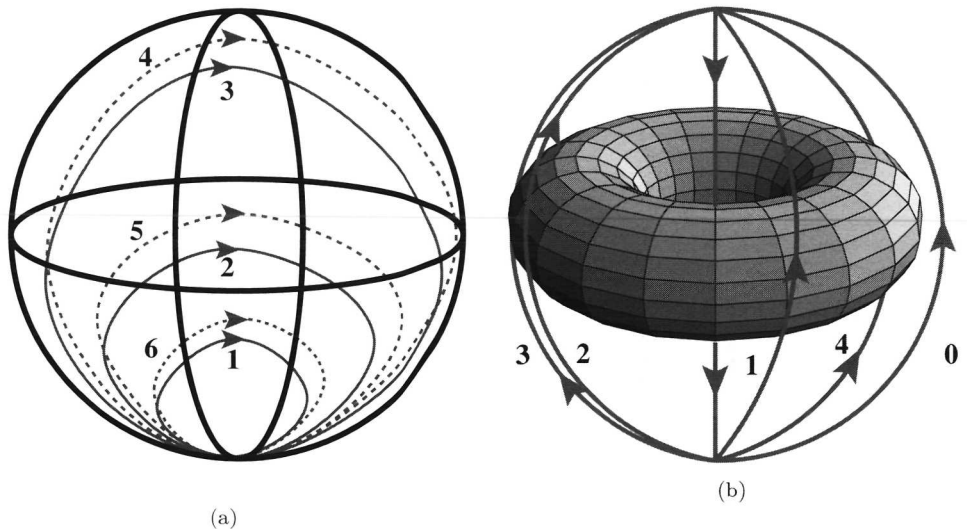


Figure 1.9: Both figures show some specific paths of a continuum of paths which. Figure (a) shows the paths used by Lubkin to classify magnetic charges, where figure (b) shows the paths used to describe the Alice ring. There is a one to one map of the paths in figure (b) to paths equivalent to the paths in figure (a) showing that a closed Alice ring can carry a magnetic charge.

We just showed that the punctured magnetic monopole becomes a magnetically Cheshire charged Alice ring. That this is possible is due to the head-tail symmetry of the Higgs field. To understand that such a configuration can indeed be stable we make an estimate for the energy of such a charged Alice ring. We approximate the energy of the circular Alice ring of radius  $R$ , by  $E_{loop} = 2\pi R \mathcal{E}_{flux}$ , with  $\mathcal{E}_{flux}$  the energy per unit length of the Alice ring, and approximate the energy of the Cheshire charge,  $E_{ches}$ , by a uniformly charged disc with radius  $R$ . The magnetic field of the latter is given by:

$$\vec{B} = \frac{-Q}{\pi R^2} \vec{\nabla} \int_0^1 \int_0^{2\pi} \frac{r' dr' d\theta'}{\sqrt{r^2 + z^2 + r'^2 - 2rr' \cos\theta'}} \quad (1.17)$$

$$\equiv \frac{Q}{R^2} \vec{a}(r, z) \quad (1.18)$$

<sup>7</sup>which preserves the winding number up to a possible sign change, but this is not important because magnetic charges of opposite sign belong to the same topological sector.

## 1.2. Alice phenomena in Alice electrodynamics

---

Where we have rescaled the coordinates by a factor of  $R$  and  $Q$  is the total charge. The field energy is then given by:

$$E_{ches} = \int \vec{B} \cdot \vec{B} R^3 d^3x \quad (1.19)$$

$$= \frac{Q^2}{R} \int \vec{a}(r, z) \cdot \vec{a}(r, z) d^3x \quad (1.20)$$

$$\equiv \frac{Q^2}{R} A \quad (1.21)$$

Where  $A$  is a dimensionless constant determined by the disc geometry. The total energy of the Alice ring of radius  $R$ , with a Cheshire charge  $Q$  is thus given by:

$$E_{tot} = 2\pi R \mathcal{E}_{flux} + \frac{Q^2}{R} A \quad (1.22)$$

We see that there are two competing,  $R$ -dependent terms and we may determine the radius of the loop which minimizes the energy, yielding:

$$R = |Q| \sqrt{\frac{A}{2\pi \mathcal{E}_{flux}}} \quad (1.23)$$

Consequently the minimal energy is given by:

$$E = \sqrt{8\pi \mathcal{E}_{flux} A} |Q| \quad (1.24)$$

Obviously this estimate can only be trusted if the radius of the Alice ring is much larger than the radius of the Alice flux and this should be checked. Nevertheless the estimate does indicate that a Cheshire charged Alice ring can be a stable configuration, where the string tension is balanced by the repulsion between the magnetic field lines. Interestingly this estimate gives an energy proportional to the magnetic charge,  $E \propto |Q|$ .

To determine whether the spherically symmetric magnetic monopole is unstable we return to the original Alice model [4]. We use a variational approach. The ansatz we employ contains the ansatz of the spherically symmetric magnetic monopole solution. We fix the ansatz by imposing cylindrical and up-down symmetry, as these are the symmetries one would expect for a magnetically Cheshire charged Alice ring. The natural boundary conditions at spatial infinity correspond to the usual boundary conditions of the spherically symmetric magnetic monopole solution. The most important thing at this moment is that our ansatz allows for Alice ring like configurations, see figure 1.10(b), and at the same time contains the ansatz of the spherically symmetric monopole solution, see figure 1.10(a). For a detailed description of the ansatz and the parameters used to describe points in the parameter space we refer to chapter 5.

We studied the system using a numerical relaxation and hysteresis procedure and determined the lowest energy configuration at specific points in the parameter space and determined the stability region of the monopole solution, see figure 1.11. We

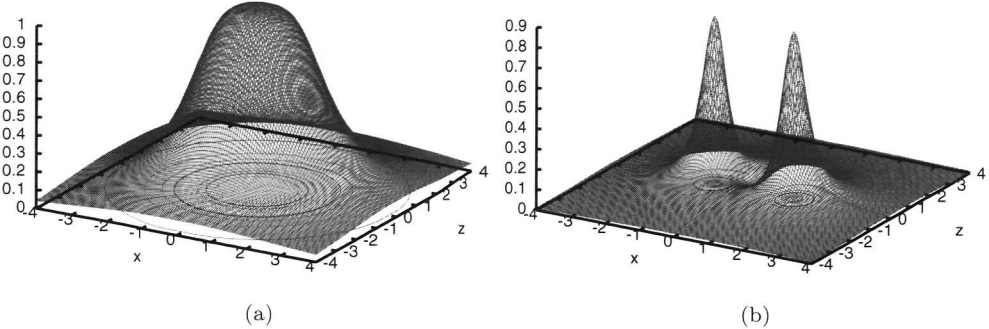


Figure 1.10: Both figures show a plot of  $1 - \frac{\text{Tr}\Phi^2}{6f^2}$  for  $y = 0$ . Figure (a) shows the typical core structure of the spherically symmetric magnetic monopole and figure (b) that of the magnetically Cheshire charged Alice ring, which lies in the  $x$ - $y$  plane at  $z = 0$ .

indeed find that the spherically symmetric magnetic monopole solution is not always the lowest energy solution in its topological sector. Even though the Alice ring configurations we found are strictly speaking not necessarily solutions to the equations of motion, they do nevertheless put an upper bound for the energy of such an exact solution. Furthermore they have the properties one would expect of a magnetically Cheshire charged Alice ring. We conclude that the spherically symmetric magnetic monopole can be unstable with respect to a decay to a magnetically Cheshire charged Alice ring.

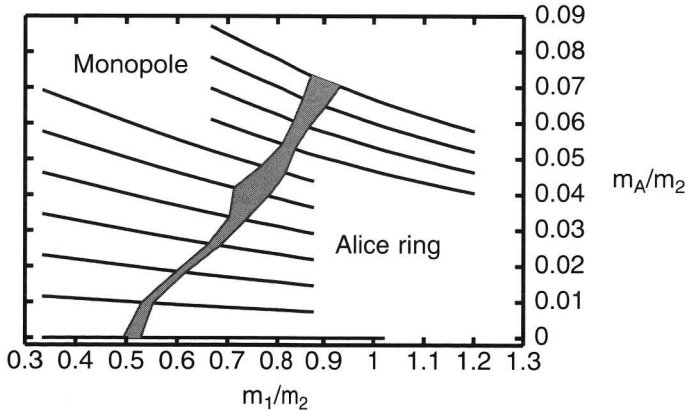


Figure 1.11: This figure shows the meta-stability line for the spherically symmetric magnetic monopole. The shaded region gives the error on the location of the line. On the left of this line the monopole and on the right the Alice ring is the lowest energy configuration within our ansatz.

We just showed that the 't Hooft-Polyakov type monopole is not always the lowest

energy configuration in AED carrying a magnetic charge. There is a region in the parameter space of the model where the magnetic charge is realized as a magnetically Cheshire charged Alice ring. Next we will conclude this lightning preview by considering an even more radical type of charge instability which appears in (2+1)-dimensional Alice electrodynamics.

### Charge instability in (2+1)-dimensions

We will discuss the stability of an external charge (pair) under the creation of a pair of Alice fluxes in (2+1)-dimensions. In section 1.2.1 in the introduction of the Cheshire charge we found that in a specific symmetric configuration the  $\mathbb{Z}_2$ -sheet could be interpreted as conducting plate. In two dimensions this also holds, but it will have a more drastic consequence. For a detailed investigation we refer to chapter 6.

To understand what may happen let us consider the following thought experiment. Assume that we have an external charge in the plane and create out of the vacuum a pair of Alice fluxes, with a  $\mathbb{Z}_2$ -sheet (or rather  $\mathbb{Z}_2$ -line) connecting them. For convenience we choose all objects, including the  $\mathbb{Z}_2$ -line say on the x-axis. Obviously this configuration has an up-down symmetry in the plane allowing us to interpret the  $\mathbb{Z}_2$ -line as a conducting “needle”, a line segment bounded by the fluxes. We see that the pair of fluxes will acquire an induced Cheshire dipole. And, as a conductor attracts a charge, the flux close to the charge will move towards the charge, while the other flux will be pushed away. Here we ignore a possible (typically parameter dependent) intrinsic flux-flux interaction which could of course also be attractive. So what happens when the flux “absorbs” the charge is basically that the charge gets converted into a Cheshire charge carried by the flux pair. This Cheshire charge results in a repulsive force between the two Alice fluxes, so the separation between the Alice fluxes will keep increasing and thereby diluting the charge indefinitely; charge effectively disappears. The notion of a static localized charge is lost. This is a novel mechanism by which charge can loose its manifest appearance, besides the well known phenomena of screening and confinement.

In this thought experiment we ignored the structure of the Alice fluxes, a possible intrinsic flux-flux interaction and the well known confining mechanism of monopoles disguised as instantons proposed by Polyakov [58, 59]. Although including these effects might change the details of the instability, the main conclusion remains unaltered. The assumptions we made can also be justified by working with a lattice model, see section 1.2.2, where there is a priori no flux-flux interaction or flux core structure and the monopole mass can be taken to be infinite, suppressing the confinement mechanism. In fact in this regime one can determine the field configurations analytically with the help of the conformal invariance of two dimensional electrodynamics. For example the potential and the field lines of two opposite charges with a flux pair in the middle are given in figure 1.12(a) and 1.12(b) respectively.

The energy gain in the field energy due to the presence of the Alice flux pair can also

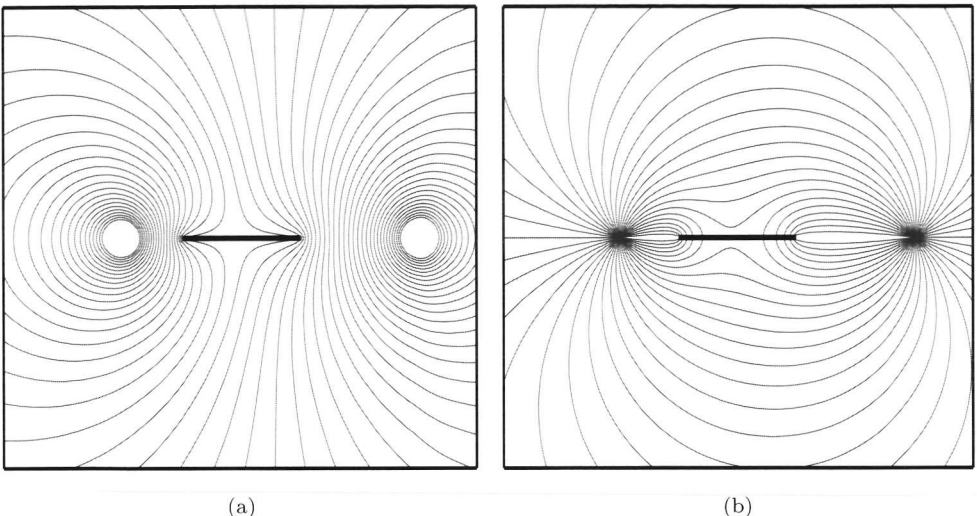


Figure 1.12: These figures show some of the equipotential lines, figure (a), and the corresponding field lines, figure (b), of two oppositely charged charges in the presence of a pair of fluxes located at the endpoints of the thick black line segment.

be determined exactly and is given by:

$$E_{f\text{pair}} = \frac{Q^2}{\pi} \log \left( \frac{1}{2} \left( 1 + \frac{1 + x_1 x_2}{\sqrt{x_1^2 - 1} \sqrt{x_2^2 - 1}} \right) \right) , \quad (1.25)$$

with  $Q$  the charge of the external charges and  $x_i$  the location of the charges with respect to the middle of the flux pair and in units of twice the distance between the fluxes.

With the help of these and other expressions we investigate several decay geometries of some charge systems in AED in chapter 6. One of the most important consequences of this instability is the fact that the potential between two charges will not grow indefinitely in (2+1)-dimensional AED irrespective of the presence of monopoles, i.e., due to this instability the potential between two external charges will saturate, see figure 6.10. So we find that (2+1)-dimensional AED is not necessarily a confining theory but may instead exhibit this novel Cheshire screening. Finally a comment on the situation in (3+1)-dimensional AED. Here one does not expect the same results, as the classical potential itself already saturates and an Alice ring can not grow without a linear cost in energy. However in the phase where the Alice fluxes condense one does expect a screening effect as one has a condensate of possible (induced) dipoles.

This completes our introduction and preview of Alice phenomena, which shows that having slightly more than electrodynamics might result in rather drastic dynamical and physical effects. These phenomena appear to be quite generic if after symmetry breaking the residual symmetry group has non-commuting discrete subgroups.

# Chapter 2

## $U(1) \times \mathbb{Z}_2$ models

In this chapter we introduce three continuum models which feature an Alice electrodynamics phase and present numerical solutions of Alice fluxes in these models. One model is the original Alice model studied by Schwarz [4], two alternative models are proposed. An advantage of these new models is that in a well defined sense the Alice flux solutions we obtain obey first order equations similar to those of the Nielsen-Olesen flux tube [60] in the abelian Higgs model in the Bogomolny limit. The contents of this chapter is mainly based on [61].

### 2.1 Alice electrodynamics

An Alice phase can be obtained by a spontaneous breaking of a larger, continuous, non-abelian symmetry group. In the original Alice model studied by Schwarz [4] a  $SU(2)$  gauge theory is spontaneously broken down to a  $U(1) \times \mathbb{Z}_2$  by a Higgs field in the 5-dimensional representation of the gauge group (see also [62, 5]). The Higgs field is chosen in this representation, because it is the smallest irreducible representation which admits  $U(1) \times \mathbb{Z}_2$  as a residual symmetry group and allows for a single valued vacuum configuration that supports Alice fluxes.

In this chapter we will discuss two alternative models, which support an Alice phase. Before doing so, we briefly review the salient features of the model discussed in [4, 62]. The action is given by:

$$S = \int d^4x \left\{ \frac{1}{4} F^{a,\mu\nu} F_{\mu\nu}^a + \frac{1}{4} \text{Tr} (D^\mu \Phi D_\mu \Phi) - V(\Phi) \right\} , \quad (2.1)$$

where the Higgs field  $\Phi = \Phi^{ab}$  is a real symmetric traceless  $3 \times 3$  matrix. The most general renormalizable potential is given by [50]:

$$V = -\frac{1}{2} \mu^2 \text{Tr} (\Phi^2) - \frac{1}{3} \gamma \text{Tr} (\Phi^3) + \frac{1}{4} \lambda (\text{Tr} (\Phi^2))^2 . \quad (2.2)$$

By a suitable choice of parameters the Higgs field will acquire a vacuum expectation value,  $\Phi_0$ . In a gauge where  $\Phi_0$  is diagonal it takes the form  $\Phi_0 = \text{diag}(-a, -b, a+b)$ . For a certain range of potential parameters one furthermore has that  $f \equiv a = b$ , so that  $\Phi_0$  is given by:

$$\Phi_0 = \begin{pmatrix} -f & 0 & 0 \\ 0 & -f & 0 \\ 0 & 0 & 2f \end{pmatrix} \quad . \quad (2.3)$$

$$\text{with } f = \frac{\gamma}{12\lambda} \left( 1 + \sqrt{1 + \frac{24\mu^2\lambda}{\gamma^2}} \right).$$

Indeed, this ground state is invariant under rotations around the  $T_3$ -axis, the  $U(1)$ -part of the Alice symmetry, and invariant under rotations by an angle  $\pi$  around any axis perpendicular to the  $T_3$ -direction, the  $\mathbb{Z}_2$ -part of the Alice symmetry. These two transformations do not commute with each other, they anti-commute, so the resulting residual gauge group is indeed  $U(1) \ltimes \mathbb{Z}_2$ . This means that we have Alice electrodynamics as the low energy effective theory in this model.

An alternative way to see the structure of the residual gauge group, is to think of the Higgs field as the symmetric traceless product of two vectors,  $\phi_1$  and  $\phi_2$ ,

$$\Phi^{ab} = \phi_1^a \phi_2^b + \phi_2^a \phi_1^b - \frac{2}{3} \delta^{ab} (\vec{\phi}_1 \cdot \vec{\phi}_2) \quad . \quad (2.4)$$

If both isovectors,  $\vec{\phi}_i$ , are non zero, there is in general only a  $\mathbb{Z}_2$  gauge symmetry left,  $\vec{\phi}_i \rightarrow \vec{\phi}'_i = -\vec{\phi}_i$ . However, in case that both isovectors are (anti-)parallel, the gauge group is  $U(1) \ltimes \mathbb{Z}_2$ . If one of the isovectors is zero, the gauge group is not broken at all and the symmetry remains  $SU(2)$ . These are the residual gauge groups which one may encounter in this model. It is easy to show that the case where the two isovectors are (anti-)parallel, corresponds to the situation where  $\Phi = \Phi_0$ .

### 2.1.1 The Alice flux solution

In this section we will present exact regular solutions, corresponding to an Alice flux tube along the  $z$ -axis, which where constructed in [63].

To have a static finite energy solution, all terms in the energy density should go to zero at spatial infinity. Thus the covariant derivatives need to vanish at spatial infinity. Let's look at the angular derivative, the condition  $D_\theta \Phi = 0$  tells us that the Higgs field has the following form at spatial infinity.

$$\Phi(\theta) = S(\theta) \Phi(0) S^{-1}(\theta) \quad , \quad (2.5)$$

with

$$S(\theta) = \exp \left( e \int_0^\theta r A_\theta d\theta \right) \quad . \quad (2.6)$$

Since we are looking for solutions which correspond to an Alice flux,  $S(2\pi)$  needs to be an element of the disconnected part of the (residual) gauge group. A simple choice

for  $A_\theta$  doing this is  $A_\theta = \frac{1}{2er} T_1$ .

This leads to the ansatz:

$$A_\theta = \frac{\alpha(r)}{2er} T_1 , \quad (2.7)$$

$$\Phi(r, \theta) = e^{\frac{\theta T_1}{2}} \Phi(r) e^{-\frac{\theta T_1}{2}} , \quad (2.8)$$

where the tensor  $\Phi(r)$  is conveniently parameterized as,

$$\Phi(r) = m(r) \begin{pmatrix} 1 & 0 & 0 \\ 0 & -\frac{1}{2} & 0 \\ 0 & 0 & -\frac{1}{2} \end{pmatrix} + q(r) \begin{pmatrix} 0 & 0 & 0 \\ 0 & \frac{3}{2} & 0 \\ 0 & 0 & -\frac{3}{2} \end{pmatrix} . \quad (2.9)$$

The part proportional to  $m(r)$  is the part of the Higgs field that is invariant under rotations generated by  $T_1$ . The boundary condition at spatial infinity is  $m(\infty) = q(\infty)$ , implying that  $\Phi(\infty)$  is of the form (2.3), i.e., the residual symmetry is  $U(1) \ltimes \mathbb{Z}_2$  indeed, where the electrodynamic  $U(1)$  is generated by  $T_3$ . At the origin,  $m$  and  $q$  have to satisfy different boundary conditions; the field  $q(r)$  needs to go to zero. The term proportional to  $m(r)$  is invariant under  $T_1$  rotations, therefore  $m(r)$  does not need to go to zero. Again, this means that the Higgs field is of the form (2.3), i.e., the unbroken gauge group is  $U(1) \ltimes \mathbb{Z}_2$ . However, the unbroken  $U(1)$  is generated by  $T_1$ . Finally, the field  $\alpha(r)$  needs to be zero at the origin and unity at spatial infinity. Inserting this ansatz in the field equations gives, after suitable rescalings, the following set of equations.

$$\partial_r^2 \alpha(r) - \frac{1}{r} \partial_r \alpha(r) = 9q^2(r)(\alpha(r) - 1) , \quad (2.10)$$

$$\begin{aligned} \partial_r^2 q(r) + \frac{1}{r} \partial_r q(r) &= \frac{(\alpha(r) - 1)^2 q(r)}{r^2} + \xi (9q^2(r) + 3m^2(r) - 2) q(r) \\ &\quad + 2\chi m(r)q(r) , \end{aligned} \quad (2.11)$$

$$\begin{aligned} \partial_r^2 m(r) + \frac{1}{r} \partial_r m(r) &= \xi (9q^2(r) + 3m^2(r) - 2) m(r) \\ &\quad + \chi (3q^2(r) - m^2(r)) . \end{aligned} \quad (2.12)$$

We summarize the boundary values for the rescaled fields below:

field	$r \rightarrow 0$	$r \rightarrow \infty$
$\alpha(r)$	0	1
$q(r)$	0	$q(\infty)$
$m(r)$	constant	$m(\infty)$

where

$$m(\infty) = q(\infty) = \frac{-\chi \pm \sqrt{\chi^2 + 24\xi^2}}{12\xi} \equiv \tilde{f}(\xi, \chi) . \quad (2.13)$$

with  $\xi = \frac{\lambda}{e^2}$  and  $\chi = \frac{\gamma\sqrt{\lambda}}{\mu e^2}$ .

The system (2.10)-(2.12) was solved numerically with the help of a relaxation method

in [63]. The solution for the potential parameter values  $\xi = 1$  and  $\chi = -1$  is given in figure 2.1.

The situation at hand is reminiscent to the one considered by Witten [64] for a  $U(1) \times \tilde{U}(1)$  model, in the sense that we have an unbroken  $U(1) \times \mathbb{Z}_2$  at the core and a different  $U(1) \times \mathbb{Z}_2$  at infinity. However, the crucial difference is, that our 'two'  $U(1)$  gauge groups do not commute with each other.

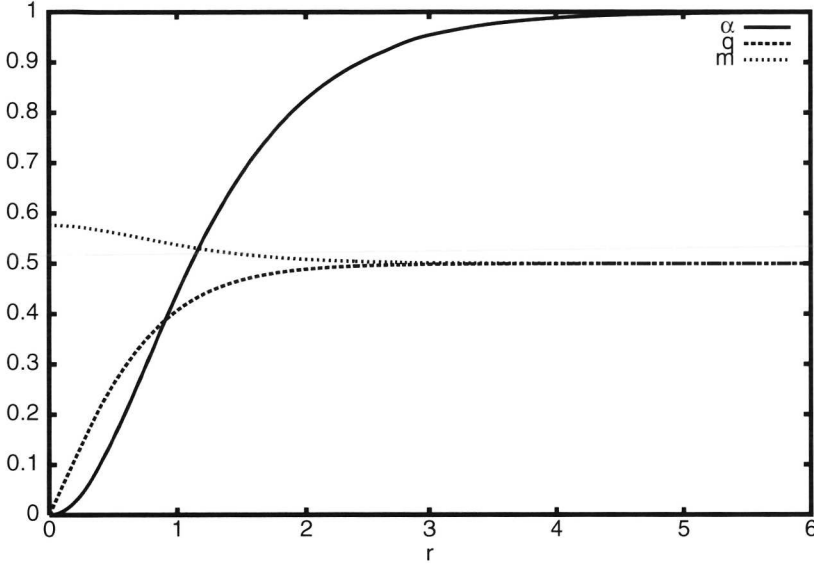


Figure 2.1: A regular solution for the fields with an Alice flux for  $\xi = 1$  and  $\chi = -1$ .

Interestingly, there is also another solution to the field equations, which we briefly discuss. If  $\chi = 0$  there is a solution with  $m(r) = 0$ . After a rescaling of  $q(r)$  one finds exactly the same equations as were obtained in the Nielsen-Olesen (NO) model by [65] for the minimal flux  $n = 1$ , provided we set the value of  $\lambda = 2\xi$ . Numerical solutions to these equations have been studied before. For a special value of  $\lambda$  one obtains the solutions by solving Bogomolny type, first order equations. The residual symmetry of this solution in our model is  $\mathbb{Z}_2$ . One may wonder whether in our model this is a stable solution. In the case of  $\gamma = 0$ , i.e.,  $\chi = 0$ , the potential (2.2) has the form:

$$V = -\mu^2 X + \lambda X^2 \quad . \quad (2.14)$$

The minimum of this potential is obviously given by  $X = \frac{\mu^2}{2\lambda}$ , with  $X = \frac{1}{2}\text{Tr}(\Phi^2)$ . Written in the components  $m$  and  $q$  this gives:

$$c_1 m^2 + c_2 q^2 = 1 \quad , \quad (2.15)$$

with  $c_1, c_2 > 0$ .

A simple rescaling of  $m$  and  $q$  yields:  $m^2 + q^2 = 1$ . As we require finite energy, this is one of the boundary conditions for the fields  $m$  and  $q$  at spatial infinity. We now see that the boundary condition of the new solution,  $m = 0$ , may be continuously changed to one where  $q = 0$ . But then the Higgs field does no longer stabilize the flux, which means that the flux will decay by spreading out and losing more and more energy. Through this process we end up in a ‘‘rotated’’ Alice phase of the theory where the  $U(1)$  generator points in the internal direction of the flux we started off with. When going from the  $m = 0$  to the  $q = 0$  boundary condition we pass an Alice phase whose  $U(1)$  generator is perpendicular to the internal direction of the flux we started with. The upshot of these observations is that, if one wants to have a stable Alice flux in an Alice phase, one needs to have  $\gamma \neq 0$ . Otherwise the decay induces a reorientation of the vacuum state in the degenerate space of all classical vacua. This concludes what we have to say about conventional Alice electrodynamics, in the remaining sections of the chapter we will focus on some alternative Alice models.

## 2.2 Alternative Alice models

In this section we introduce two alternative models, which exhibit an Alice electrodynamic phase. In these alternative models we choose the Higgs field(s) in the adjoint (3) representation of  $SO(3)$ . This obviously means that the Higgs field is not single valued in the presence of an Alice flux, but this can be ‘‘solved’’ in two more or less similar ways. One way is to put the internal space of the Higgs field ( $X$ ) on a  $\mathbb{Z}_2$  orbifold, i.e.,  $X$  and  $-X$  are identified with each other. The other way is to use (at least) two Higgs fields and put the total internal space of these two Higgs fields ( $X$  and  $Y$ ) on a  $S_2$  orbifold, i.e., identify the points  $(X, Y)$  and  $(Y, X)$ .

The action we use for both models is given by:

$$S = \int d^4x \left\{ \text{Tr} \left( \frac{1}{4} F^{\mu\nu} F_{\mu\nu} + \frac{1}{2} D^\mu X D_\mu X + \frac{1}{2} D^\mu Y D_\mu Y - \frac{\hat{\gamma}}{2} [X, Y]^2 \right) - \frac{\hat{\lambda}}{4} (\text{Tr} (X^2 + Y^2) - f^2)^2 \right\} . \quad (2.16)$$

Both theories allow the presence of an Alice flux. In the  $S_2$  model it means that one studies the twisted sector of the theory.

### 2.2.1 Alice flux solutions

We now turn to the construction of regular cylindrically symmetric (numerical) solutions corresponding to an Alice flux. At spatial infinity one has  $D_\theta X = 0$ , implying that the Higgs field should have the following form there.

$$X(\theta) = S(\theta)X(0)S^{-1}(\theta) . \quad (2.17)$$

with  $S(\theta)$  the same as in (2.6).

The flux associated with  $S(\theta)$  is topologically stable if the element of the gauge group associated with  $S(2\pi)$  is an element of the disconnected part of the residual gauge group. A simple choice<sup>1</sup> is:  $A_\theta = \frac{1}{2er} T_1$ . This puts the Alice flux in the internal  $T_1$  direction. Writing the Higgs field as  $X = x^a T_a$ , it follows that  $X(\theta)$  has the following form:

$$X(\theta) = e^{\frac{T_1 \theta}{2}} \begin{pmatrix} x^1(0) \\ x^2(0) \\ x^3(0) \end{pmatrix} . \quad (2.18)$$

and thus that  $X(2\pi)$  is given by:

$$X(2\pi) = \begin{pmatrix} x^1(0) \\ -x^2(0) \\ -x^3(0) \end{pmatrix} . \quad (2.19)$$

The same holds, of course, for the other Higgs field. Because the two models differ slightly in constructing the ansatz, we will treat them separately for the moment.

### The $\mathbb{Z}_2$ model:

For the  $\mathbb{Z}_2$  model the boundary condition specified above implies that either  $x^1 = 0$  or  $x^2 = x^3 = 0$ . Only in the first case, however, is  $S(2\pi)$  an element of the disconnected part of the gauge group. Thus we have to put  $x^1 = 0$ . Later we will see that this choice is important in order to obtain first order equations. At this point it is convenient to introduce a different basis for the generators of the gauge group, a basis naturally linked to the orientation of the Higgs field. Its elements are given by:

$$S_a(\theta) = e^{\frac{T_1 \theta}{2}} T_a e^{-\frac{T_1 \theta}{2}} . \quad (2.20)$$

Now we write the Higgs field as  $X = x^a S_a$ , where also in this language one has to put  $x^1 = 0$  to secure the possibility of a topological stable solution.

In this model a single Higgs field would suffice, but for reasons of similarity we will use two. Our ansatz then reads:

$$A_\theta = \frac{\alpha(r)}{2er} S_1 . \quad (2.21)$$

$$X = a(r) S_3 . \quad (2.22)$$

$$Y = c(r) S_1 . \quad (2.23)$$

### The $S_2$ model:

The 'double valuedness' is only allowed if one uses an orbifold interpretation. So we impose a strict relation between  $X$  and  $Y$ .

$$X(\theta + 2\pi) = \begin{pmatrix} x^1(\theta) \\ -x^2(\theta) \\ -x^3(\theta) \end{pmatrix} = \begin{pmatrix} y^1(\theta) \\ y^2(\theta) \\ y^3(\theta) \end{pmatrix} = Y(\theta) . \quad (2.24)$$

<sup>1</sup> At this point we can not yet say that this is an element of the disconnected part of the residual gauge group, but this will be done consistently below.

Leading to:  $x^1 = y^1$ ,  $x^2 = -y^2$  and  $x^3 = -y^3$ . Again we are going to work with the twisted generators (2.20). A consistent ansatz is the following one:

$$A_\theta = \frac{\alpha(r)}{2er} S_1 , \quad (2.25)$$

$$X = a(r) S_3 + c(r) S_1 , \quad (2.26)$$

$$Y = -a(r) S_3 + c(r) S_1 . \quad (2.27)$$

For both cases one may insert the appropriate ansatz in the field equations. This yields after a suitable rescaling, the same set of differential equations for both models:

$$\partial_r^2 \alpha(r) - \frac{1}{r} \partial_r \alpha(r) = (\alpha(r) - 1) a^2(r) , \quad (2.28)$$

$$\begin{aligned} \partial_r^2 a(r) + \frac{1}{r} \partial_r a(r) &= \frac{(\alpha(r) - 1)^2}{4r^2} a(r) + \lambda a(r) (a^2(r) + c^2(r) - 1) \\ &\quad + \gamma c^2(r) a(r) , \end{aligned} \quad (2.29)$$

$$\partial_r^2 c(r) + \frac{1}{r} \partial_r c(r) = \gamma a^2(r) c(r) + \lambda c(r) (a^2(r) + c^2(r) - 1) . \quad (2.30)$$

The asymptotic values of the fields are as follows:

field	$r \rightarrow 0$	$r \rightarrow \infty$
$\alpha(r)$	0	1
$a(r)$	0	1
$c(r)$	constant	0

The boundary conditions are such that  $S(2\pi)$  is an element of the disconnected part of the residual gauge group.

We have constructed numerical solutions to these equations, for different values of  $\lambda$  (and  $\gamma$ ), with the use of a “shooting” method, see figures 2.2 and 2.2. As a matter of fact, we only found solutions for which  $c(r) = 0$ , although our starting values were chosen quite general. This implies that there is no dependence of the solutions we found, on  $\gamma$ .

In fact if  $c(r) = 0$ , the equations become the same as in the case of a Nielsen-Olesen (NO)flux with the critical value of the Landau coupling parameter leading to first order Bogomolny equations. However, there is an important difference with the NO case. The “winding” number of the Alice flux is fractional and equals  $n = \frac{1}{2}$ , a value which is not admissible in the NO model. This is clearly a consequence of the different breaking schemes of the theories in question.

There is a special role in these theories for the parameter  $\gamma$ . If we set  $\gamma = 0$  the equations are very similar to the equations (2.10)-(2.12) with  $\chi = 0$ . Though  $\gamma$  appears to play no role as long as  $c(r) = 0$ , this is not quite the case. We don't want  $\gamma$  to vanish because then we run more or less into the same problem as in the conventional model for Alice electrodynamics with  $\chi = 0$ . The solution with  $c(r) = 0$  would still be a solution of the field equations, but the flux would no longer be stable. It would be allowed to decay into the vacuum. In fact in the alternative models it is

quite clear what happens at  $\gamma = 0$ , the potential term proportional to  $\gamma$  – assuming it is nonzero – ensures that there is no continuous path in the vacuum manifold connecting the  $c = 0$  to the  $a = 0$  boundary condition<sup>2</sup>. If  $\gamma = 0$  such a path does exist.

There is a simple relation between the  $\mathbb{Z}_2$  model with one Higgs field and the  $S_2$  model with two Higgs fields, in the presence of an Alice string. In the presence of an Alice string the field component of the Higgs field parallel to the Alice flux is zero in the  $\mathbb{Z}_2$  model, whereas in the  $S_2$  model this is in general only true far away from the core. So, in some sense the  $\mathbb{Z}_2$  model is a long wavelength approximation of the  $S_2$  model, but remarkably enough, it does support solutions which are regular everywhere nevertheless. The action of both models becomes the same, up to a rescaling, if the components parallel to the Alice flux, of the Higgs fields in the  $S_2$  model, are set equal to zero.

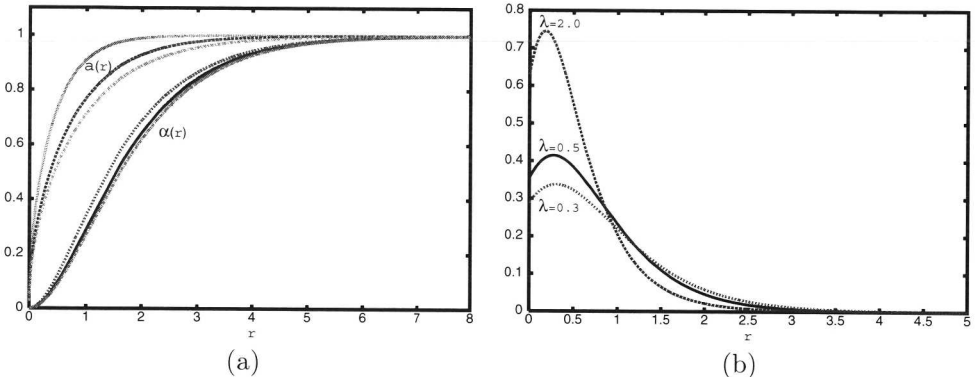


Figure 2.2: The fields  $\alpha(r)$  and  $a(r)$ , figure (a), and the energy density times  $r$  of the Alice flux, figure (b), for  $\lambda = 2.0 \dots 0.5 \dots 0.3$

### 2.2.2 First order equations

As mentioned before, if one sets  $c(r) = 0$ , the set of equations, (2.28)-(2.30), reduces to the same set that one would obtain in the NO model for a solution with winding number  $n = \frac{1}{2}$ . It thus appears that one can, in the sector that contains a topologically stable Alice flux, project both theories on a sector of the NO model. This raises the question whether it would be possible to find first order equations in both models. In the  $\mathbb{Z}_2$  model, with only a single Higgs field, this projection is the clearest. For the rest of this section we will therefore concentrate on this case.

One of the features of the NO theory is that for a certain value of the coupling constant  $\lambda$ , the solutions can be obtained from first order equations. These first order equations can be found *à la* Bogomolny, by rewriting the energy density as a sum of

<sup>2</sup>Remember, there is also the boundary condition  $a^2 + c^2 = 1$ .

squares plus a topological term. In the case of static solutions, the energy density and the Lagrangian differ only by a sign, implying that extrema of the energy are also extrema of the Lagrangian. Consequently, solutions of minimal energy are stable static solutions of the full set of second order field equations. The energy of the  $\mathbb{Z}_2$  model is given by:

$$E = \frac{1}{2} \int d^3x \left\{ \text{Tr} (E_i^2 + B_i^2 + (D_i X)^2 + (D_t X)^2) + \frac{\lambda}{2} ((x^1)^2 + (x^2)^2 + (x^3)^2 - 1) \right\} . \quad (2.31)$$

In the static case with no electric fields, in the gauge  $A_t = 0$ , one has  $E_i = \partial_t A_i = 0$  and  $D_t X = \partial_t X = 0$ , reducing the expression to,

$$E = \frac{1}{2} \int d^3x \left\{ \text{Tr} (B_i^2 + (D_i X)^2) + \frac{\lambda}{2} ((x^1)^2 + (x^2)^2 + (x^3)^2 - 1) \right\} . \quad (2.32)$$

Restricting ourselves to the plane, the energy written in components is given by:

$$E = \frac{1}{2} \int d^2x \left\{ (B_z^1)^2 + (B_z^2)^2 + (B_z^3)^2 + ((D_\nu X)^1)^2 + ((D_\nu X)^2)^2 + ((D_\nu X)^3)^2 + \frac{\lambda}{2} ((x^1)^2 + (x^2)^2 + (x^3)^2 - 1) \right\} . \quad (2.33)$$

where now the upper label refers to the internal directions (in the normal, non-twisted basis) and the lower label to the spatial directions. From this expression we are unable to obtain first order equations, however, if we restrict ourselves to the subspace of solutions containing an Alice flux, there is something we can do. Let's call the internal direction in which the Alice flux 'points' the '1' direction, so if one is looking for topological stable fluxes one needs to have  $x^1 = 0$ , as argued before. In that case we may write the energy as,

$$E = \frac{1}{2} \int d^2x \left\{ (B_z^1)^2 + (B_z^2)^2 + (B_z^3)^2 + (([A_1, X]^1)^2 + ([A_2, X]^1)^2 + (\partial_1 x^2 + A_1^1 x^3)^2 + (\partial_1 x^3 - A_1^1 x^2)^2 + (\partial_2 x^2 + A_2^1 x^3)^2 + (\partial_2 x^3 + A_2^1 x^2)^2 + \frac{\lambda}{2} ((x^2)^2 + (x^3)^2 - 1) \right\} . \quad (2.34)$$

For the case of  $\lambda = \frac{1}{2}$  this can be brought into the form:

$$E = \frac{1}{2} \int d^2x \left\{ (B_z^2)^2 + (B_z^3)^2 + ((\partial_1 x^2 + A_1^1 x^3) \mp (\partial_2 x^3 - A_2^1 x^2))^2 + (([A_1, X]^1)^2 + ([A_2, X]^1)^2 + \left( B_z^1 \pm \frac{1}{2} ((x^2)^2 + (x^3)^2 - 1) \right)^2 + ((\partial_2 x^2 + A_2^1 x^3) \pm (\partial_1 x^3 - A_1^1 x^2))^2 \right\}$$

$$\begin{aligned} & \pm [A_1, A_2]^1 \left( (x^2)^2 + (x^3)^2 - 1 \right) \} \\ & \pm \frac{1}{2} \int d^2x (B_z + [A_1, A_2])^1 \quad . \end{aligned} \quad (2.35)$$

Still, there appears to be a problem, because there are two terms in this expression of the energy density, which are not squares and as we will show later, only one of them is proportional to the winding number. The other term,  $[A_1, A_2]^1 \left( (x^2)^2 + (x^3)^2 - 1 \right)$ , therefore appears to be problematic. This problem can fortunately be cured rather straightforwardly. Remember that we are already in a ‘gauge’  $A_t = 0$ . In this situation the residual gauge freedom of time independent gauge transformations may be used to put the term  $[A_1, A_2]^1$  equal to zero. In this gauge the energy density consists only of squares and a term proportional to the winding number. The minimum of the energy is now easily obtained by putting all squares in the energy density equal to zero. This then yields a set of first order equations of which the solutions are also solutions of the full field equations. The first order equations, including the gauge conditions, are:

$$[A_1, A_2]^1 = 0 \quad . \quad (2.36)$$

$$B_z^2 = 0 \quad . \quad (2.37)$$

$$B_z^3 = 0 \quad . \quad (2.38)$$

$$[A_1, X]^1 = 0 \quad , \quad (2.39)$$

$$[A_2, X]^1 = 0 \quad . \quad (2.40)$$

$$B_z^1 \pm \frac{1}{2} \left( (x^2)^2 + (x^3)^2 - 1 \right) = 0 \quad . \quad (2.41)$$

$$(\partial_1 x^2 + A_1^1 x^3) \mp (\partial_2 x^3 - A_2^1 x^2) = 0 \quad . \quad (2.42)$$

$$(\partial_2 x^2 + A_2^1 x^3) \pm (\partial_1 x^3 - A_1^1 x^2) = 0 \quad . \quad (2.43)$$

The last three equations are identical to those that were obtained in the NO model. The energy of solutions to this set of equations are fully determined by the term:  $\int d^2x (B_z + [A_1, A_2])^1$ , which is proportional to the winding number, as we show next. The general expression for  $X$  in the presence of an Alice flux in the first isospin direction ‘along’  $T_1$ , becomes:

$$\begin{aligned} X &= x(r) e^{2\pi i \chi(\theta) T_1} T_2 = x(r) \cos(2\pi \chi(\theta)) T_2 + x(r) \sin(2\pi \chi(\theta)) T_3 \\ &\equiv a T_2 + b T_3 \quad . \end{aligned} \quad (2.44)$$

with  $\chi(\theta + 2\pi) = \chi(\theta) + \frac{1}{2}$ . For  $r \rightarrow \infty$  one has  $x(r \rightarrow \infty) = 1$ , and the winding number can be extracted from the asymptotics by:

$$\frac{-i}{2\pi} \oint^{r \rightarrow \infty} d\ln(a + i * b) = n = \frac{1}{2} \quad . \quad (2.45)$$

For  $r \rightarrow \infty$  one also has the spatial covariant derivatives  $DX = 0$  or:

$$\partial X = [A, X] \quad , \quad (2.46)$$

or in components:

$$[A, X]^1 = 0 \quad , \quad (2.47)$$

$$\partial a = -A^1 b \quad , \quad (2.48)$$

$$\partial b = A^1 a \quad . \quad (2.49)$$

From this one finds  $\partial \ln(a + i * b) = i * A^1$ , which means that:

$$\frac{-i}{2\pi} \oint^{r \rightarrow \infty} d \ln(a + i * b) = \frac{1}{2\pi} \oint^{r \rightarrow \infty} d\vec{l} \hat{l} \cdot A^1 = \frac{1}{2\pi} \int d^2 x \left( B_z^1 + [A_1, A_2]^1 \right) \quad . \quad (2.50)$$

Thus the rescaled energy of the solutions is equal to  $\frac{\pi}{2}$ . Note that the above expressions do not look gauge invariant because we are evaluating a gauge invariant expression in a particular gauge.

One should, of course, check whether the first order equations actually do have any solutions of the type we are interested in. By inserting the ansatz used before and putting  $c(r)$  to zero, one arrives at the following set of coupled non-linear first order equations.

$$r \partial_r a(r) = \frac{1}{2} (1 - \alpha(r)) a(r) \quad , \quad (2.51)$$

$$\frac{1}{r} \partial_r \alpha(r) = 1 - a^2(r) \quad . \quad (2.52)$$

Now, these turn out to be a special case of the equations encountered before by De Vega and Schaposnik [65] in their study of the NO model. They were obviously only interested in the case of integer winding number, whereas we are interested in the case of fractional winding number  $n = \frac{1}{2}$ . The corresponding numerical solution is given in figures 2.2 and 2.2.

We have attained our goal of this subsection, of obtaining a set of first order equations, of which the solutions are also static minima of the energy (with no electric fields). As is well-known, first order equations play a deep role in gauge theories. Bogomolny [66] explained, for the NO model, that solutions which come from the first order equations are also minima of the energy, which implied the neutral stability of such solutions. Later it was shown [67] that the occurrence of so-called Bogomolny equations is tightly connected to the existence of a super-symmetric extension of the theory. The explicit super symmetry extension of the NO model was given by [68] and in agreement with [67] showed that the first order equations indeed come together with an increase of super-symmetry. In our models we found first order equations whose solutions are also solutions to the full set of second order field equations. We showed that the solutions are also minima of the energy. This obviously raises the question if these first order solutions can also be explained by the existence of a super-symmetric extension of our models. A superficial analysis suggests that this is not the case, basically because we can only recover the Bogomolny argument within the context of a very restrictive ansatz. In this respect the situation is similar to that encountered in the study of regular  $\mathbb{Z}_N$  monopoles [69].

## 2.3 Conclusions

In this chapter we proposed two new models which both possess an Alice electrodynamics phase. For both models we constructed solutions corresponding to a topologically stable Alice flux. We found a way to project the theories on the Nielsen Olesen model and, in that way, obtained first order equations. Solutions to these first order equations corresponding to minima of the energy (without electric fields) were constructed numerically.

We close with a brief remark concerning the zero modes of our solution. Weinberg [70] showed that in the NO model, for the critical value  $\lambda = \frac{1}{2}$ , a flux with winding number  $n$  has  $2n$  zero modes. These modes are interpreted as being the positions of the unit fluxes. At first sight this appears to give problems for the case of  $n = \frac{1}{2}$ , but carefully redoing section IV of the article mentioned, in particular using the fact that our fields are allowed to be double valued, one may show that the answer for  $n = \frac{1}{2}$  is that there are again two zero modes, as one would expect.

# Chapter 3

# Lattice Alice electrodynamics

In the previous chapter we examined three continuum models of AED and determined Alice flux solutions numerically. In this chapter we will introduce and investigate a lattice model of AED. We present results of numerical simulations and some (analytical) approximations of a compact  $U(1) \times \mathbb{Z}_2$  lattice gauge theory, including an extra bare mass term for Alice fluxes. The subtle interplay between Alice fluxes and (Cheshire) magnetic charges is analyzed. We determine the phase diagram and some characteristics of the model in three and four dimensions. The results of the numerical simulations in various regimes of the parameter space of the model compare well with some analytic approximations. This chapter is mainly based on [71].

The chapter is organized as follows. We start with a brief introduction of lattice gauge theory. In section 3.2 we specify the lattice AED model in detail. In section 3.3 we give the numerical results we obtained for the phase diagrams of the model in dimensions three and four and in section 3.4 we present some analytic approximations related to the phase diagram and other measurable quantities. In the final section we summarize the results and conclude.

## 3.1 A brief introduction to lattice gauge theory

In this section we will briefly introduce lattice gauge theory. for a more thorough introduction we refer to [51, 52]. As is well known most quantum field theories need regularization. The possibility we will focus on is a lattice regularization. There one assumes that space-time can be represented by a lattice. An obvious drawback of this regularization is the breaking of the Lorentz symmetry, but a major advantage is that in this form some questions in the theory can be handled non-perturbatively.

A simple way to introduce lattice gauge theory is to focus on the parallel transporter. In the continuum the parallel transporter,  $U(C_{xy})$ , along a curve,  $C_{xy}$ , from  $y$  to  $x$  is

defined by the path-ordered product:

$$U(C_{xy}) = P \exp \left( -i \int_{C_{xy}} dz_\mu A_\mu(z) \right) \quad . \quad (3.1)$$

where  $A_\mu(z)$  is the gauge field.

Let us look at the parallel transporter of a square path in the  $(\mu, \nu)$ -plane with sides of length  $a$ ,  $C_{\mu\nu,a}(x)$ . We divide the path in four straight segments of length  $a$  and assume the gauge field to be constant along each segment. To lowest order in  $a$  this gives:

$$U(C_{\mu\nu,a}(x)) = \exp [i (a^2 F_{\mu\nu} + O(a^3))] \quad , \quad (3.2)$$

where we have used the discretized partial derivative.

To lowest order in  $a$  the real part of the trace of such a closed path is equal to:

$$\Re(\text{Tr}\{U(C_{\mu\nu,a}(x))\}) = 1 - \frac{a^4}{2} \text{Tr}\left\{(F_{\mu\nu})^2\right\} + \dots \quad , \quad (3.3)$$

with no summation over  $\mu$  and  $\nu$  and the trace normalized such that  $\text{Tr}(\mathbb{I}) = 1$ .

This is exactly the structure one can use to construct a gauge invariant action for gauge fields on a lattice which in the naive continuum limit reduces to the continuum action for the gauge fields, up to an irrelevant constant.

A cubic lattice can obviously be build up from these type of minimal square paths, where  $a$  is the lattice distance. Summing over all these minimal square paths of the cubic lattice represents the space-time integral and the summation over  $\mu$  and  $\nu$  in the continuum limit. This is a simple and straightforward way to construct a gauge invariant action for a gauge theory on a lattice with the desired naive continuum limit.

In lattice gauge theories it is typically much more convenient to work in terms of the  $U$ -fields instead of the  $A$ -fields, which are of course related. The  $U$ -fields can be thought of as directed variables living on the links of the lattice, the link variables. The lattice action in terms of the link variables, the well known Wilson action [53], is given by:

$$S = \frac{1}{g^2} \sum_p \Re \left( \text{Tr} \left\{ \left( U_1 U_2 U_3^\dagger U_4^\dagger \right)_p \right\} \right) \quad (3.4)$$

$$= \frac{1}{g^2} \sum_p \Re(\text{Tr}\{U_p\}) \quad , \quad (3.5)$$

where  $U_p = U(C_{\mu\nu,a}(x))$  and the sum over  $p$  represents the sum over all minimal square paths, the plaquettes, and we have put  $a = 1$ .

In the next section we will find that lattice Alice electrodynamics is very similar to  $U(1)$  lattice gauge theory. To get some understanding of  $U(1)$  lattice gauge theory we will go into some relevant details of this theory.

### 3.1. A brief introduction to lattice gauge theory

As  $U(1)$  gauge theory is an abelian gauge theory there is no need for the trace in the action. In fact for  $U(1)$  gauge theory the lattice action becomes<sup>1</sup>:

$$S = -\frac{1}{g^2} \sum_p \cos(F_p) \quad . \quad (3.6)$$

As lattice calculations are typically done in a Euclidean space-time instead of on a Minkovskian space-time the action obtains a minus sign through the Wick rotation. One of the important and interesting features of this lattice regularization is that it allows for magnetic monopoles. In the following we will try to make this clear.

It is important to note that the action density due to the field strength only depends on the field strength modulo  $2\pi$ . We may write:

$$F_p = F_{\mu\nu}(x) = F_{\mu\nu}^{mod}(x) + 2\pi\tilde{D}_{\mu\nu}(x) \quad . \quad (3.7)$$

with  $F_{\mu\nu}(x) \bmod 2\pi \equiv F_{\mu\nu}^{mod}(x) \in \langle -\pi, \pi \rangle$ ,  $\tilde{D}_{\mu\nu}(x) \in \mathbb{Z}$  and  $\tilde{D}_{\mu\nu}(x) = -\tilde{D}_{\nu\mu}(x)$ . The integer field  $\tilde{D}$  has no effect on the action density as the action density has a period of  $2\pi$ . Thus we have:

$$S = -\frac{1}{g^2} \sum_p \cos(F_p) = -\frac{1}{g^2} \sum_p \cos(F_p^{mod}) \quad . \quad (3.8)$$

Although there is a Bianchi identity for  $F_{\mu\nu}(x)$  the splitting of the field strength into a physical and a 'redundant' term allows for a magnetic monopole current of the physical field. For the physical field strength  $F_{\mu\nu}^{mod}(x)$  the possibly nonzero monopole current is given by:

$$\partial_\mu \tilde{F}_{\mu\nu}^{mod}(x) = 2\pi k_\nu(x) \quad , \quad (3.9)$$

with

$$k_\nu(x) = \partial_\mu D_{\mu\nu}(x) \quad , \quad (3.10)$$

where  $D_{\mu\nu}(x) = \frac{1}{2}\epsilon_{\mu\nu\rho\sigma}\tilde{D}_{\rho\sigma}(x)$  and  $\tilde{F}_{\mu\nu}^{mod}(x) = \frac{1}{2}\epsilon_{\mu\nu\rho\sigma}F_{\rho\sigma}^{mod}(x)$ .

The integer field  $D_{\mu\nu}(x)$  is identified as the Dirac-sheet and it is this field which is used in locating magnetic monopoles in a specific configuration. Obviously if out of any volume more (or less) Dirac strings enter than leave there is a net magnetic charge inside this volume. The magnetic charges live inside the unit-cells of the lattice or more specifically they live on the dual lattice.

We end this short introduction to lattice gauge theory with a remark on the possible charges of the magnetic monopoles. A direct consequence of the fact that  $F_{\mu\nu}^{mod}(x) \in \langle -\pi, \pi \rangle$  is that the magnetic charge/current within a unit-cell can only have some quantized values.

$$k_\mu(x) = 0, \pm 1, \pm 2 \quad . \quad (3.11)$$

---

<sup>1</sup>We do note that this is not the only way to put compact  $U(1)$  gauge theory on a lattice and that it is also possible to have a non-compact  $U(1)$  lattice gauge theory.

## 3.2 Lattice Alice electrodynamics

In this section we introduce the specific Lattice Alice ElectroDynamics (LAED) model we will study. First we explain the different terms that appear in the action and then we discuss how magnetic monopoles and instantons are realized and can be measured in this model. Finally we say a few things about the computational implementation of the model.

### 3.2.1 The action

Alice phases can be generated by spontaneously breaking  $SU(2)$  to  $U(1) \times \mathbb{Z}_2$ . In this case it is clear that Alice loops, monopoles and Cheshire charges may arise as regular classical finite energy solutions. In the study presented in this chapter we restrict ourselves to compact  $U(1) \times \mathbb{Z}_2$  gauge theory with an extra bare mass term for the Alice fluxes. Our lattice formulation of the theory allows for the formation of Alice fluxes and magnetic monopoles<sup>2</sup>. The action we will use is given by:

$$S = \frac{1}{g^2} \sum_p \left\{ -\Re \left( \text{Tr} \left\{ (U_1 U_2 U_3^\dagger U_4^\dagger)_p \right\} \right) + m_f (P_f)_p \right\} . \quad (3.12)$$

The first part represents the normal Wilson [53] plaquette action for the gauge theory, which we introduced in the previous section. The second term is the extra bare mass term for the  $\mathbb{Z}_2$  fluxes in the model.  $P_f$  is a functional of the  $\mathbb{Z}_2$  degrees of freedom which, when evaluated on a plaquette, equals one if the plaquette is pierced by a  $\mathbb{Z}_2$  flux, and equals zero if not. The parameter  $m_f$  is the extra bare mass (in three dimensions) or tension (in four dimensions) for the Alice flux.

In principle one can also add an extra bare monopole mass term to the action. We have refrained from doing so because it is computationally much more involved and because we can realize all four phases in the model without this term (see table 3.1). To define suitable link variables for LAED we use the fact that compact  $U(1) \times \mathbb{Z}_2$  can be conveniently embedded in  $SU(2)$  as follows:

$$U_\nu(x) = e^{iA_\nu(x)\tau_3} \tau_1^{a_\nu(x)} . \quad (3.13)$$

with  $a_\nu(x) \in \{0, 1\}$  and  $A_\nu(x) \in \langle -\pi, \pi \rangle$ .

Thus  $a_\nu$  represents the  $\mathbb{Z}_2$  gauge variable and  $A_\nu$  the compact  $U(1)$  gauge variable of the theory. We say that, if  $a_\nu(x) = 1$  a  $\mathbb{Z}_2$ -sheet in 3D, or a  $\mathbb{Z}_2$ -volume in 4D, crosses the link, implying that the  $\mathbb{Z}_2$ -sheets live on the dual lattice. These  $\mathbb{Z}_2$ -sheets can, of course, be moved around by local  $\mathbb{Z}_2$  gauge transformations. A gauge transformation of the links is given by:

$$U_\nu(x) \rightarrow \Omega(x) U_\nu(x) \Omega(x + \hat{\nu})^\dagger , \quad (3.14)$$

<sup>2</sup>It also allows for the formation of Cheshire charges, but their non-locality makes them hard to detect, see section 3.2.2

with  $\Omega(x) = e^{i\Sigma(x)\tau_3}\tau_1^{\sigma(x)}$ , where  $\sigma(x) \in \{0, 1\}$  and  $\Sigma(x) \in \langle -\pi, \pi \rangle$ .

The boundaries of the  $\mathbb{Z}_2$ -sheets, however, cannot be moved around by local  $\mathbb{Z}_2$  gauge transformations, this in analogy with the endpoints of Dirac strings (being magnetic monopoles) in the compact  $U(1)$  gauge theory. This is exactly what one should expect, since the boundaries of the  $\mathbb{Z}_2$ -sheets are closed Alice flux<sup>3</sup> loops, which are physical objects carrying energy. Bearing this in mind it is easy to locate the Alice fluxes, namely by just counting the number of  $\mathbb{Z}_2$ -sheets crossing the links of a plaquette. If an even number of  $\mathbb{Z}_2$ -sheets crosses the links of the plaquette, then no Alice flux pierces the plaquette, but if an odd number does, then that means that an Alice flux does pierce the plaquette. This observation allows one to define the  $P_f$  operator, which applied to a plaquette measures the presence of an Alice flux,

$$P_f = \frac{1}{2} \left( 1 - (-1)^{\sum_{i=1}^4 a_i} \right) \quad , \quad (3.15)$$

where the four  $a_i$  summed over belong to links  $U_1, U_2, U_3$  and  $U_4$ , bounding a single plaquette. Equations (3.12), (3.13) and (3.15) define our LAED model.

### 3.2.2 The problem of locating monopoles (or instantons)

In this model of LAED in four dimensions, there are magnetic monopoles, in three dimensions these appear as instantons. There are a few intricacies in detecting them compared to the usual compact  $U(1)$  lattice gauge theory. In this section we will explain under what circumstances and how we can detect a monopole/instanton in LAED. As our model of LAED has a lot of similarities with compact  $U(1)$  lattice gauge theory, we try to use these similarities in determining the monopole content of a configuration.

Let us first consider the case that there are no Alice fluxes present. Clearly, this corresponds to the limit of an infinitely large mass,  $m_f$ , for the flux. In this case there may still be closed  $\mathbb{Z}_2$  surfaces, but these surfaces are not physical and can be moved around by making suitable local  $\mathbb{Z}_2$  transformations. Suppose we want to determine the monopole content of a specific cube in such a configuration. We would like to see if a Dirac string ends in the cube, just as one does for compact  $U(1)$  lattice gauge theory. We distinguish two cases, the first where no  $\mathbb{Z}_2$ -sheet crosses the cube of interest and the second where one or more  $\mathbb{Z}_2$ -sheets do cross the cube.

In the first case we determine the monopole content of the cube just as in compact  $U(1)$  lattice gauge theory. In the second case we should construct a new or more general definition due to the presence of the  $\mathbb{Z}_2$ -sheets. Bearing in mind that a monopole is a physical object which cannot be moved around by gauge transformations, one may use local  $\mathbb{Z}_2$  gauge transformations to gauge the  $\mathbb{Z}_2$ -sheets away from the cube of interest. After this procedure we can again determine the monopole content by the methods of compact  $U(1)$  lattice gauge theory.

<sup>3</sup>To avoid confusion we note that in the  $\mathbb{Z}_n$  literature one typically calls these objects vortices instead of fluxes.

$\mathbb{Z}_2$ -sheets can be gauged out of the cube of interest in several different ways. One would expect this not to make any difference to the outcome of the measurement of the monopole charge of the cube of interest, but it does! As we mentioned in the chapter 1, monopoles of opposite sign belong to the same topological class. For the measurement of the monopole charge of a single cube this means that one cannot distinguish between positive and negative charges. To see that this is the case, let us consider a cube which is not intersected by a  $\mathbb{Z}_2$ -sheet. If one performs a 'global'  $\mathbb{Z}_2$  gauge transformation to all the links of this cube, this has the same effect as pulling a  $\mathbb{Z}_2$ -sheet through the cube; all the  $U(1)$  degrees of freedom change sign, since  $\tau_1 e^{iA\tau_3} \tau_1 = e^{-iA\tau_3}$ , see equation (3.14). Obviously this means that the outcome of the measurement of the magnetic charge of the cube changes sign. Hence only the absolute value of the magnetic charge is a locally gauge invariant quantity, i.e., an observable.

Next we consider the situation where fluxes are present. Now we have two different type of cubes, cubes which are pierced by a flux and cubes which are not. The latter are obviously equivalent to the cubes we just discussed. Thus at this point we may restrict our considerations to cubes which are pierced by fluxes. The statement is, that for a cube which is pierced by a flux, the notion of a gauge invariant magnetic charge breaks down completely. Let us explain why this is the case.

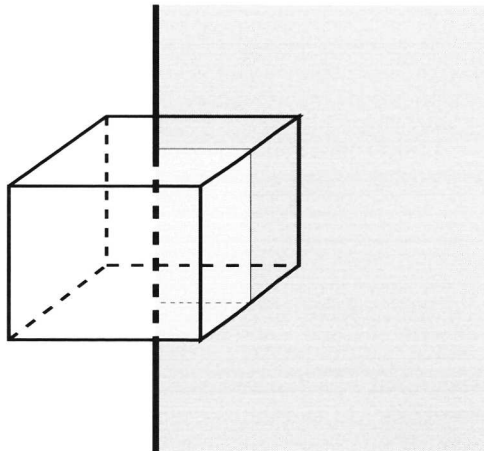


Figure 3.1: A cube that is pierced by a flux which is the boundary of a  $\mathbb{Z}_2$ -sheet.

If an Alice flux pierces through a cube, it is obviously not possible to gauge the  $\mathbb{Z}_2$ -sheet out of the cube. In figure 3.1 we depicted a cube pierced by a flux and the  $\mathbb{Z}_2$ -sheet connected to the flux. If one tries to define Dirac strings through the plaquettes bounding the cube of interest one gets into all sorts of trouble. For the plaquettes where no flux pierces through one can up to a sign determine the (real magnetic flux through the) Dirac string. This sign problem seems to be a minor one, as it appears to be for the monopole charge itself, but that is not true, because there

is a separate sign ambiguity for the Dirac strings through each of the plaquettes and not just a single overall sign, as was the case for a cube not pierced by a flux. This means that in such a cube, even the absolute value of the net magnetic charge is not an invariant quantity.

Yet another problem arises if one wants to define the Dirac string through a plaquette which is pierced by a flux, because an odd number of  $\mathbb{Z}_2$ -sheets cross the links bounding the plaquette. The problem basically follows directly from Alice electrodynamics itself, where if one sweeps a  $\mathbb{Z}_2$ -sheet through a  $U(1)$  link field, this will change sign. So even the sign of the individual  $U(1)$  link variables is not defined uniquely on a plaquette which is intersected by an odd number of sheets, *even if one looks only at that particular plaquette*. This obstruction to defining the magnetic flux through such a plaquette, is just a manifestation of what is generally called the obstruction to globally define a  $U(1)$  charge in the presence of an Alice flux in Alice electrodynamics.

However not all is lost. The previous discussion only shows that it is impossible to determine the magnetic charge of a cube, or more general of a volume, whose bounding surface is pierced by a flux. There is however no problem in determining the magnetic charge of a volume which contains a loop of flux not crossing the boundary.

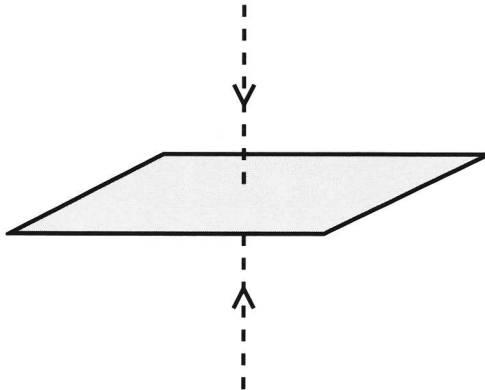


Figure 3.2: This figure shows an Alice loop with its  $\mathbb{Z}_2$ -sheet. The  $\mathbb{Z}_2$ -sheet is pierced by a Dirac string, which changes sign/direction once it passes the  $\mathbb{Z}_2$ -sheet. In this configuration the Alice loop carries a magnetic Cheshire charge.

To see this consider the configuration given in figure 3.2. A configuration is shown of an Alice loop and a Dirac string piercing the  $\mathbb{Z}_2$ -sheet bounded by the Alice loop. This figure demonstrates, that an Alice loop configuration is capable of carrying a magnetic charge. We note that there is no Dirac string coming from the flux itself (this is actually possible and even necessary for the unit charged Alice loop). Remember that we are, for plaquettes not pierced by a flux, able to determine the Dirac string up to a sign. We also note that any attempt to measure the location of the monopole will fail. It looks like that the cube where the the Dirac string pierces the  $\mathbb{Z}_2$ -sheet does contain a magnetic charge, but as the position of the sheet is gauge dependent this is

just a gauge illusion. Yet, drawing a closed 2-surface around the loop there is a gauge invariant quantity of magnetic flux emanating from that surface, i.e., there is magnetic charge inside. This magnetic charge is present, not as a localized or even localizable quantity, but rather as a global property carried by a closed Alice loop as a whole, in which case one speaks of a magnetic “Cheshire” charge. And indeed, although one can determine the magnetic charge carried by the Alice loop as a whole, one can not assign this magnetic charge to any of the cubes inside the volume containing the loop. These nonlocalizable charges may in the continuum even be energetically favored. We will show in chapter 5 that 't Hooft-Polyakov type monopoles may decay into their Cheshire versions.

To see that a Cheshire charge configuration is physically relevant in our LAED model we briefly study a configuration of a magnetic monopole and an Alice loop. We fix the position of both objects by hand and only allow changes in the gauge variables which do not change the position of these objects. We want to show that also in LAED an Alice loop can carry a magnetic Cheshire charge. As the lattice we use has periodic boundary conditions the total magnetic monopole charge is zero, i.e., there is also an anti-monopole present. In the limit of  $g \rightarrow 0$ , the naive classical limit, and  $m_{flux} \rightarrow \infty$  one does not expect there to be any other defects present. In this limit there appear to be two possibilities: either the anti-monopole is located next to the monopole or it is absorbed by the Alice loop in the form of a Cheshire charge. The latter configuration is the one which we are interested in. In general it is a question of energetics which configuration is preferred<sup>4</sup>, and the energy of the field configuration obviously depends on the size of the Alice loop and its relative location with respect to the monopole. Now we will consider a configuration where the anti-monopole is absorbed by the Alice loop.

In this configuration the monopole and the Alice loop lie in one plane, the  $xy$  plane. The Alice loop is a square and the middle of one side is in front of the monopole. In figure 3.3 we plotted the  $z$  component of the magnetic field just above and below the plane in the dual lattice in which the configuration of the monopole and the Alice loop lies. The monopole and the Alice loop have not been plotted, but it should be clear where they are, they live on the dual  $xyz$  lattice. The plot is in the special  $\mathbb{Z}_2$  gauge, where the only  $\mathbb{Z}_2$  sheet is the minimal surface bounded by the Alice loop.

From figure 3.3 it should be clear that the Alice loop carries the magnetic charge of the anti-monopole as the  $z$  component of the magnetic field has a different sign just above/below the Alice loop than just above/below the monopole. We also checked that there were no other monopoles in the system and determined the magnetic charge of the Alice loop, the Cheshire charge. We see that also in LAED the Alice loop can carry a magnetic Cheshire charge and it makes clear that one can not define the position of a magnetic charge on an Alice string.

We conclude, that once we enter a phase where there are very many Alice fluxes around, detecting and localizing magnetic charge becomes a hairy business. The only useful thing one may still do, is to measure the fraction of monopole carrying cubes of

---

<sup>4</sup>If we had an extra bare mass term for the monopole we could simply send it to infinity to force the anti-monopole to be absorbed by the Alice loop

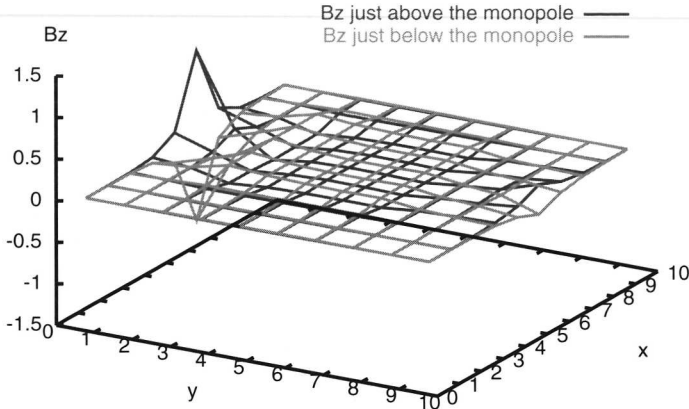


Figure 3.3: This plot shows the  $z$  component of the magnetic field just above and just below the plane in which the monopole and Alice loop lie. It clearly shows that the Alice loop carries a magnetic Cheshire charge.

the number of cubes *not* pierced by an Alice flux. In view of these observations, when in the following we talk about the monopole density, we mean the average absolute charge per unpierced cube and when we talk about flux density we mean the fraction of plaquettes pierced by an Alice flux, i.e.,  $\langle P_f \rangle$ , unless stated otherwise.

### 3.2.3 Implementation of the model

Although formula (3.13) suggests that we should implement LAED using (Pauli) matrices we have not done so. Instead, we exploited the fact that the structure of our  $U(1) \times \mathbb{Z}_2$  gauge theory is very close to that of the compact  $U(1)$ . The only effect of the  $\mathbb{Z}_2$  degrees of freedom is the appearance of Alice fluxes and  $\mathbb{Z}_2$ -sheets. If there are an odd number of  $a$  variables equal to one in a plaquette, then the plaquette is pierced by a  $\mathbb{Z}_2$  flux and the first term in the action is always zero irrespective of the values of the  $A$  fields. This can be understood as a consequence of the fact that the  $U(1)$  symmetry is globally frustrated in the presence of an Alice flux. If, in the contrary, there are an even or zero number of  $a$  variables equal to one in a plaquette, the  $a$  variables can be gauged away, changing only the sign of some of the  $A$  fields and the action is just the action of compact  $U(1)$ . In view of these observations, we have for our simulations used the following simple action, which is equivalent to the action of formula (3.12), but does not require any matrix calculations.

$$S = \frac{1}{g^2} \sum_p \left\{ -(1 - P_f) \cos \tilde{F} + m_f P_f \right\}_p , \quad (3.16)$$

where  $\tilde{F}$  is the  $F$  of  $U(1)$  after the  $\mathbb{Z}_2$  fields have been gauge transformed out of the plaquette, which is always possible if  $P_f = 0$ .

We have investigated this model, using a combination of a Monte Carlo method for the  $A_\nu(x)$  variables, and a heat bath method for the  $a_\nu(x)$  variables. We examined the model on a periodic hyper cubic lattice of size  $10^d$ , where  $d$  is the dimension. Although we will not go into detail on the order of the phase transitions we mention that it has been suggested [72], that the order, oddly enough, would depend on the imposed boundary conditions. Three dimensional ED has attracted a lot of attention, the last few years, due to its potential applicability to models of high  $T_c$  superconductors [73, 74, 75].

Our LAED model contains a pure compact  $U(1)$  and a  $\mathbb{Z}_2$  gauge theory in different limits of the model. In the limit of  $m_f \rightarrow \infty$  the model is equal to pure compact  $U(1)$  gauge theory. In the limit of  $g^2 \rightarrow \infty$  while keeping  $m_f/g^2$  finite the model is equal to  $\mathbb{Z}_2$  gauge theory. Before we proceed we like to mention a few things about the  $\mathbb{Z}_2$  gauge theory to avoid confusion later on. In  $\mathbb{Z}_2$  gauge theory there is only one parameter, in the  $\mathbb{Z}_2$  limit of our model this parameter is  $m_f/g^2$ . Normally, the  $\mathbb{Z}_2$  gauge theory is only studied for positive values of its parameter. However, in our situation we are also interested in the region where  $m_f/g^2$  becomes negative. In the pure  $\mathbb{Z}_2$  gauge theory the region of positive and negative values of the parameter form a mirror image of each other. Note that this mirror map is different from the usual duality that is also present in  $\mathbb{Z}_n$  type gauge theories. This mirror symmetry holds, at least, for a hyper cubic lattice, where one may map the negative coupling side on the positive side if one replaces “fluxes” by “no-fluxes” in every sense. So “no-fluxes” are the places where “no flux” pierces through a plaquette, i.e., they are the holes in the flux condensate. The model can equally well be described by either of the two objects. This mirror symmetry follows from the fact that for a hyper cubic lattice both objects, fluxes and no-fluxes, form closed loops in three dimensions and closed surfaces in four dimensions. This shows that the regions of positive values and negative values of  $m_f/g^2$  can be naively mapped onto each other. As we will show, in LAED the Alice mirror symmetry is broken by the interactions with the  $U(1)$  gauge fields for finite values of  $g^2$ .

### 3.3 The phase diagram in three and four dimensions

In this section we present various numerical results for the LAED model. Because we have two types of topological objects in the theory, which may or may not condense, one may in principle expect four phases. It is quite easy to anticipate where in the parameter space the four phases could occur, as we have indicated in table 3.1.

In figure 3.4(a) we have plotted the flux density and the monopole density in four dimensions. It is clear that various interesting transitions do occur. Using a hysteresis type of analysis we could determine the order of these transitions, and we found that all but one, are of first order. Only the transition from the phase with only Alice fluxes condensed, to the phase where both Alice fluxes and monopoles are condensed, is different. In fact, it does appear not to be a phase transition at all, but rather a crossover phenomenon, see also section 3.4.4 and the discussion in section 3.4.5.

### 3.3. The phase diagram in three and four dimensions

	$m_f$ small	$m_f$ large
$g^2$ small	Fluxes	No Condensate
$g^2$ large	Fluxes and Monopoles/ Instantons	Monopoles/ Instantons

Table 3.1: The four phases of LAED.

In figure 3.4(b) we have plotted some contours for the Alice flux and monopole densities. The curves indicate where the first order phase transitions [76, 77] take place, but also show the change of the first order monopole transition if no fluxes are condensed, to the crossover monopole transition if fluxes are condensed.

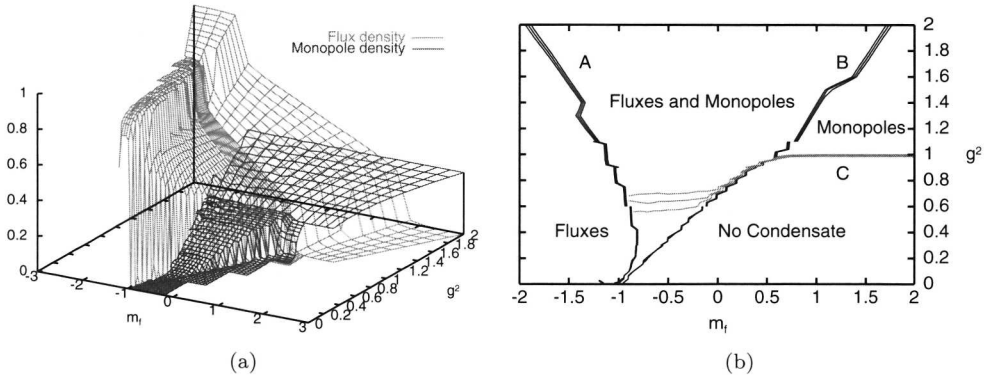


Figure 3.4:

(a): The 4-dimensional flux and the monopole densities are plotted as a function of  $m_f$  and  $g^2$ . The four different phases of table 3.1 can be clearly distinguished.

(b): A plot of some specific monopole and the Alice flux density contours in four dimensions. We identify the four phases of the model. The lines denoted  $B$  mark the transition involving the Alice fluxes, where to the left of  $B$  the fluxes are condensed. The lines  $A$  correspond to a second phase transition involving the fluxes. The lines  $C$  denote the monopole transition, notice the splitting of the height lines once the Alice fluxes are condensed.

Note that in figures 3.4(a) and 3.4(b) we have only plotted the monopole density up to the 'second' flux density transition, line A in figure 3.4(b), where the flux density jumps to about one and only very few cubes (if any) are left where no flux pierces through, making the fluctuations for the monopole measurement very large.

Though in our limited model we find all of the anticipated four phases, each characterized by some condensate, we do not find all possible transitions from one phase to another. There is apparently no transition from the phase with condensed monopoles

and no fluxes to the phase with condensed fluxes and no monopoles.

In appropriate limits of the model we recover the results for the lattice gauge theories of compact  $U(1)$  and  $\mathbb{Z}_2$  separately, consistent with equation (3.16). The pure  $U(1)$  gauge theory arises in the limit of  $m_f \rightarrow \infty$ , where the Alice fluxes are suppressed and the only feature reminiscent of the  $\mathbb{Z}_2$  part of the gauge theory are pure  $\mathbb{Z}_2$  gauge transformations, which of course do not affect any of the physics. In this limit we therefore expect only the transition corresponding to monopole condensation. The pure  $\mathbb{Z}_2$  gauge theory arises in the limit of  $g^2 \rightarrow \infty$ , while keeping  $m_f/g^2$  finite, which is usually only studied with  $m_f/g^2 \geq 0$ . We verified that the limiting behaviors of the results of our simulations are in agreement with the known results of the  $\mathbb{Z}_2$  and  $U(1)$  gauge theories [78, 79, 80, 81], see also [82] and references therein.

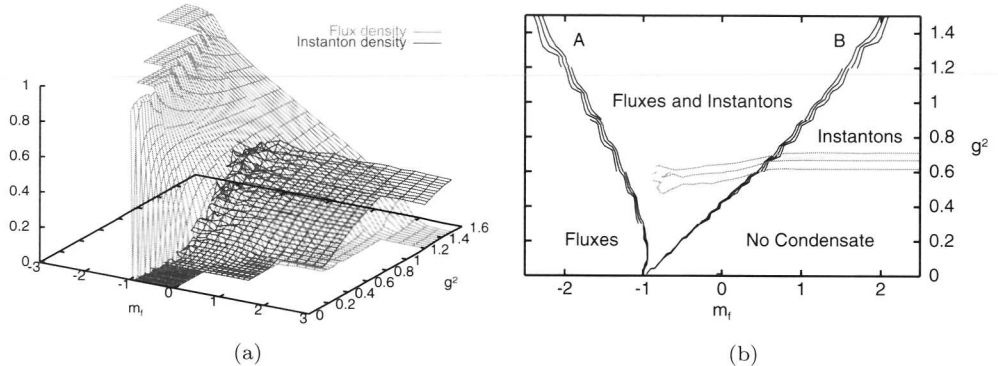


Figure 3.5:

(a): The 3-dimensional flux and instanton densities are plotted as a function of  $m_f$  and  $g^2$ . The four different phases of table 3.1 are clearly distinguishable.

(b): In this figure we plotted some specific height lines of the instanton and the Alice flux density in three dimensions. We identify the four phases of the model. The lines  $B$  correspond to the condensation line of the Alice fluxes, to the left of it the fluxes are condensed. The lines  $A$  correspond to a second phase transition involving the fluxes Line  $A$ . In comparison with figure 3.4(b) there is no line  $C$ . In three dimensions the instanton condensation is always a crossover.

In figure 3.5(a) we plotted the results for the instanton and Alice flux density in three dimensions. Also in this case we encounter all four phases of the theory, but the transitions are of different order. The instanton condensation is always a crossover and the flux condensation appears to be of second order, which it certainly should be in the  $\mathbb{Z}_2$  gauge theory limit [79]. We did not determine the order of the flux condensation for small  $g^2$ .

In figure 3.5(a) the transition for small values of  $g^2$  appears to become a first order phase transition, but this is mainly due to the fact that we use  $m_f$  and  $g^2$  to parameterize the model, whereas the, in some sense more natural, choice of  $(m_f + 1)/g^2$  and  $1/g^2$  could give a different picture, which is also true for the four dimensional case. We will come back to this point in section 3.4.5.

In figure 3.5(b) we, just as in figure 3.4(b), plotted specific height lines of the instanton

and Alice flux density. These lines show the location of the Alice flux phase transitions and divide the parameter space up in the four different regions linked to the phases. Again in the  $U(1)$  and  $\mathbb{Z}_2$  limit we recover the results of these pure gauge theories separately.

In three dimensions the flux density becomes very high before the second phase transition of the fluxes, line A in figure 3.5(b), occurs and consequently the fluctuations of the instanton density measurements become very large in a larger region.

## 3.4 Analytic and other approximations

LAED contains both pure compact  $U(1)$  and  $\mathbb{Z}_2$  gauge theory. As both of these theories have been studied thoroughly over the years, our aim is not to make estimates for these models, but rather to treat their (numerical) results as known and focus on the interaction of these two models in LAED. To this end we give (analytical) approximations of some characteristic quantities of the model. We subsequently discuss the average action of unpierced plaquettes<sup>5</sup>, the flux condensation lines, the contours of constant flux density in the region between the two flux condensation lines  $A$  and  $B$  and the monopole/instanton density. We conclude this section with a brief discussion of the approximations we made.

### 3.4.1 The average action of unpierced plaquettes

To approximate the average action per unpierced plaquette,  $-\langle \cos \tilde{F} \rangle$ , we split the parameter space of the model into two regions, a region where the  $\mathbb{Z}_2$  fluxes do not condense and the region where they do.

In the region where the  $\mathbb{Z}_2$  fluxes do not condense we approximate the theory by a pure  $U(1)$  gauge theory (in the present context considered to be given) and  $-\langle \cos \tilde{F} \rangle$  is approximated accordingly, i.e., we ignore the effect which the few Alice fluxes have, that may be present. In the region where the fluxes do condense and the flux density is large, we approximate the average action of unpierced plaquettes by the average action of a single plaquette. The  $U(1)$  link variables are irrelevant to plaquettes pierced by a flux, as follows from formula (3.16). In the limit of a high flux density the plaquettes which are not pierced by a flux become isolated in the sense that the value of the  $U(1)$  degrees of freedom have almost no effect on the surrounding plaquettes. Thus we can approximate  $-\langle \cos \tilde{F} \rangle$  in the condensed phase by:

$$\langle \cos \tilde{F} \rangle \approx \frac{\int_0^{2\pi} \frac{d\tilde{F}}{2\pi} \cos \tilde{F} e^{\frac{\cos \tilde{F}}{g^2}}}{\int_0^{2\pi} \frac{d\tilde{F}}{2\pi} e^{\frac{\cos \tilde{F}}{g^2}}} = \frac{I_1\left(\frac{1}{g^2}\right)}{I_0\left(\frac{1}{g^2}\right)} . \quad (3.17)$$

where the functions  $I_0$  and  $I_1$  are modified Bessel functions.

---

<sup>5</sup>The total average action per plaquette is easily determined by this result and the flux density.

The difference between these two limits, the single plaquette and the  $U(1)$  limit, vanishes for large  $g^2$ . In four dimensions, for small  $g^2$ , the fraction of pierced fluxes typically is very large in the flux condensed phase. Thus we may expect that the two limits describe the model for any value of  $g^2$ . In three dimensions there is no such jump in the flux density and we expect an intermediate region, for small  $g^2$ , to be present.

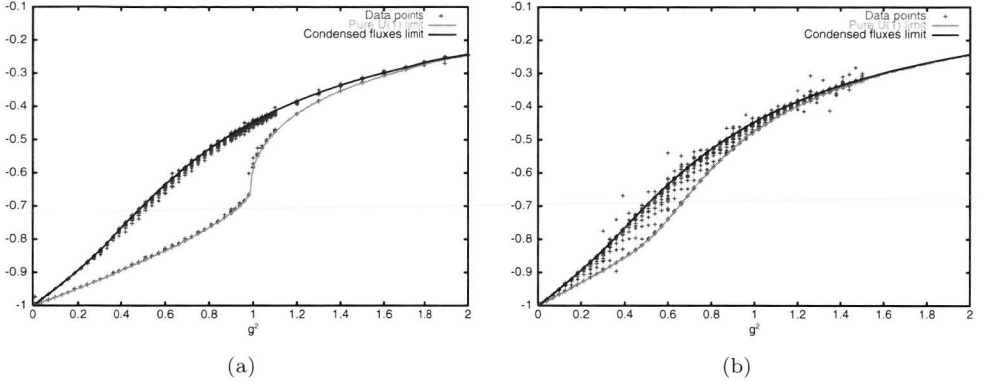


Figure 3.6:

(a): The average plaquette action  $-\langle \cos \tilde{F} \rangle$  in four dimensions. All the data points, i.e., including those corresponding to different values of  $m_f$  and  $g^2$ , lie either on the pure  $U(1)$  line or (almost) on the approximation for condensed fluxes phase. The division is so clear due to the strong first order  $\mathbb{Z}_2$  transition, i.e., in the flux condensed phase the flux density is fairly high for small  $g^2$ .

(b): The average plaquette action  $-\langle \cos \tilde{F} \rangle$  in three dimensions. Here the transition from the one region to the other is much more smooth, because the  $\mathbb{Z}_2$  transition in three dimensions is only of second order, also the pure  $U(1)$  result deviates much less from the flux condensed limit. The points outside the region between the two limits are points where the flux density is very high, implying that the fluctuations become very large.

In figure 3.6(a) we plotted  $-\langle \cos \tilde{F} \rangle$  as a function of  $g^2$  in four dimensions. We see that the data splits up into two lines. Part of the data points lie on the pure  $U(1)$  line while the other part lies (almost) on the single plaquette line. This strict separation of the data points in these two sets is due to the strong first order behavior of the  $\mathbb{Z}_2$  flux condensation for small  $g^2$ . We see that each point is very well described by either the first or the second approximation indeed.

In figure 3.6(b) we plotted  $-\langle \cos \tilde{F} \rangle$  as a function of  $g^2$  in three dimensions. The two approximations now generate the boundaries between which the data points lie. The fact that there is no clear division of the data in two sets in three dimensions, is due the  $\mathbb{Z}_2$  phase transition being of second order. The flux density grows gradually across the transition region. That points appear also outside the region bounded by the two approximations is due to very large fluctuations when the flux density is high, i.e., when there is a small number of unpierced plaquettes.

### 3.4.2 The condensation lines of the Alice fluxes

To approximate the location of the Alice flux condensation lines in the parameter space of the model we make use of an action,  $S$ , versus entropy,  $Ent$ , argument. The weight factor of a configuration is determined by  $e^{Ent-S}$ . The important quantity is the relative weight factor,  $e^{\Delta Ent - \Delta S}$ , between configurations. Assuming that  $Ent - S$  of the object that condenses is additive with respect to the so called background, we find that  $\Delta Ent - \Delta S = Ent_{object} - S_{object}$ . Now typically the location of the critical point can be approximated by  $Ent_{object} = S_{object}$ .

As we saw in figures 3.4(b) and 3.5(b) there are two flux condensation lines in LAED. In the  $\mathbb{Z}_2$  gauge theory these are just each others mirror image. For finite  $g^2$  this symmetry between the two condensation lines is broken due to the interactions with the  $U(1)$  fields. We may still compare them, in the sense that at the first transition line, B, the fluxes condense, while at the other, A, the “no-fluxes” condense. The coupling between the  $\mathbb{Z}_2$  and the  $U(1)$  fields manifests itself as follows: if a flux is created then a piece of the  $U(1)$  fields is “eaten” away in the sense that the  $U(1)$  fields become irrelevant because they are projected out and do not affect the action of the plaquettes involved. This is an effect that we have to take into account, and as we shall see, this can be done very accurately for the no-flux condensation line, but only partially for the flux condensation line.

#### The four dimensional case:

First we determine the transition line of the no-flux condensate with the help of the action versus entropy argument. When a no-loop (i.e., a loop of no-flux) is created, the plaquettes through which it pierces carry a  $U(1)$  action. We determine the no-flux density and will assume that the contributions of the  $U(1)$  field of a plaquette are independent of each other. We then approximate the location of the condensation line by assuming that the average over the  $U(1)$  degrees of freedom in the relative weight factor for a plaquette is equal to one. This gives us:

$$\ln \left( \int_0^{2\pi} \frac{d\tilde{F}}{2\pi} e^{c_{nl} + \frac{m_f}{g^2} + \frac{\cos \tilde{F}}{g^2}} \right) = 0 \quad . \quad (3.18)$$

where  $c_{nl}$  denotes the given value of the condensation point of the no-loops in the pure  $\mathbb{Z}_2$  gauge theory limit and we used  $\Delta S = -\frac{m_f}{g^2} - \frac{\cos \tilde{F}}{g^2}$  per plaquette. We note that the value of  $c_{nl}$  equals to minus the value for the loops,  $c_l$ , as follows from the mirror symmetry of the  $\mathbb{Z}_2$  gauge theory, as we discussed at the end of section 3.2.3. From now on we will adopt the notation  $c_{nl} = -c_{4D} (\equiv -c_l)$ .

Formula (3.18) leads to the following equation for the transition curve in the  $(m_f, g^2)$  plane:

$$m_f = -g^2 c_{4D} - g^2 \ln I_0 \left( \frac{1}{g^2} \right) \quad . \quad (3.19)$$

As can be seen in figure 3.7(a) the approximation of the no-loop condensation line is very good.

We can try to do the same for the Alice loop condensation line. We use again  $Ent_{object} = S_{object}$ , but are now not able to include all contributions. The entropy and action contribution of the loop are clear, one thing that changes in equation (3.19) is the sign in front of the first term on the r.h.s.. The problem is a reliable estimate of the  $U(1)$  contribution. Obviously we may no longer assume that the  $U(1)$  contribution of each plaquette is independent. On the other hand it is known that the correlation length decreases exponentially in the confining phase, which implies that we should expect this approximation to still work if  $g^2 > g_c^2 \approx 1$ .

We can also approximate the Alice loop condensation line in a slightly different way, where we use the contribution to the action of the  $U(1)$  fields as given by the pure  $U(1)$  theory and ignore the change in the entropy due to the  $U(1)$  fields. For the action we then take:

$$S_{object} = \left( \frac{m_f}{g^2} + \frac{\langle \cos \tilde{F} \rangle}{g^2} \right) . \quad (3.20)$$

with  $\langle \cos \tilde{F} \rangle$  the average of  $\cos \tilde{F}$  for given  $g^2$  and is equal to  $\langle \cos F \rangle$  of pure  $U(1)$  gauge theory as follows from the previous section (which is evaluated numerically and in the present context considered as given). This leads to the following approximation for the position of the condensation line for the loops:

$$m_f = g^2 c_{4D} - \langle \cos \tilde{F} \rangle . \quad (3.21)$$

We note that in the pure  $\mathbb{Z}_2$  limit, the second term on the r.h.s. of equations (3.19) and (3.21) becomes zero and that  $c_{4D}$  and its three dimensional analogue  $c_{3D}$  follow from pure  $\mathbb{Z}_2$  gauge theory results as mentioned before. In fact, they are even known analytically [78]. In the limit of  $g^2 \rightarrow 0$  the only state that is allowed, is the global minimum, which means that the condensation lines need to go to  $m_f = -1$  for  $g^2 \rightarrow 0$ . This is true for both approximations.

In figure 3.7(a) we have plotted the approximations for the condensation lines in four dimensions and some specific height lines, which characterize the position of the phase transitions. We see that the approximation of the condensation of the no-loops is very good. For  $g^2 > 1$  the same method works also very well for the loop condensation line. The other approximation for the loop condensation line does not work as well, but we qualitatively understand why.

### The three dimensional case:

In three dimensions we follow the same strategy. We repeat the arguments given for the four dimensional case, leading to exactly the same equations (3.19) and (3.21), where we only have to replace the four dimensional quantities by their three dimensional counterparts. In particular  $c_{4D}$  is replaced by  $c_{3D}$  and  $\langle \cos \tilde{F} \rangle_{4D}$  is replaced by  $\langle \cos \tilde{F} \rangle_{3D}$ .

In figure 3.7(b) we plotted the resulting condensation lines for the three dimensional theory. The plot shows some specific height lines which characterize the phase transitions as well as the approximations for the lines where the phase transitions should occur. Again we find that the approximation for the no-flux condensation line is very

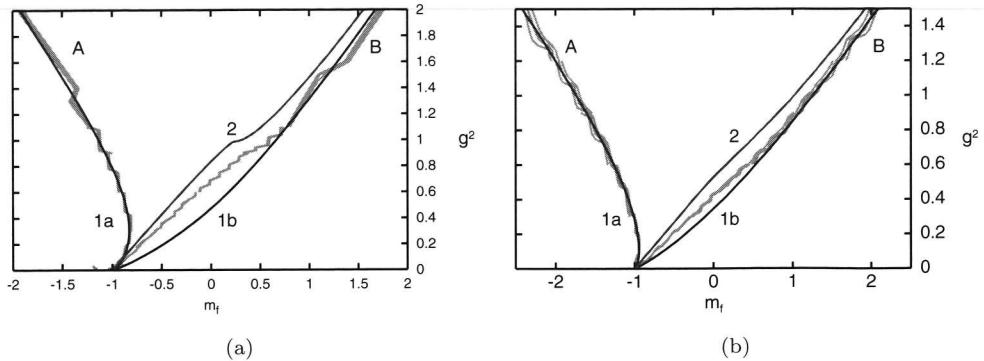


Figure 3.7:

(a): A plot of the phase transition lines, A and B, in four dimensions and of the approximations we made. The approximation for the no-loop condensation line, 1a, is very good. For  $g^2 > 1$  the same approximation works also very well for the loop condensation line, 1b, while the other approximation, 2, deviates in a qualitatively expected way from the loop condensation line.

(b): A plot of the phase transition lines, A and B, in three dimensions and of the approximations we made. The approximation for the no-flux condensation line, 1a, is very good. For  $g^2 > 0.6$  the same approximation works also very well for the flux condensation line, 1b, while the other approximation, 2, deviates in an expected way from the flux condensation line.

good. The approximation of the analogue of equation (3.19) is very good for larger values of  $g^2$ , whereas the deviation of the other approximation to the flux condensation line is qualitatively understood.

### 3.4.3 Contours of constant flux density

In this subsection we will approximate the flux density in the region between the two flux condensation lines, by assuming that in this region the correlation lengths of both fields are zero, so that it suffices to look at the single plaquette.

This means that we get the same answer for the three and four dimensional case. The fraction of plaquettes being pierced by an Alice flux,  $\rho_f$ , can be approximated by:

$$\rho_f \approx \frac{e^{ent_f - S_f}}{e^{ent_f - S_f} + e^{ent_{nf}} \int_0^{2\pi} \frac{d\tilde{F}}{2\pi} e^{-S_{\tilde{F}}} } . \quad (3.22)$$

Using  $ent_f = ent_{nf}$  and  $S_f = \frac{m_f}{g^2}$  this gives:

$$m_f = g^2 \ln \left( \frac{1 - \rho_f}{\rho_f} \right) - g^2 \ln \left( \int_0^{2\pi} \frac{d\tilde{F}}{2\pi} e^{-S_{\tilde{F}}} \right) , \quad (3.23)$$

which leads to:

$$m_f = g^2 \ln \left( \frac{1 - \rho_f}{\rho_f} \right) - g^2 \ln \left( I_0 \left( \frac{1}{g^2} \right) \right) . \quad (3.24)$$

Note that in the limit  $g^2 \rightarrow 0$  we find that all the height lines meet at  $m_f = -1$ , just as one should expect, whereas in the  $\mathbb{Z}_2$  limit one obtains that  $\frac{m_f}{g^2} = \ln\left(\frac{1-\rho_f}{\rho_f}\right)$ .

In four dimensions, within the region of the two condensation lines, which is the region we are probing, our approximation works very well, see figure 3.8(a). In three dimensions the approximation does not work in the whole region, but works very well between the height lines 0.7 and 0.3, see figure 3.8(b).

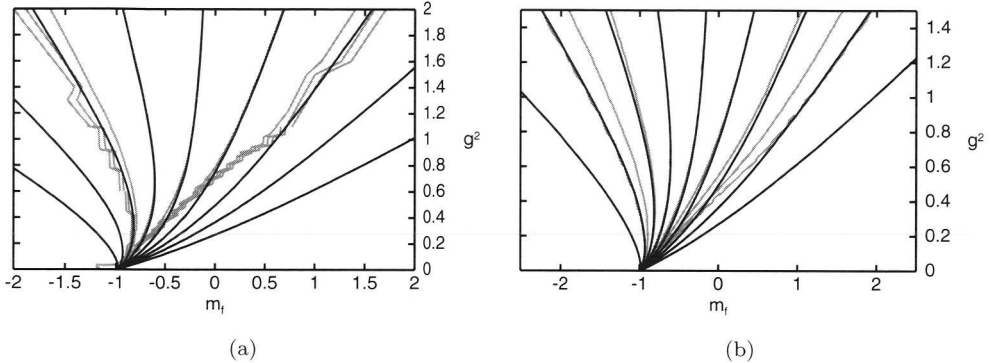


Figure 3.8:

(a): Contour lines of the flux density in four dimensions and their approximations. We plotted from, left to right, the height lines:  $0.9, 0.8, \dots, 0.2, 0.1$ . The approximations for the height lines  $0.6, \dots, 0.4$  are perfect up to the point where they reach the condensation line.

(b): Contour lines of the flux density in three dimensions and their approximations. We plotted from, left to right, the height lines:  $0.9, 0.8, \dots, 0.2, 0.1$ . The approximations for the height lines  $0.7, \dots, 0.3$  are very good up to the point where they reach the condensation line.

The approximation of the flux density, equation (3.24), can be split into two parts. The first term on the right hand side is due to the  $\mathbb{Z}_2$  degrees of freedom. In the  $\mathbb{Z}_2$  limit this term can be compared with pure  $\mathbb{Z}_2$  gauge theory, which we did not use as input in this estimate. The second term on the right hand side is due to the  $U(1)$  degrees of freedom. Moving away from the 0.5 height line makes the approximation of  $\mathbb{Z}_2$  term less good while moving from the 0.9 height line to the 0.1 height line makes the  $U(1)$  term less good. The validity of the  $U(1)$  term can be seen by fitting the  $\mathbb{Z}_2$  part of the approximation with results from pure  $\mathbb{Z}_2$  gauge theory. This gives a perfect fit for all values  $g^2$  for a high flux density, but as one expects, fails in the region of low flux density and small  $g^2$ .

### 3.4.4 The monopole/instanton density

In this subsection we will approximate the monopole/instanton density. In the phase where the Alice fluxes do not condense the monopole condensation line and height lines are easily understood. In this phase there are almost no fluxes, and ignoring these the model becomes a pure  $U(1)$  theory and one expects the monopole density to behave accordingly, allowing us to use the known numerical results.

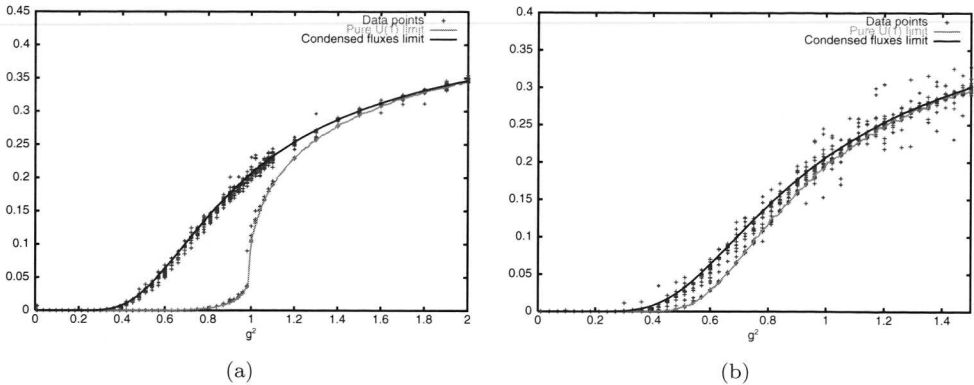


Figure 3.9:

(a): A plot of the monopole density. Just as in figure 3.6(a) all the data points, i.e., including those for different values of  $m_f$  and  $g^2$ , perfectly match the two different approximations. The monopole density is or equal to the pure  $U(1)$  monopole density or is (almost) equal to the approximation for the condensed fluxes phase.

(b): A plot of the instanton density. The instanton density lies between the two different approximations. That the data does not jump from one line to the other line is due to the fact that the  $\mathbb{Z}_2$  transition is much softer in three dimensions. The points outside the region between the two limits are points where the flux density is very high, implying that the statistics is bad.

In the phase where the Alice fluxes do condense we may approximate the monopole density by the monopole density of a single cube. That this can be done follows basically from the results of sections 3.4.1 and 3.4.3. The cubes not pierced by any  $\mathbb{Z}_2$  flux are in the condensed phase isolated in the sense that the  $U(1)$  degrees of freedom of the links have hardly any effect on the surrounding plaquettes. This makes it safe to use the single cube approximation in the phase where the fluxes have condensed.

We determined the single cube density by using random link values, with which we determined the energy of the cube, the charge inside the cube and the entropy of the configuration. With this information we calculated the monopole density for different values of  $g^2$  and compared it with the data points we found. This approximation is the same for the three and four dimensional model, though in three dimensions these are of course instantons.

Just as in section 3.4.1 one expects the two approximations to describe the model very well in four dimensions, but in three dimensions one expects an intermediate region. This is exactly what we find, see figures 3.9(a) and 3.9(b). Again we note that the points outside the region bounded by the two approximations are points where the flux density is very high, i.e., the fluctuations become very large.

### 3.4.5 Discussion

The approximations we made in the last few sections describe the model fairly well. In four dimensions the approximations work extremely well. The phase with condensed

fluxes can apparently be understood as a phase where the correlation lengths of the fields are vanishingly small. In three dimensions the division of the phase space is not as clear, but our approximation of the height lines of the flux density does imply a region where the correlation length of both fields is also vanishingly small. If the Alice fluxes do not condense the theory is very well described by a pure compact  $U(1)$  gauge theory.

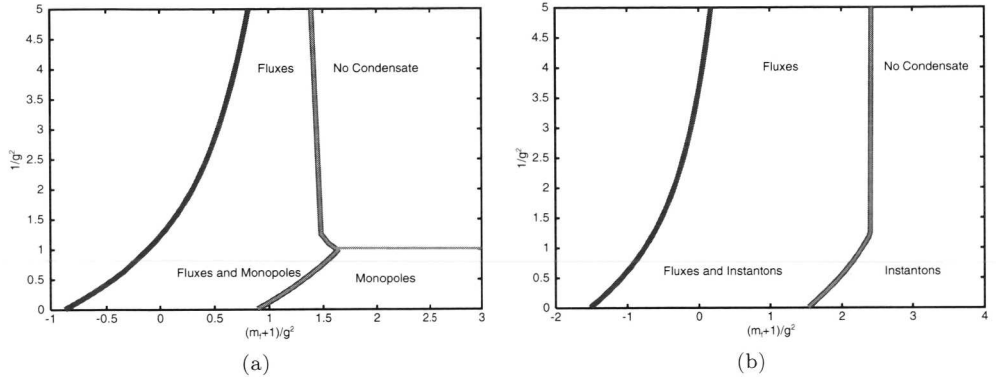


Figure 3.10: The phase diagrams of four, (a), and three, (b), dimensional LAED in the new parameters. The details and implications are explained in the text.

As mentioned before, the fact that all the contour lines of the flux density come together at  $m_f = -1$  for  $g^2 \rightarrow 0$ , does not mean that the phase transition becomes or stays first order. It is mainly due to the choice of parameters that all the contour lines of the flux density come together. If one uses the in some sense more natural parameters  $(m_f + 1)/g^2$  and  $1/g^2$ , it is not at all clear that this will happen. This is illustrated in figure 3.10, where we have plotted the phase diagram of the model in terms of the conventional parameters. The crossover transitions are not marked, they are associated to regions with different condensates not separated by a phase transition line. Although there is a second flux transition line, the “no-flux” condensation, there is no monopole/instanton transition at this point. We deduce this from the results of section 3.4.4. That we are not able to determine the monopole/instanton density there is due to the fact that the fluctuations are very large in that region of parameter space. However one would expect the single cube approximation of section 3.4.4 also to be valid in that region of parameter space.

The position of the monopole transition line, see figure 3.10(a) is also following from the results of section 3.4.4. We pointed out that the monopole data splits up into two regions, the regions where the fluxes have or have not condensed. This means that the  $U(1)$  monopole transition line splits up and follows the (first) flux transition line. We have drawn it all the way along this flux condensation line, but it is not yet clear whether there is always a monopole transition. For  $g^2 \rightarrow 0$  and  $g^2 \rightarrow \infty$  the difference in the monopole density between the two regions becomes smaller and smaller.

To some extend the same is true for the instanton density, see figure 3.10(b). Although

in that case there is an intermediate region, see section 3.4.4. In this region the instanton density grows with increasing flux density, and since in this region the flux density has a transition one would expect also the instanton density to show a transition. The data also appears to imply this, but is not shown here. Again it is not clear what happens to this transition in the limits of  $g^2 \rightarrow 0$  and  $g^2 \rightarrow \infty$ . In these limits the difference of the instanton density between the regions where the fluxes have or have not condensed goes to zero.

## 3.5 Conclusions and outlook

In this chapter we have studied Alice electrodynamics on a lattice, with a model that allows the formation of magnetic monopoles and Alice fluxes. It includes the usual Wilson lattice action for the  $U(1)$  gauge theory and has an extra bare mass term for Alice fluxes. This term suffices to reach all four phases of Alice electrodynamics given in table 3.1.

We have determined the regions in phase space corresponding to the four different phases of LAED and presented results on some measurable quantities; the monopole density, the flux density and  $\langle \cos \tilde{F} \rangle$ . We then approximated the locations of the flux and the so called no-flux condensation line in the phase diagram of the model, both in three and four dimensions. These approximations worked very well except for the flux condensation line for small values of the gauge coupling. The other approximations we made also all work quite well, with the remark that in three dimensions there is an intermediate region which we have not yet investigated. We successfully compared our numerical results with approximations of the flux density between the flux and the no-flux condensation line, the monopole/instanton density,  $\langle \cos \tilde{F} \rangle$  and the position of the monopole condensation line. The monopole condensation becomes a crossover in the region where the Alice fluxes are condensed. In section 3.4.5 we gave the resulting phase diagrams.

It would be interesting to examine the fate of the phase transitions in the monopole and instanton density induced by condensing Alice fluxes for small and large values of  $g^2$ . For small values of  $g^2$  it is also not clear if the two flux transitions merge or not in the parameter space with the coordinates  $(m_f + 1)/g^2$  and  $1/g^2$ .



# Chapter 4

# Dynamical vacuum selection

In the last two chapters we introduced several models containing an AED phase. In the coming chapters we will study some effects which are related to the Alice effect in AED. However in this chapter we will investigate a generic feature of field theories with flat directions in their potential and a non-trivial topology. The common factor of the coming three chapters is the mixture of topological defects and a notion of instability.

In this chapter, which is based on [83], we show that in field theories with topologically stable kinks and flat directions in their potential, a so-called dynamical vacuum selection (DVS) takes place in the non-trivial, soliton sector of the theory. We explore this DVS mechanism using a specific model. For this model we show that there is only a static kink solution when very specific boundary conditions are met, section 4.2.2, very similar to the case of vortices in two dimensions. In the case of other boundary conditions a scalar cloud is expelled to infinity, leaving a static kink behind, section 4.2.4. Other circumstances under which DVS may or may not take place are discussed as well.

## 4.1 Introduction

In this chapter we examine topological defects in theories with flat directions in their potential. Flat directions in the scalar potential are quite natural in the context of supersymmetric models. As was noticed in [54], in spite of the fact that a model does allow topologically stable vortices, not all admissible boundary conditions in a given model with flat directions are compatible with the existence of a static vortex solution. In [55] such vortices in theories with flat directions were studied, and it was shown that in the presence of a topologically stable vortex, a specific vacuum is dynamically selected. In this chapter we focus on the one dimensional case and show that also for theories in one dimension with flat directions not all boundary conditions allow the existence of a static kink. We will show that a specific vacuum is

dynamically selected in the presence of such a kink or domain wall. Although we will use a specific model, it will become clear that dynamical vacuum selection (DVS) is a general feature for theories with flat directions in one dimension.

To be a bit more specific we will discuss a class of models which have two copies of a scalar Higgs field and a potential of the following form.

$$V(\phi_1, \phi_2) = \frac{\lambda}{4} (\phi_1^2 - \phi_2^2 - f^2)^2 \quad . \quad (4.1)$$

in analogy with the model studied in [55].

In section 4.2 we focus on the one dimensional model, in section 4.3 we comment on the two dimensional model which was discussed in [55], and in section 4.4, we show with the help of a Bogomolny [66] type argument that there is no DVS in the three dimensional case, as was already anticipated in [55]. We end the chapter with some conclusions and a brief discussion.

## 4.2 DVS in 1 dimension

In this section we investigate DVS in a specific one dimensional model. First we introduce the model, subsequently we prove that there is only a static kink solution for a very specific non trivial boundary condition out of a continuum of allowed boundary conditions. Finally we investigate the kink dynamics if this specific boundary condition is not met and we find that indeed the DVS mechanism becomes operative.

### 4.2.1 The model

We consider a model with two real scalar fields and a potential which allows for the formation of topologically stable kinks and which furthermore features a flat direction. The model is given by:

$$\mathcal{L} = \int dx \left\{ \frac{1}{2} (\partial_\mu \phi_1)^2 + \frac{1}{2} (\partial_\mu \phi_2)^2 - \frac{\lambda}{4} (\phi_1^2 - \phi_2^2 - f^2)^2 \right\} \quad , \quad (4.2)$$

with  $\phi_1$  and  $\phi_2$  two real scalar fields.

It is quite clear that this model contains topologically stable kinks, which have to satisfy the spatial boundary conditions  $\phi_1(\pm\infty) = \sqrt{f^2 + \phi_2(\pm\infty)^2}$  and  $\phi_1(\mp\infty) = -\sqrt{f^2 + \phi_2(\mp\infty)^2}$ . Note that the boundary values of  $\phi_2$  do not influence the topological charge of the kink. Thus there is a two parameter class of topologically stable kinks present in this model, labeled by  $(\phi_2(-\infty); \phi_2(+\infty))$ . In the next section we investigate the class of static kink solutions in this model when real space is taken infinite. This class as we will show is in fact very small.

### 4.2.2 Static kinks

Naively one might expect to be able to find a static kink solution (assuming real space to be infinite) for any set of the boundary values of  $\phi_2$  in the topologically nontrivial sector. However this turns out not to be true. What we will show is that there is only one very specific set of boundary values of  $\phi_2$  for which a static kink solution exists.

To obtain a static configuration, we set the time derivatives equal to zero and extremize the resulting Hamiltonian. The Hamiltonian of this model can be interpreted as the action of a point particle in a two dimensional potential, and we may analyze the system through this mechanical analogue. More explicitly, after making the following identifications:  $x \rightarrow t$ ,  $\phi_1 \rightarrow x$  and  $\phi_2 \rightarrow y$ , we get the following action:

$$S = \int dt \left\{ \frac{1}{2} (\partial_t x)^2 + \frac{1}{2} (\partial_t y)^2 + \frac{\lambda}{4} (x^2 - y^2 - f^2)^2 \right\} . \quad (4.3)$$

This system corresponds to a point particle moving in the inverse potential:  $V(x, y) = -\frac{\lambda}{4} (x^2 - y^2 - f^2)^2$ .

The problem of finding a static kink solution is now translated to finding a solution to the equations of motion of the point particle, which moves from one point on one line of maxima of the potential,  $x = \pm \sqrt{f^2 + y^2}$ , at  $t \rightarrow -\infty$  to an other point on the other line of maxima,  $x = \mp \sqrt{f^2 + y^2}$ , at  $t \rightarrow \infty$  (see figure 4.1).

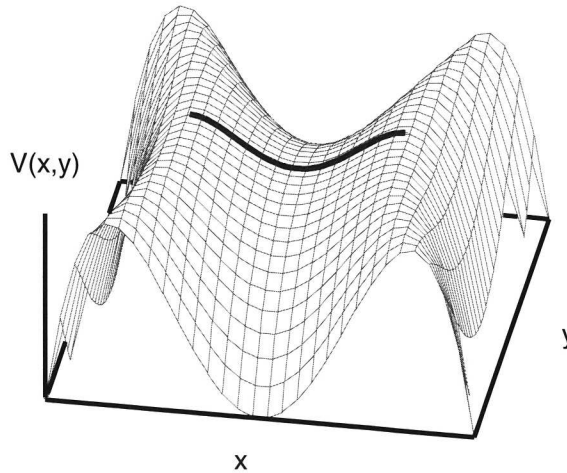


Figure 4.1: The two dimensional potential for the point particle. The only path satisfying the desired boundary conditions is the path with  $y(t) = 0$ . This path represents the only static kink solution in an infinite space, for which  $\phi_2(x) = 0$ .

At  $t \rightarrow -\infty$  the particle should be at rest in one of the maxima of the potential.

At  $t \rightarrow \infty$  the particle needs to be at rest in one of the other set of maxima of the potential. Obviously there is only one path which satisfies these boundary conditions and that is the path with  $y = 0$ . Any path starting with  $y(t \rightarrow -\infty) \neq 0$  in one of the maxima of the potential will never again reach a maximum of the potential. In such a case it is easy to prove that the kinetic energy of the particle associated with component of the motion in the  $y$ -direction will increase monotonically in time and therefore the particle can never climb out of the potential well again, i.e., will not be able to satisfy the boundary condition at  $t \rightarrow \infty$ . Translating this back to the kink solutions, this means that one can only have a static kink solution if the boundary conditions of  $\phi_2$  are  $\phi_2(\pm\infty) = 0$  and moreover for the static solution we get  $\phi_2(x) = 0$ . Thus the only static kink solution for this model in an infinite space is equal to the usual kink solution.

A crucial step in deriving this result was the infinite size of real space. If space is finite the argument changes dramatically. In the mechanical analogue this would mean that the particle can have an initial velocity (and direction of this velocity), so that the entire class of boundary configurations is allowed.

A natural question to ask is, what happens if the boundary conditions of  $\phi_2$  are *not* of the specific form  $\phi_2(\pm\infty) = 0$ . As we just demonstrated, there can not be a static kink solution with these boundary conditions and we are led to ask how the configuration will develop in time. Later on we will study the dynamics of such a configuration and find that DVS will take place. Before we turn to this question we take a closer look at the structure of the static kink solutions in a finite space and at how the boundary conditions effect the core structure of the kink.

### 4.2.3 Kinks in finite space

In this section we study static kink solutions in a finite space with fixed boundary conditions. These kinks correspond to the so called restricted instantons in quantum mechanics [84]. We first want to introduce the massless modulus field,  $z$ , which is of paramount interest to us in the rest of the chapter. In the broken phase of the theory this field corresponds to the degree of freedom in the flat direction of the potential. On the vacuum manifold we have  $\phi_1^2 - \phi_2^2 = f^2$ . We can parameterize the degree of freedom in the flat direction of the potential by writing:  $\phi_1 = f \cosh u$  and  $\phi_2 = f \sinh u$ . To get the canonical kinetic term we change from  $u$  to the modulus field  $z$ , which is given by:

$$z = f \int_0^u du' \sqrt{\cosh 2u'} \quad . \quad (4.4)$$

This field  $z$  obeys the free massless equations of motion. From the construction for this specific case it is evident that there is always a massless mode if there is a flat direction in the potential. The dynamics and statics (energy) of this massless mode are the crucial ingredients in DVS. They allow one to show directly, that there can be DVS in one and two dimensions but not in three or higher dimensions.

Let us return to the restricted kinks. It is not hard to anticipate what the solution of a kink will look like if the size of the space,  $2R_\infty$ , is much larger than the core size of the kink,  $2R_c$ . Consider the configuration of a kink of size  $2R_c$ , where outside the core of the kink the vacuum manifold is reached exponentially fast. To this kink we add a tail at each side in which the scalar fields stay in the vacuum manifold but move to the prescribed boundary value at  $x = \pm R_\infty$ . In the limit of  $R_\infty \rightarrow \infty$  we should recover the unique static solution we found before. Thus the kink solution we should use to describe the core of the kink is this special case where  $\phi_2 = 0$ .

So we approximate the restricted kink solution by a configuration which is a superposition of two linear tails and a kink with  $\phi_2 = 0$ . Clearly the tails and the kink independently satisfy the field equations, so it is only due to the overlap that the field equations are not quite satisfied. The violation to the equations of motion due to the overlap is proportional to  $z_\pm/R_\infty$  in the action, and this justifies the approximation we made in the limit of small  $z_\pm/R_\infty$ . With the help of a relaxation program we numerically determined the static kink solution for various values of the parameters, see figure 4.2. In all our figures and numerical simulations we take  $\lambda = f = 1$ , any other values of  $\lambda$  and  $f$  follow by rescaling the fields and the space coordinate.

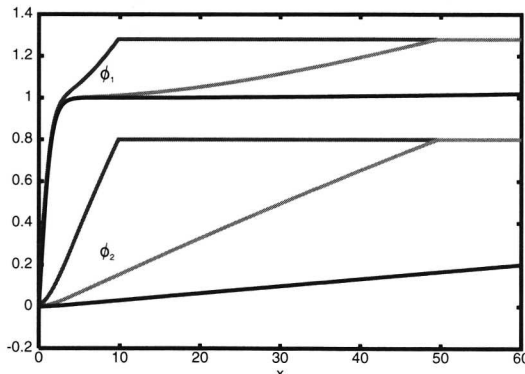


Figure 4.2: The fields for the restricted kinks for different values of  $R_\infty$ . The values of  $R_\infty$  are  $R_\infty = 10$ ,  $R_\infty = 50$  and  $R_\infty = 250$ . The boundary conditions on  $\phi_2$  are  $\phi_2(\pm R_\infty) = \pm 0.8$ . The fields for negative values of  $x$  just follow from symmetry of the configuration and are not plotted. This figure clearly shows the separation of the solution in the kink and a tail in the limit of small  $z_\pm/R_\infty$ .

Using these approximate restricted kink solutions we can also determine the position of the kink with respect to the boundaries of the space. We can get an estimate by minimizing the energy in the tails. Both tails want to spread as much as they can to lower the energy, so if there is an asymmetry in the boundary conditions of  $\phi_2$ , this will certainly have an effect on the position of the kink. We approximate the position of the kink by minimizing the sum of the energy of the two tails, which is given by:

$$E_{tail} = \frac{z_+^2}{R_+} + \frac{z_-^2}{R_-} , \quad (4.5)$$

with  $R_+ + R_- = 2R_\infty$  and  $z_\pm$  the values of the modulus field at the boundaries of space.

Minimizing this energy under the restriction  $R_+ + R_- = 2R_\infty$  gives:

$$R_+ = \frac{2}{1 + \left| \frac{z_-}{z_+} \right|} R_\infty \quad ; \quad R_- = \frac{2}{1 + \left| \frac{z_+}{z_-} \right|} R_\infty \quad , \quad (4.6)$$

with  $R_+$  and  $R_-$  the distance between the core of the kink and the  $+R_\infty$  and  $-R_\infty$  boundary of space respectively. Note that the position of the kink in this estimate does not depend on the relative sign between the boundary conditions on  $\phi_2$  at  $+R_\infty$  and  $-R_\infty$ . We tested this simple estimate numerically and found it to work quite well, see figure 4.3. It should be clear that for  $R_\pm < R_c$  the estimates of  $R_+$  and  $R_-$  break down.

In figures 4.3(a) and 4.3(b) we plotted the numerical data for the position of the kink and the estimated position of the kink. We show the results of numerical simulations for  $R_\infty = 50$ , where we defined the position of the kink by the zero of the  $\phi_1$  field. The boundary conditions we put on  $\phi_2$  are  $\phi_2(R_\infty) = 2 + \delta$  and  $\phi_2(-R_\infty) = \pm 2 \mp \delta$ , with  $\delta$  running from zero to two. In figure 4.3(a) we plotted  $R_-$  as a function of  $z_+/z_-$ , where in 4.3(b) we plotted  $R_-$  as a function of  $\delta$ . The plots show a good agreement between the estimate and the numerical data. They also show the independence of the position of the kink on the sign of  $z_-/z_+$ , which is equal to the sign of  $\phi_2(-R_\infty)/\phi_2(+R_\infty)$ .

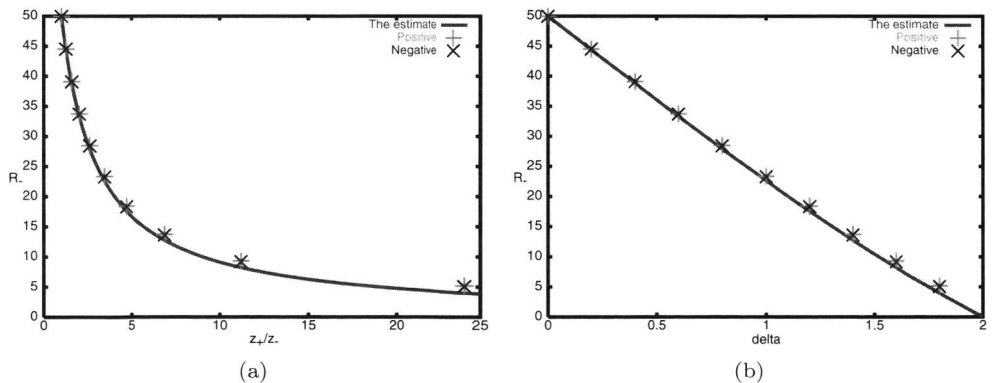


Figure 4.3:

The estimate for  $R_-$  and the numerically obtained values of  $R_-$  as a function of  $z_+/z_-$ , figure (a), and of  $\delta$ , figure (b), with  $R_\infty = 50$ . The boundary values of  $\phi_2$  are  $\phi_2(R_\infty) = 2 + \delta$  and  $\phi_2(-R_\infty) = \pm 2 \mp \delta$ . The figures show that the estimate of the position of the kink works very well and that the position of the kink is independent of the sign of  $\phi_2(-R_\infty)/\phi_2(+R_\infty)$  as prescribed by our estimate.

In the limit of small  $z_\pm/R_\infty$  we have a good understanding of the static kink solution. In the next section we will study the dynamics of the non static kink solutions, which occur if the boundary values of the  $\phi_2$  field are not zero.

#### 4.2.4 Non static kink configurations

In section 4.2.2 we proved that in an infinite space there is only a static kink solution to the field equations for a specific set of boundary values of  $\phi_2$ , notably  $\phi_2(\pm\infty) = 0$ . In any other case there is no static kink solution to the equations of motion. In this section we will investigate the behavior of these non static kinks and find the DVS. The modulus field  $z$  obeys the free massless equation of motion, which in one dimension is given by:

$$-\partial_t^2 z(x, t) + \partial_x^2 z(x, t) = 0 \quad . \quad (4.7)$$

Thus the modulus field is given by  $z(x, t) = z_r(t - x) + z_l(t + x)$ . This shows that the modulus field propagates with the speed of light. Next we will look at some specific dynamical simulations. In the light of the previous discussion of constrained kinks it is clear what should happen in an infinite space. The kink will 'eject' a so called scalar cloud, the tail, to infinity; the cloud will move with the speed of light, and will dynamically select the vacuum with  $\phi_2 = 0$ .

We look at two types of initial configurations. One corresponds with the solution of a restricted kink, which we numerically determined in the previous section. The other initial configuration is a configuration with constant  $\phi_2$  and for  $\phi_1$  the static kink solution with  $f^2$  replaced by  $f^2 + \phi_2^2$ , see equation (4.8). Both types of initial configurations we assume to be at rest at  $t = 0$ .

Lets us first examine the latter case. Again in our numerical simulations we take  $\lambda = f = 1$ , and start with:

$$\phi_2(x) = \phi_2 \quad ; \quad \phi_1(x) = \sqrt{1 + \phi_2^2} \tanh \left( \frac{1}{2} \sqrt{2} \sqrt{1 + \phi_2^2} x \right), \quad (4.8)$$

taking  $\partial_t \phi_1(t)|_{t=0} = \partial_t \phi_2(t)|_{t=0} = 0$ . As expected, we find that the scalar cloud moves away with the speed of light and the special vacuum with  $\phi_2 = 0$  is dynamically selected, see figure 4.4(a).

The initial condition with the restricted kink as the initial configuration yields a similar result. We determined the solution of the restricted kink, with  $R_\infty = 50$  and  $\phi_2(\pm R_\infty) = 0.8$ , with the help of a relaxation program and used it as the initial configuration of the dynamical process. Again we take  $\partial_t \phi_2(t)|_{t=0} = \partial_t \phi_1(t)|_{t=0} = 0$ . Also here the special vacuum with  $\phi_2 = 0$  is dynamically selected, see figure 4.4(b).

After the vacuum has been selected the kink can still be excited, which is clear in the first case, equation (4.8). In the case where the restricted kink has been chosen as initial configuration, the kink is only slightly excited locally, due to the overlap of the kink and the modulus field. We conclude that this part of the dynamics depends on the initial condition, but does not effect the vacuum selection part of the dynamics.

### 4.3 DVS in 2 dimensions

In this section we briefly recall known results of DVS in two dimensions, as discussed in [55]. Witten in [54] already observed, that in several models not all boundary

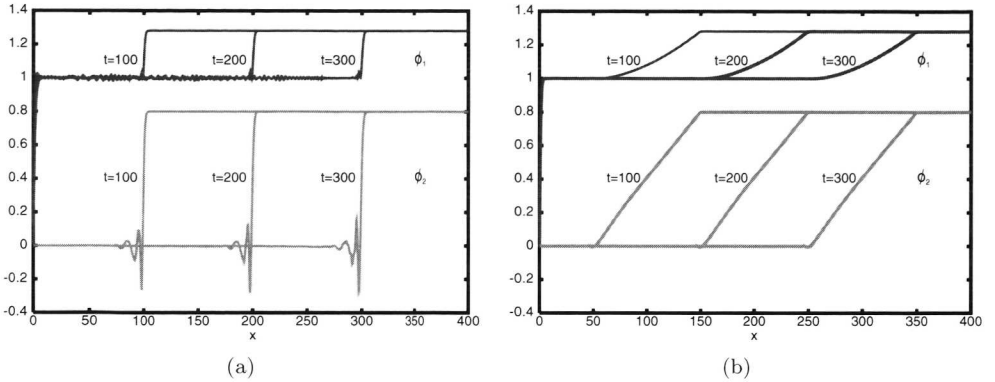


Figure 4.4:

(a):The dynamics of the kink with  $\phi_2(x) = \phi_2 = 0.8$  and  $\phi_1(x)$  given by equation (4.8) at  $t = 0$ . The figure shows snapshots of the fields  $\phi_1(x)$  and  $\phi_2(x)$  at  $t = 100$ ,  $t = 200$  and  $t = 300$ . This shows the DVS and the speed of the scalar cloud.

(b):The dynamics of the restricted kink with  $\phi_2(\pm R_\infty) = 0.8$  and  $R_\infty = 50$  at  $t = 0$ . The figure shows snapshots of the fields  $\phi_1(x)$  and  $\phi_2(x)$  at  $t = 100$ ,  $t = 200$  and  $t = 300$ . This shows the DVS and the speed of the scalar cloud.

The values of the fields for negative values of  $x$  follow from symmetry of the configuration and are not plotted.

conditions allow for static vortex solutions. In the model, studied in [55] there is also a potential of the form  $\frac{\lambda}{4}(|\phi_1|^2 - |\phi_2|^2 - f^2)^2$ . The Higgs fields they use are now complex scalar fields, oppositely charged under a local  $U(1)$ . Also in this model the vacuum  $\phi_2 = 0$  is dynamically selected in a topologically nontrivial sector of the theory. In [56] it was pointed out that this specific vacuum was selected to minimize the mass of the massive gauge boson.

Again the main idea behind the DVS is the fact that one can make a tail with the modulus field, which brings fields from one point of the vacuum manifold to an other point in the same connected component of the vacuum manifold. In two dimensions the energy cost of such a tail is inversely proportional to  $\ln \frac{R_\infty}{R_c}$  and can be made arbitrarily small in an infinite space. Although the dynamics of the modulus field is a bit different in two dimensions from the dynamics in one dimension, the conclusion is the same: DVS takes place. For more details on DVS in two dimensions we refer to [54], [55] and [56].

## 4.4 No DVS in 3 dimensions

To conclude we look at a specific model in three dimensions to argue that DVS does not work in three dimensions (as was already mentioned in [55]). The crucial observation here is that a tail in which the modulus field connects one point of the vacuum manifold to another point in the same connected component, will cost a finite amount of energy. In three dimensions the energy of such a modulus field is

proportional to  $\frac{R_c R_\infty}{R_\infty - R_c}$ , which does not go to zero in the limit of  $R_\infty \rightarrow \infty$ , suggesting that there is no DVS in three dimensions.

To make this more explicit we discuss a model which has a local  $SU(2)$  symmetry and two scalar Higgs fields in the vector representation of the local gauge group. The potential will again have the form  $\frac{\lambda}{4} (\text{Tr}(\phi_1^2) - \text{Tr}(\phi_2^2) - f^2)^2$ . In this model the  $SU(2)$  gauge symmetry is spontaneously broken to  $U(1)$  and topologically stable magnetic monopoles can form. The action of the model is given by:

$$S = \int d^4x \left\{ \frac{1}{4} F_{\mu\nu}^a F^{a,\mu\nu} + \frac{1}{2} \text{Tr}((D_\mu \phi_1)^2) + \frac{1}{2} \text{Tr}((D_\mu \phi_2)^2) - \frac{\lambda}{4} (\text{Tr}(\phi_1^2) - \text{Tr}(\phi_2^2) - f^2)^2 \right\} . \quad (4.9)$$

We will try to find static monopole solutions in the BPS limit, i.e., we keep the boundary terms fixed but put  $\lambda$  to zero. We note that the fields  $\phi_1$  and  $\phi_2$  need to be parallel to each other in the internal space at spatial infinity in order to have a finite energy solution, and to have an unbroken  $U(1)$  in the first place. We will focus on static configurations where  $\text{Tr}(\phi_2(r \rightarrow \infty)^2)$  does not depend on the spatial angles.

To find static solutions we have to extremize the energy:

$$E = \int d^3x \left\{ \frac{1}{2} B^2 + \frac{1}{2} \text{Tr}((D_i \phi_1)^2) + \frac{1}{2} \text{Tr}((D_i \phi_2)^2) \right\} . \quad (4.10)$$

To be able to get the BPS equations we first make the following rescalings:  $\phi_1 \rightarrow \cosh u \phi_1, \phi_2 \rightarrow \sinh u \phi_2, x_i \rightarrow \frac{1}{\sqrt{\cosh 2u}} x_i$  and  $A_i \rightarrow \sqrt{\cosh 2u} A_i$ , where  $\text{Tr}(\phi_2(\infty)^2) = f^2 \sinh^2 u$ . Note the similarity with the usual BPS dyon. Now we can write the energy in the following form:

$$E = \frac{1}{\sqrt{\cosh 2u}} \int d^3x \left\{ \cosh^2 u \left( \frac{1}{2} B^2 + \frac{1}{2} \text{Tr}((D_i \phi_1)^2) \right) + \sinh^2 u \left( \frac{1}{2} B^2 + \frac{1}{2} \text{Tr}((D_i \phi_2)^2) \right) \right\} . \quad (4.11)$$

From this we get the usual BPS equations for the monopole twice, one for  $\phi_1$  and one for  $\phi_2$ . They reduce to one set of BPS equations under the assumption  $\phi_1 = \phi_2$ <sup>1</sup>, whose solution is well known. The energy of the monopole is simply given by:

$$E_{\text{mon}} = \sqrt{\cosh 2u} E_{\text{mon}; u=0} , \quad (4.12)$$

where  $E_{\text{mon}; u=0}$  is the energy of the monopole in absence of  $\phi_2$ .

This shows that the core structure of the monopole is affected by the boundary conditions of the  $\phi_2$  field and that there is no DVS. This in contrast to the results found in one and two dimensions.

<sup>1</sup>This is possible since the rescaled fields  $\phi_1$  and  $\phi_2$  have the same boundary conditions.

## 4.5 Conclusions and outlook

In this chapter we showed the possibility of dynamical vacuum selection (DVS) in one dimensional field theories with flat directions. We examined this DVS with the help of a specific model. For this model we proved that there is only one specific boundary condition which allows a static kink solution in an infinite space. In a finite space any boundary condition allows the formation of a static kink. With the help of a relaxation program we numerically determined these restricted kinks. They can be very well described by one specific kink with a scalar cloud on each side of the kink. This description of the restricted kink also correctly predicts the position of the kink with respect to the boundaries of the space as a function of the boundary conditions. Using a numerical simulation we examined the dynamical properties of configurations with boundary conditions which do not allow a static solution in an infinite space. These simulations confirm the DVS, which was expected to occur, from the result of the restricted kinks and the field equation for the modulus field.

It should be clear that DVS in one dimension is not specific for the one dimensional model we considered. It is a general feature of one dimensional models with flat directions. The argument relies crucially on the scaling of the energy of the tails, the scalar clouds, of the restricted kinks. In these scalar clouds only the modulus field changes. More generally this shows that DVS is only possible in one and, as was shown before [55], in two dimensions, but not in three or higher dimensions. For completeness we briefly mentioned the two dimensional case and included an explicit example of a three dimensional model where DVS does not work.

It remains of course possible that a model has more than one possible static configuration in an infinite space [85], but the DVS will just pick out one of the possible static solitons and including tunneling it will eventually always select the vacuum corresponding to the static soliton with the lowest energy. Although this DVS selects a lowest energy static soliton solution there can still be a vacuum and core degeneracy left if the ground state of the topologically non trivial sector is degenerate, as was for example found in [56].

It would be interesting to study DVS, due to the presence of a soliton, in a theory where the selected vacuum is lifted from the classical vacuum manifold by quantum mechanical (or thermal) corrections. Obviously this cannot happen if a supersymmetric BPS soliton is selected by the DVS, since the energy of such a BPS soliton is protected against quantum mechanical corrections. On the length scale where the quantum mechanical corrections to the vacuum manifold would become important the DVS alters and most likely a type of restricted soliton will become the new selected vacuum. The tail(s) of these restricted solitons will have a length of the order determined by the quantum mechanical corrections to the classical vacuum manifold.

The processes we described in this chapter can be interpreted in two ways. One is the dynamical vacuum selection interpretation which we anticipated throughout the chapter. In the other interpretation, which is much closer to the coming chapters, the process can be seen as a possible instability of a kink or vortex solution in a theory with flat directions in its potential.

# Chapter 5

## A monopole core instability

In the previous chapter we investigated a possible instability of topological defects in theories with flat directions in their potential. We saw that such a instability is not possible for magnetic monopoles. In this chapter we investigate a different type of instability which is possible for the magnetic monopole. We present results on a core instability of the 't Hooft Polyakov type monopoles. This instability, where the spherical core decays in a toroidal one, typically occurs in models in which charge conjugation is gauged. However, we will argue that a core instability of 't Hooft Polyakov type monopoles is quite a generic feature of models with charged Higgs particles. We also discuss a third conceivable configuration denoted as "split core", which brings us to some details of the numerical methods we employed. This chapter is mainly based on [86, 87].

### 5.1 Introduction

Since the pioneering work of 't Hooft and Polyakov [88, 89] magnetic monopoles have been studied in detail in many different models. In this chapter we address the question of stability of the core of the fundamental, spherically symmetric, monopole configuration, a stability which appears to be so obvious that it was never seriously questioned. We will show that in the original AED model [4] the spherically symmetric unit charge magnetic monopole is not the global minimal energy solution for all parameter values in the model. We determine the regions in parameter space where this instability occurs and present some details of the numerical simulations we performed. The fact that the core topology is not fixed by the boundary conditions at infinity and different core topologies can be deformed into each other was already established earlier [90].

As we will indicate, Alice theories have a special topological feature which makes it plausible that such a core deformation really can be favored energetically. We will also argue that a core deformation is typically energetically favored in models where

the charged Higgs particles are light compared to the neutral Higgs particles. Our interest in this problem was rekindled by some observations made in theories with global symmetries [91, 92, 93, 94].

This chapter is organized as follows. We start with a brief motivation for studying the monopole core meta-/instability in AED. Next we introduce the specific model and discuss in some detail the numerical simulations we performed and present our the main results. We end this chapter with conclusions and an outlook.

## 5.2 The core instability

Alice electrodynamics (AED) is a gauge theory with gauge group  $H = U(1) \ltimes \mathbb{Z}_2 \sim O(2)$ . As we saw in chapter 1 this theory allows for Alice fluxes and Cheshire charges [4, 5]. In this chapter the Cheshire phenomenon in AED is of great importance to us as it supports the possible core meta-/instability of the spherically symmetric magnetic monopole solution.

It was pointed out long ago that there are interesting issues concerning the core stability of magnetic monopoles. Fixing the asymptotics of the Higgs field, the core (i.e., the zeros of the Higgs field) may have different topologies, notably that of a “ring” rather than the conventional “point”<sup>1</sup>. These core topologies are *cobordant*, i.e., they can be smoothly deformed into each other and it is a question of energetics what will be the lowest energy monopole state [90]. In AED such a core deformation would be accompanied by the rather unusual delocalized version of (magnetic) charge, the so called *magnetic Cheshire charge*. Cheshire charge is a key feature of AED and is a general phenomenon in field theories with (topologically) stable fluxes which are not elements of the center of the unbroken gauge group.

In the specific AED model we consider the Higgs field is a symmetric tensor, whose vacuum expectation value may be depicted as a bidirectional arrow. In AED we can “punch a hole” in the spherically symmetric monopole and deform it into an Alice ring, this configuration is consistent with the continuity requirement on the order parameter because of its head-tail symmetry. In figure 5.1 we plotted the two different core regions one expects to find for a magnetic monopole in AED. In this chapter we determine in what part of the parameter space of the model the monopole is meta-/unstable and where we expect the spherically symmetric monopole to compete with a magnetically, Cheshire charged Alice ring. Figure 5.1(a) represents the spherically symmetric magnetic monopole and figure 5.1(b) represents the magnetically Cheshire charged Alice ring. The fact that the core of the defect can really deform into a torus is due to the head-tail symmetry of the Higgs field in the broken phase. We note that the Higgs field only rotates over an angle  $\pi$  when going around a single flux, see figure 5.1(d). This is the hallmark for an Alice flux, so the core deformed spherical

---

<sup>1</sup>In fact in AED the Higgs field can typically only be represented by a director field if it is in the vacuum manifold. Thus the Higgs field need not go to zero inside the core of a defect. However for the spherically symmetric magnetic monopole solution the Higgs field does go to zero, but for the Alice loop solution it does not.

monopole is in fact an Alice ring carrying a magnetic Cheshire charge.

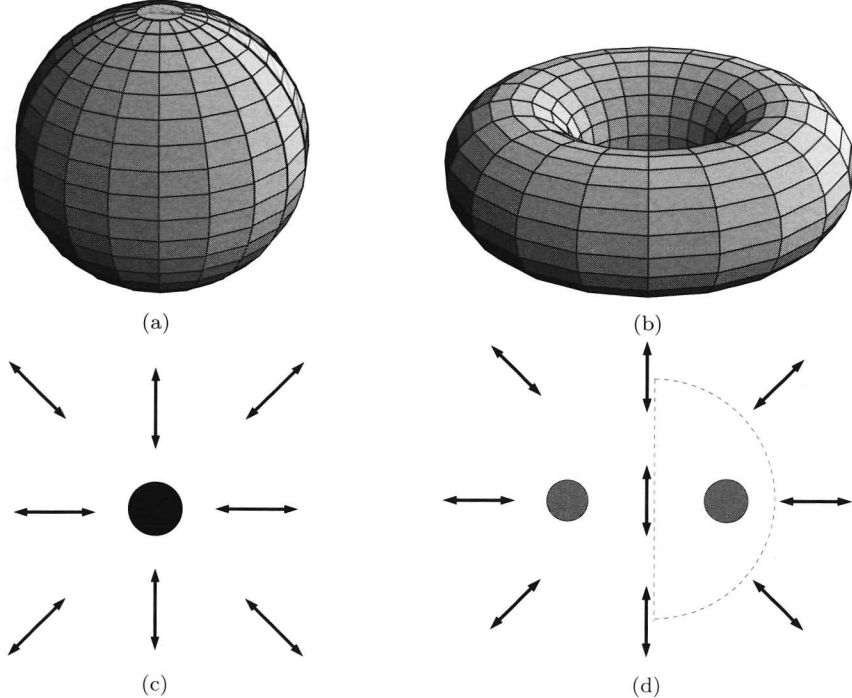


Figure 5.1: These figures show the two different core structures of a magnetic defect which are naturally present in AED. Figure (a) represents the spherically symmetric magnetic monopole, the 't Hooft Polyakov type monopole, and figure (b) represents the magnetically, Cheshire charged Alice ring. Figures (c) and (d) represent a slice of the different core topologies including the Higgs field.

### 5.3 The Alice model

To answer stability questions related to the spherically symmetric monopole configuration (or the Cheshire charged Alice ring) we consider an explicit model. We use the original tensor Alice model [62], but we will argue that the results obtained are quite general and model independent. For completeness and notational convenience we briefly summarize the model. The action is given by:

$$S = \int d^4x \left\{ \frac{1}{4} F^{a,\mu\nu} F_{\mu\nu}^a + \frac{1}{4} \text{Tr}(D^\mu \Phi D_\mu \Phi) - V(\Phi) \right\} , \quad (5.1)$$

where the Higgs field  $\Phi = \Phi^{ab}$  is a real, symmetric, traceless  $3 \times 3$  matrix, i.e.,  $\Phi$  is in the five dimensional representation of  $SO(3)$  and  $D_\mu \Phi = \partial_\mu \Phi - ie[A_\mu, \Phi]$ , with

$A_\mu = A_\mu^a T_a$ , where  $T_a$  are the generators of  $SO(3)$ . The most general renormalizable potential is given by [50]:

$$V = -\frac{1}{2}\mu^2 \text{Tr}(\Phi^2) - \frac{1}{3}\gamma \text{Tr}(\Phi^3) + \frac{1}{4}\lambda (\text{Tr}(\Phi^2))^2 \quad . \quad (5.2)$$

with the parameter  $\gamma > 0$ , since  $(\Phi, \gamma) = (-\Phi, -\gamma)$ . For a suitable range of the parameters in the potential, the gauge symmetry of the model will be broken to the symmetry of AED. In the “unitary” gauge, where the Higgs field is diagonal, the ground state is (up to permutations) given by the following matrix:

$$\Phi_0 = \begin{pmatrix} -f & 0 & 0 \\ 0 & -f & 0 \\ 0 & 0 & 2f \end{pmatrix} \quad . \quad (5.3)$$

$$\text{with } f = \frac{\gamma}{12\lambda} \left( 1 + \sqrt{1 + \frac{24\mu^2\lambda}{\gamma^2}} \right).$$

The full action has four parameters,  $e, \mu^2, \gamma, \lambda$ , this number can be reduced to two dimensionless parameters by appropriate rescalings of the variables. A physical choice for these dimensionless parameters is to take the ratio’s of the masses that one finds from perturbing around the homogeneous minimum. To determine these, we write the action in the unitary gauge where the massless components of  $\Phi$  have been absorbed by the gauge fields. The physical components of the Higgs field may be expanded as:

$$\Phi(x^\mu) = \Phi_0 + \sqrt{2}\phi_1(x^\mu)E_1 + \sqrt{2}\phi_2(x^\mu)R_3(a(x^\mu))E_2R_3(a(x^\mu))^T \quad , \quad (5.4)$$

with:

$$\begin{aligned} E_1 &= \frac{1}{\sqrt{6}} \begin{pmatrix} -1 & 0 & 0 \\ 0 & -1 & 0 \\ 0 & 0 & 2 \end{pmatrix} ; \quad E_2 = \frac{1}{\sqrt{2}} \begin{pmatrix} 1 & 0 & 0 \\ 0 & -1 & 0 \\ 0 & 0 & 0 \end{pmatrix} ; \\ E_3 &= \frac{1}{\sqrt{2}} \begin{pmatrix} 0 & 0 & 1 \\ 0 & 0 & 0 \\ 1 & 0 & 0 \end{pmatrix} \end{aligned} \quad (5.5)$$

and  $R_i$  are the usual rotation matrices. To second order, the potential  $V(\Phi)$  takes the following form<sup>2</sup>:

$$V(\Phi) = \text{const.} + (2\mu^2 + \gamma f)\phi_1^2 + 3\gamma f|\phi_2|^2 + \dots \quad . \quad (5.6)$$

yielding the two distinct masses of the Higgs modes. Next we look at the ‘kinetic’ term,  $\frac{1}{4}\text{Tr}(D^\mu\Phi D_\mu\Phi)$ , of the Higgs field. Inserting the previous expressions for the Higgs field, we find:

$$\frac{1}{4}\text{Tr}(D^\mu\Phi D_\mu\Phi) = \frac{1}{2}(\partial_\mu\phi_1)^2 + \frac{1}{2}|D_\mu^3\phi_2|^2 + \frac{9}{2}e^2f^2\left(\left(A_\mu^1\right)^2 + \left(A_\mu^2\right)^2\right) + \dots \quad , \quad (5.7)$$

<sup>2</sup>It is most convenient to use  $\phi_2$  for the combination  $\phi_2 e^{ia}$ , since these two Higgs modes,  $\phi_2$  and  $a$ , combine to form one complex charged field, from now on called  $\phi_2$ .

with:  $D_\mu^3 = \partial_\mu - i2eA_\mu^3$ . The second term shows that the  $\phi_2$  component of the Higgs field carries a charge  $2e$  with respect to the unbroken  $U(1)$  component  $A_\mu^3$  of the gauge field. The first term describes the usual charge neutral Higgs particle and the third term yields the mass of the charged gauge fields. So the relevant lowest order action is given by:

$$S = \int d^4x \left\{ \frac{1}{4}F_{\mu\nu}^a F^{a,\mu\nu} + \frac{1}{2}(\partial_\mu\phi_1)^2 + \frac{1}{2}|D_\mu^3\phi_2|^2 - \frac{1}{2}m_1^2\phi_1^2 - \frac{1}{2}m_2^2|\phi_2|^2 - \frac{1}{2}m_A^2\left(\left(A_\mu^1\right)^2 + \left(A_\mu^2\right)^2\right) + \dots \right\} , \quad (5.8)$$

with  $m_1^2 = 4\mu^2 + 2\gamma f$ ,  $m_2^2 = 6\gamma f$  and  $m_A^2 = 9e^2f^2$ .

Two degrees of freedom of the five dimensional Higgs field are 'eaten' by the broken gauge fields, one degree of freedom forms the real neutral scalar field and two degrees of freedom form the complex (doubly charged) scalar field. To specify a point in the classical parameter space we may, up to irrelevant rescalings, use the dimensionless mass ratio's  $\frac{m_1}{m_2}$  and  $\frac{m_A}{m_2}$ . We note that the value of  $\frac{m_1}{m_2}$  needs to be larger or equal to  $\frac{1}{3}$ , because for smaller values of  $\frac{1}{3}$  the groundstate corresponds to the symmetric unbroken vacuum. Note that we found three mass scales in this problem. For the simulations, which we will describe in the next section, this means that we will have to deal with three different length scales.

## 5.4 Numerical simulations

In this section we will describe in some detail the numerical simulations we performed to determine the instability and the meta-stability regions for the spherically symmetric monopole, in the parameter space of the model. First though, we introduce the ansatz. We end the section with the discussion of a typical set of numerical experiments.

### 5.4.1 The variational ansatz

As mentioned before we will use a variational approach. In such an approach the configurations one finds are typically not exact solutions to the equations of motion. However as the ansatz we will use contains the ansatz for the exact spherically symmetric solution we may still study the instability and the meta-stability of this solution. This means that the instability and the meta-stability regions we will find for the monopole, are lower bounds, in the sense that those instability regions can only become larger as the ansatz becomes less restrictive.

As we expect the competing configuration of the spherically symmetric magnetic monopole to be the magnetically Cheshire charged Alice ring, we base our ansatz on cylindrical symmetry. The ansatz we will use also has a reflection symmetry with respect to the  $z=0$ -plane. We impose this reflection symmetry to eliminate the

(almost) zero mode in the energy due to the position of the defect along the  $z$ -axis. The ansatz for the Higgs field is:

$$\Phi(z, \rho, \theta = 0) = \phi_1(z, \rho)E_1 + \phi_2(z, \rho)E_2 + \phi_3(z, \rho)E_3 \quad (5.9)$$

and

$$\Phi(z, \rho, \theta) = R_3(\theta)\Phi(z, \rho, \theta = 0)R_3(\theta)^T. \quad (5.10)$$

The ansatz for the gauge fields is simply given by  $eA_i^j = -\epsilon_{ijk}\frac{x^k}{x^2}A(z, \rho)$ , very similar to the one for the spherically symmetric monopole [88], except that we allow  $A(z, \rho)$  to depend on  $\rho$  and  $z$  and not only on  $r = \sqrt{\rho^2 + z^2}$ . The boundary conditions for  $r \rightarrow \infty$  are the boundary conditions of the spherically symmetric monopole [62], i.e.,  $A(z, \rho)$  goes to one and the Higgs field to  $\Phi(z, \rho, \theta) = R_3(\theta)R_2(\arccos(\frac{z}{r}))\Phi_0R_2(\arccos(\frac{z}{r}))^T R_3(\theta)^T$ . The boundary conditions at  $\rho = 0$  and  $z = 0$  follow by imposing the cylindrical and reflection symmetry and are given in the table below:

	$\rho = 0$	$z = 0$
$\phi_1$	$\partial_\rho\phi_1 = 0$	$\partial_z\phi_1 = 0$
$\phi_2$	$\partial_\rho\phi_2 = \phi_2 = 0$	$\partial_z\phi_2 = 0$
$\phi_3$	$\phi_3 = 0$	$\phi_3 = 0$
$A$	$\partial_\rho A = 0$	$\partial_z A = 0$

It is easy to see that these boundary conditions are also met by the spherically symmetric monopole, so it is indeed contained in our more general ansatz. With the help of this model and ansatz we study the stability of the spherically symmetric magnetic monopole. Before we present the results we describe the numerical methods we employ, and a typical set of experiments.

### 5.4.2 Some numerical details

We mentioned in section 5.3 that the AED model has three mass scales, i.e., three relevant length scales. However we examine a region of parameter space in which only two of those are relevant. That is the core geometry of the defect and the region where the Higgs field is not in the vacuum manifold on the one hand, and the inverse mass of the gauge fields - which is typically much larger - on the other. To be able to adequately capture both scales we use a space and configuration dependent lattice spacing. In fact we will use two types of lattices. In figure 5.2 we schematically give the step sizes as a function of the point number (in one dimension). The two dimensional lattices we will use have the same type of lattice in both directions.

The only difference between the two lattices is that in the second, figure 5.2(b), there are extra lattice points near  $r = 0$  and  $z = 0$  and thus it has more lattice points. However the same part of space is covered by both lattices. Although the difference between the two lattices is quite small we will encounter a specific lattice dependence, which turns out to be an artifact, but nevertheless will be of use later on.

To obtain the minima of the energy within the ansatz for the different values of the parameters of the model, we used a Monte Carlo based cooling method. In this

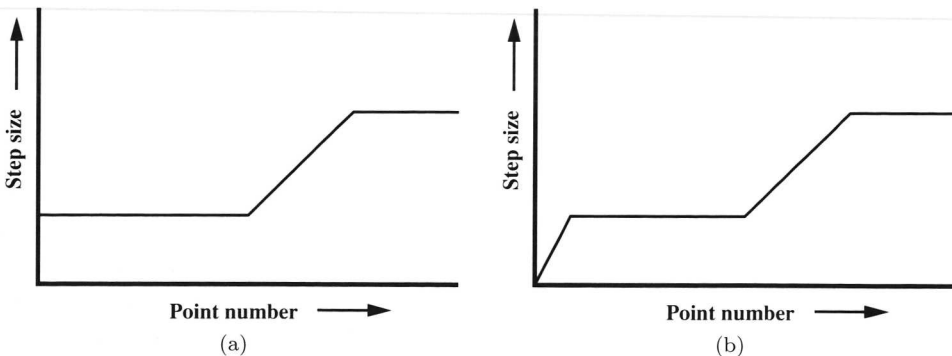


Figure 5.2: The two different types of lattices. The first part covers the core structure of the defects where the second part captures the region where the gauge fields - which have a much smaller mass - show nontrivial behavior. The only difference of a lattice of type (b) with respect to lattice of type (a) is a few extra lattice points near  $r = 0$  and  $z = 0$ .

method one introduces a temperature and gives a configuration with energy  $E$  a weight factor equal to  $e^{-\frac{E}{T}}$ . In the limit of  $T \rightarrow 0$  only the configuration with the lowest energy survives. Assuming there are no flat directions this procedure selects a unique configuration. With the help of a Monte Carlo mechanism different configurations are sampled. We keep sampling at a specific temperature as long as the energy of the system averaged over a preset number of sweeps<sup>3</sup> (typically 10) decreases and do this a minimal number of times (typically 3). When this average energy no longer decreases we lower the temperature (typically by 10%) and repeat the process until the total energy drop at a specific temperature becomes lower than a predetermined relative energy change (typically  $\sim 10^{-6}\%$ ). During this process we keep the acceptance rate of the Monte Carlo steps locally fixed for all fields. This means that we introduced a maximum step size for each field at each position and automatically adjust it to get the preferred acceptance rate. Since the change due to temperature change is easily captured we determined the desired maximum step sizes in the beginning of the cooling mechanism and further only correct for the trivial temperature changes, i.e., as  $T$  changes in  $aT$ ,  $\delta_{field}$  changes in  $\sqrt{a}\delta_{field}$ . This assumes that the energy change depends quadratically on the field change which is what one naively expects near a stable configuration, and indeed, that criterion worked nicely.

The procedure we just described is used to determine stable configurations within our ansatz for the different values of the parameters of the model. To be able to determine the meta-stability and instability regions of the monopole in the parameter space of the model we perform hysteresis type experiments. This means that we determine the lowest energy configuration for a specific point in the parameter space and use this configuration as the starting point for the determination of a stable configuration at a point nearby in the parameter space. As the change in the parameter space is only small one would expect the new configuration also to be close to the previous

<sup>3</sup>In one sweep all variables undergo one Monte Carlo step, i.e., are allowed to change once.

one. We determine the new configuration again with the help of the cooling method<sup>4</sup>. We repeat this process and move along a trajectory in the parameter space and back again. We choose these paths such that the lowest energy configurations on each end of the trajectory are different type of configurations: a spherical monopole and a Cheshire charged Alice ring. To keep things numerically simple we keep the mass of the gauge fields constant during a hysteresis experiment. This restriction selects specific trajectories in the two dimensional parameter space, which are given by:

$$\frac{m_A}{m_2} = \frac{2 \left( \frac{m_A}{m_2} \right)^{\frac{1}{3}}}{3 \sqrt{\frac{1}{3} + \left( \frac{m_1}{m_2} \right)^2}}, \quad (5.11)$$

with  $\left( \frac{m_A}{m_2} \right)^{\frac{1}{3}}$  the value of  $\frac{m_A}{m_2}$  at the minimal value of  $\frac{m_1}{m_2} = \frac{1}{3}$ .

This restriction allows us to keep the total space covered by the same lattice throughout the hysteresis. In a single hysteresis experiment the size of the core does not change much, so we keep the lattice fixed throughout a single hysteresis experiment.

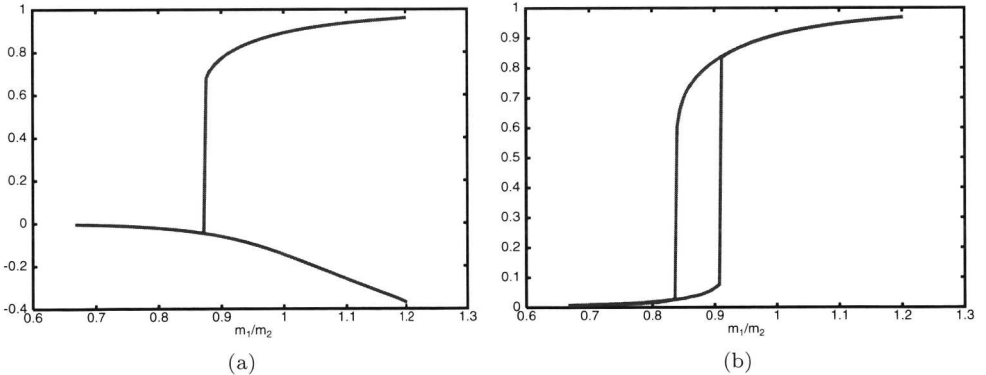


Figure 5.3: The two typical results of the hysteresis experiments for the different lattice types projected on the  $\frac{m_1}{m_2}$ -axis. Figure (a) corresponds to a lattice of type (a) and figure (b) corresponds to a lattice of type (b).

Figures 5.3(a) and (b) show the typical hysteresis results. The figures show the values of the field variable  $\frac{\phi_1}{\sqrt{6}f}$  at  $r = z = 0$ . This variable is a normalized order parameter in the sense that its value equals zero for the spherical monopole, and one for the Alice ring. A negative value of the order parameter is also possible and corresponds to a

<sup>4</sup>The temperature at which the secondary cooling process starts is smaller than the starting temperature of the initial cooling process. This starting temperature of the secondary cooling processes determines the energy barriers which can be overcome. Only in the limit where this temperature goes to zero can one really claim that a configuration becomes unstable. However for finite temperature one can still show the instability under small, but finite, perturbations. This is what we mean if we claim to find an instability of a specific type of configuration.

new type of configuration, the so called *split core*, see figure 5.4(c) and also [92, 93]. Figure 5.3(b) shows what one would expect for a hysteresis type of experiment for a lattice of type (b) while figure 5.3(a) shows a different behavior and corresponds to a lattice of type (a).

In figure 5.3(a) the split core configuration appears and although this configuration typically has more energy then a Cheshire charged Alice ring configuration, it does appear to be meta-stable. In [92, 93] this object was discussed for the global analog of AED, a nematic liquid crystal theory, and it was argued that this configuration is due to the cylindrical symmetry restriction of the ansatz used to explore the solution-space. Here we found that it might as well be just a lattice artifact as it depends on the lattice type used in the hysteresis experiments. Although this split-core configuration may be viewed as an undesirable feature caused by lattice and/or symmetry artifacts, we will see that it can be turned into a useful tool.

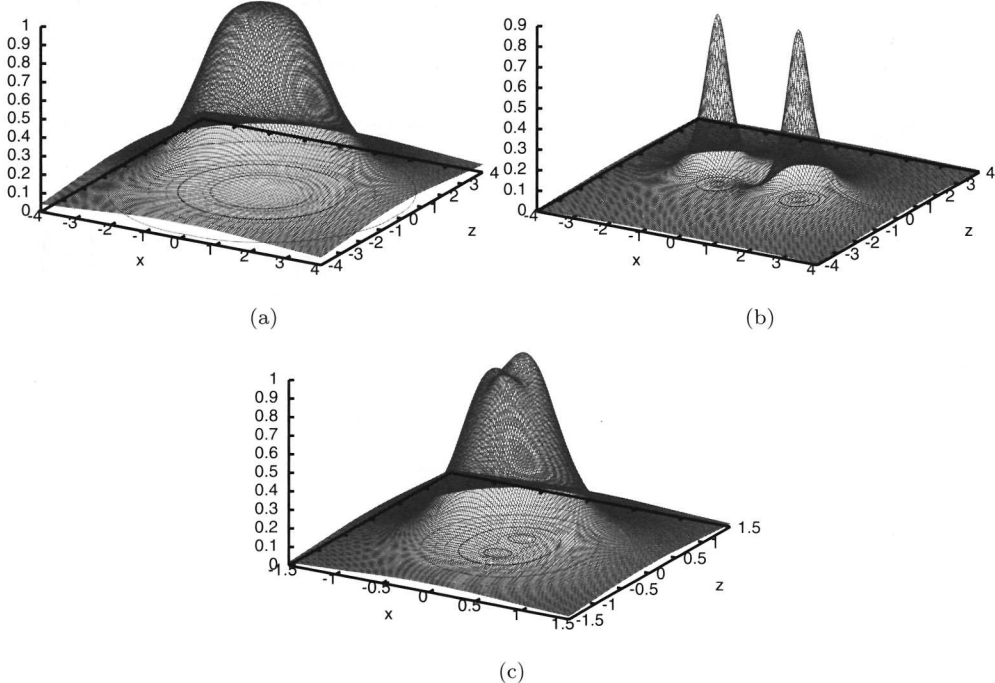


Figure 5.4: These figures show the three typical core structures we encountered in the numerical simulations. All three figures show a slice of the core structure at  $y = 0$  and in the figures the value of  $1 - \frac{\text{Tr}\Phi^2}{6f^2}$  is plotted. In figure (a) we plotted the core structure of the spherically symmetric magnetic monopole at  $\frac{m_1}{m_2} = 0.57$  and  $\frac{m_A}{m_2} = 0.0095$ . In figure (b) we plotted the core structure of the magnetically Cheshire charged Alice ring at  $\frac{m_1}{m_2} = 0.88$  and  $\frac{m_A}{m_2} = 0.0073$  and in figure (c) we plotted the core structure of the split core configuration at  $\frac{m_1}{m_2} = 1.12$  and  $\frac{m_A}{m_2} = 0.0425$ .

### 5.4.3 A typical set of experiments

As mentioned before we do hysteresis type experiments along specific trajectories in the parameter space of the model. Next we look at a typical set of such experiments. We did the hysteresis experiment for three different numbers of lattice points, where we only changed the number of lattice points describing the core of the configuration. One could of course also change the number of points outside the core but we found that that did not make any difference in the observables we examined and did not affect the stability of the configurations. We performed numerical simulations with  $25 \times 25$  ( $27 \times 27$ ),  $50 \times 50$  ( $54 \times 54$ ) and  $100 \times 100$  ( $108 \times 108$ ) lattice points describing the core structure for each line in the parameter space we considered. The figures 5.5(a-d) are the typical results of such an investigation. The figures show two different observables: the relative energy difference of the two branches of the hysteresis, and the quantity  $\frac{\phi_1(0,0)}{\sqrt{6}f}$ . The figures 5.5(a) and 5.5(b) belong to lattices of type (a) and the figures 5.5(c) and 5.5(d) belong to lattices of type (b). All figures show the results obtained with the three different number of lattice points, with the lines A, B and C corresponding to  $25 \times 25$  ( $27 \times 27$ ),  $50 \times 50$  ( $54 \times 54$ ) and  $100 \times 100$  ( $108 \times 108$ ) points describing the core structure respectively.

Let us first compare the figures 5.5(a) and 5.5(c). These figures show the values of  $\frac{\phi_1(0,0)}{\sqrt{6}f}$ . In both figures we see that qualitatively the lines A, B and C do not differ very much, but quantitatively they do. The steep part of the lines corresponds to the local instability of the Cheshire charged Alice ring and the spherical monopole. In both figures 5.5(a) and 5.5(c) we see that the Alice ring becomes locally unstable with respect to the monopole for low enough values of  $\frac{m_1}{m_2}$ . In figure 5.5(c) we see that for large enough values of  $\frac{m_1}{m_2}$  the monopole becomes unstable with respect to the Alice ring, whereas in figure 5.5(a) we see that the monopole slowly transforms into a split core configuration, see figure 5.4(c), and does not become locally unstable with respect to the Alice ring. In figure 5.5(b) we do see that this split-core configuration is globally unstable with respect to the Alice ring configuration as it costs more energy.

Now let us examine and compare the figures 5.5(b) and 5.5(d). First we note that the relative energy differences are very small, being of the order of pro-mils. This is one of the reasons why the minimal relative energy difference step in the cooling mechanism is chosen so small, of the order of  $10^{-5}$  pro-mil. In the regions where both branches of the hysteresis give the same configuration, see figures 5.5(a) and 5.5(c), the relative energy difference is equal to zero on the scale of the figures 5.5(b) and 5.5(d). The other segment of the curves is the interesting part, in figure 5.5(b) and 5.5(d). The point where this segment of the curves goes to zero is the point where the spherically magnetic monopole solution is no longer the lowest energy configuration within our ansatz, i.e., it is the point where the monopole becomes globally unstable. As we use more lattice points to probe this meta-stability this point moves only very slightly. Typically one should extrapolate the results to infinitely many points, but here we can use a different approach. We will exploit the results of the two different types of lattice. In the limit of infinitely many lattice points both lattice types will move

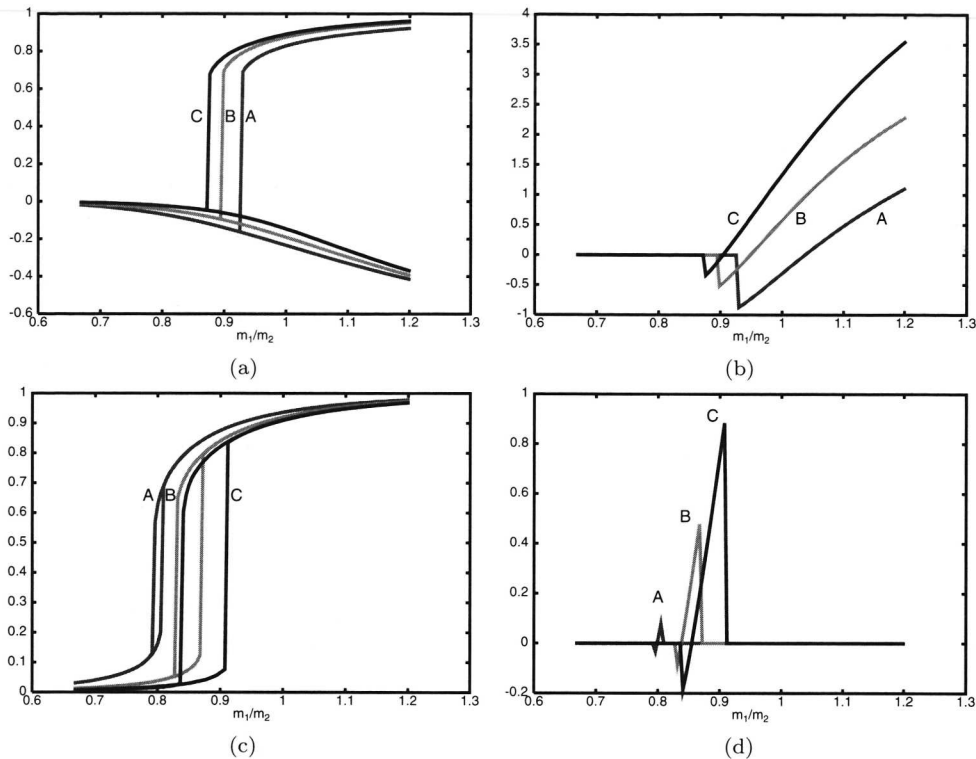


Figure 5.5: These figures show the results of a typical set of experiments of a specific line in the parameter space, with the results projected on the  $\frac{m_1}{m_2}$ -axis. Figures (a) and (b) correspond to a lattice of type (a), while figures (c) and (d) correspond to a lattice of type (b). In the figures (a) and (c) the value of  $\frac{\phi_1(0,0)}{\sqrt{6}f}$  is plotted, while in the figures (b) and (d) the relative energy differences of the two branches of the hysteresis plotted in pro-mils. The lines A, B and C correspond to  $25 \times 25$  ( $27 \times 27$ ),  $50 \times 50$  ( $54 \times 54$ ) and  $100 \times 100$  ( $108 \times 108$ ) lattice points respectively describing the core structure.

to the same point. However in the figure 5.5(b) we see that this point is approached from the right while in figure 5.5(d) it is approached from the left<sup>5</sup> when increasing the number of lattice points. Obviously this helps us to determine the position of the point where the monopole becomes globally unstable, as well as the error in the position of the point. So we may turn the lattice dependence into a useful tool to determine the global stability of the spherically symmetric monopole solution.

For most trajectories through the parameter space the same feature can be used to determine the point where the Alice ring configuration becomes locally unstable with respect to the monopole. However this point is not as interesting, since the Alice ring configuration is not necessarily an exact solution to the equations of motion.

<sup>5</sup>We observed this feature for all the trajectories through parameter space we considered.

Both lattice types also show a local instability of the spherically symmetric monopole solution. In figure 5.5(c) this happens at a clear point, but from figure 5.5(a) where the monopole changes into a split-core configuration, it is a bit harder to fix the point where this happens as it appears to be a continuous process. Although the position of this point is unclear, from figure 5.5(a), it is at least clear that this point moves in the same direction for both types of lattices as follows from figures 5.5(a) and 5.5(c). With the help of the results of both types of lattice we determine the global instability point of the spherically symmetric monopole solution and local instability point of Alice ring configuration. To determine the monopole instability point we only use the results from the lattices of type (b) as they clearly show the point where the monopole solution becomes locally unstable.

### 5.5 The results

Let us now turn to results of our investigations. First we describe how we extracted the results from the hysteresis type of experiments. There are two important results. In the first place, there is the line bounding the region in parameter space where the spherically symmetric magnetic monopole solution is no longer the lowest energy configuration. Crossing that line the solution only becomes meta-stable. Although our variational method does not prove that the configuration which has the lowest energy is a Cheshire charged Alice ring solution, in that case it actually does imply it, as we find that a Cheshire charged Alice ring configuration minimizes the energy for those parameter values within our ansatz. In the second place there is the other line bounding the region where the spherically symmetric magnetic monopole solution is no longer a locally stable solution. Finally we also determined the line at which the Alice ring configuration becomes locally unstable, but as explained before, this line is of least interest as the Alice ring configuration (with our ansatz) is typically not a solution to the equations of motion of the model.

In figure 5.6(a-c) we give the results for the meta-stability and instability lines. Figure 5.6(c) shows the meta-stability line for the spherically symmetric magnetic monopole solution. We showed in section 5.4.3 that we use the results of both lattice types to determine the monopole meta-stability line. As the meta-stability lines determined with the help of the two lattice types move oppositely and towards each other for an increasing number of lattice points, we use both results to determine the meta-stability line. The plot shows the lines on which we did the hysteresis type of experiments, the two monopole meta-stability lines determined by the different lattice types and a shaded region which is to represent the error in the position of the monopole meta-stability line. Thus we did not extrapolate the results from both types of lattices to an infinite number of lattice points we just used the results from the lattices with the most lattice points to corner the meta-stability line, see figure 5.6(c). This line shows that the spherically symmetric magnetic monopole is not always the lowest energy solution and cuts the parameter space into two regions.

To determine the position of the instability line of the spherically magnetic monopole

solution, see figure 5.6(b), we just use the results from the type (b) lattices as these show a clear point where the monopole becomes unstable. This does mean we have to extrapolate our results to a lattice with an infinite number of points. For all lines in the parameter space we investigated we observed that the change of the position, projected on the  $\frac{m_1}{m_2}$ -axis, of this point from the  $27 \times 27$  to the  $54 \times 54$  lattice is about twice as big as the change in the position from the  $54 \times 54$  to the  $108 \times 108$  lattice. We estimate the position of the monopole instability point by extrapolating this behavior to a lattice of an infinite number of lattice points. This means that the estimated position of the instability point lies at the same distance from the  $108 \times 108$ -point as the  $54 \times 54$ -point only on the other side. The error we estimate as twice this distance. In figure 5.6(b) we plotted these results. We plotted the lines on which we did the hysteresis experiments. The shaded region is to represent the error in the position of the monopole instability line and we plotted the instability line obtained from the data of the  $108 \times 108$  lattices. The estimate of the instability line itself is not plotted but is right in the middle of the shaded region.

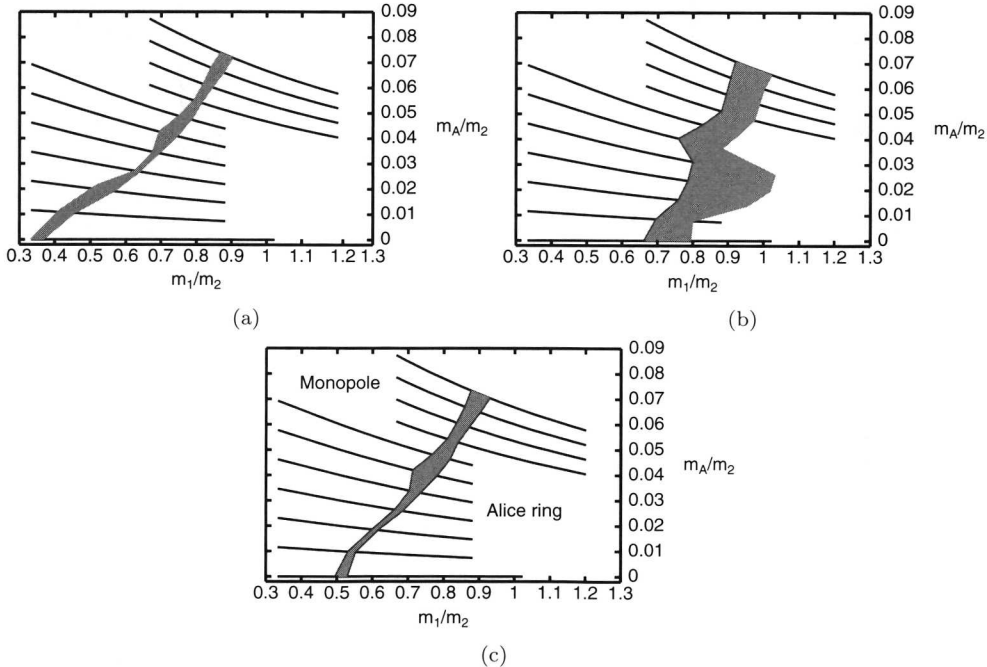


Figure 5.6: These figures show the stability results from the hysteresis type of experiments we did on the specific lines in the parameter space of the model. The shaded regions give the errors of the lines. Figure (a) shows the local instability line of the Alice ring configuration. Figure (b) shows the monopole instability line and figure (c) shows the monopole meta-stability line.

In figure 5.6(a) we plotted the instability line of the Alice ring configuration. For most of the lines through the parameter space we used the same technique as for the

monopole meta-stability line, for the rest we used the same principle as we used for the monopole instability line.

Again we note that due to the fact that we used a variational approach the monopole meta-stability and instability lines are upper bounds in the sense that if less restrictions are forced upon the configurations these lines can only move to the left, i.e., in favor of the Cheshire charged Alice ring.

It is quite easy to understand why the Alice ring is the lowest energy configuration in the limit of large values of  $\frac{m_1}{m_2}$  and the monopole is the lowest energy solution in the limit of small  $\frac{m_1}{m_2}$ . The two masses  $m_1$  and  $m_2$  correspond to energy costs in deviations of the Higgs field from the vacuum manifold. Deviations pure in the 'length' of the Higgs field correspond to  $m_1$ . While deviations in the non-uniaxial direction correspond to  $m_2$ . In the limit of  $\frac{m_1}{m_2} \rightarrow 0^6$  the non-uniaxial deviations are suppressed and the spherically symmetric (uniaxial) magnetic monopole is the lowest energy solution. In the limit of  $\frac{m_1}{m_2} \rightarrow \infty$  one would expect an 'escape' in the non-uniaxial direction. This signals the meta-stability of the monopole and implies that the Cheshire charged Alice ring is the lowest energy solution. In this case the length of the Higgs field never becomes zero<sup>7</sup> as can be seen in figure 5.4(b), i.e., the quantity  $\left(1 - \frac{\text{Tr}\Phi^2}{6f^2}\right)$  never becomes equal to one.

We pointed out that one of the main factors determining the monopole core meta-stability is the mass ratio  $\frac{m_1}{m_2}$  of the charged and neutral Higgs particles. As the mass of the charged excitation becomes much smaller than the mass of the neutral excitation the 't Hooft Polyakov magnetic monopole is expected to become meta-stable. Clearly this argument holds generically and one expects a core meta-/instability to be a general feature of the 't Hooft Polyakov magnetic monopole in models with charged Higgs excitations. The nice thing of Alice type models is that they naturally suggest an alternative configuration to the 't Hooft Polyakov type monopoles: the magnetically Cheshire charged Alice loop.

## 5.6 Conclusions and outlook

In this chapter we investigated the core structure of the unit charge magnetic monopole and discussed the numerical methods we employed in some detail. We showed that the core structure of the magnetic monopole is not necessarily spherically symmetric. The model has three mass scales, two of them refer to the Higgs field, one to its length and the other to deviation from the uniaxial direction. The third mass scale is set by the mass of the broken gauge fields. The topologically non-trivial boundary conditions can be met by an "escape" in a non-uniaxial direction. This possibility allows for the length of the Higgs field to stay finite in the core and not go to zero as

<sup>6</sup>Note that this limit can in fact not be taken as the minimum value of  $\frac{m_1}{m_2}$  at which the broken vacuum is still the true vacuum is equal to  $\frac{1}{3}$ . For smaller values of  $\frac{m_1}{m_2}$  the unbroken vacuum is the true vacuum. We come back to this point in the conclusions and outlook section.

<sup>7</sup>Not shown here, but we also find that the minimum length of the Higgs field in the case of the Alice loop increases for increasing  $\frac{m_1}{m_2}$  as this argument indicates.

would be necessary otherwise. As the ratio of the masses,  $\frac{m_1}{m_2}$ , increases it becomes harder energetically to decrease the length of the Higgs field and one would expect an escape in the non-uniaxial direction.

At the end of section 5.5 we argued that a core instability of the 't Hooft Polyakov magnetic monopole is a general feature of models with charged excitations of the Higgs field. The instability occurs in the region of the parameter space where the charged excitations are much lighter than the neutral excitations. In Alice electrodynamics there is also an other, somewhat independent motivation to question the core stability of the spherically symmetric magnetic monopole, provided by the possibility of an Alice ring which can carry a magnetic Cheshire charge.

Within our ansatz we determined the meta- and instability regions of the spherically symmetric magnetic monopole. We also found that, as expected, the competing configuration is the magnetically Cheshire charged Alice ring. We did also stumble upon the somewhat unwanted split-core configurations but fortunately they never became the lowest energy solutions. As we used a variational approach we cannot claim that the Alice ring configurations we found are exact solutions to the equations of motion. However they do have every feature which one would expect from an exact Alice ring solution. Also, because we used a variational approach the regions of meta-stability and global-stability of the spherically magnetic monopole are with respect to energetic upper bounds so that with respect to the exact solutions, these regions can only become smaller.

As a final comment we want to come back to the fact that the minimum value of  $\frac{m_1}{m_2} = \frac{1}{3}$  for which the broken vacuum is the true vacuum. In section 5.5 we gave a simple explanation of why the spherically magnetic monopole becomes globally unstable in the limit of large values of  $\frac{m_1}{m_2}$ . In the opposite limit one would expect the monopole to be the spherically magnetic monopole to be the global stable solution. However as the minimum value of  $\frac{m_1}{m_2} = \frac{1}{3}$  there is no guarantee that this ever happens. It could just be that in this or similar models the 't Hooft Polyakov type magnetic monopole is never globally stable.



# Chapter 6

## Charge instabilities in (2+1)-dimensions

In the previous two chapters we investigated possible instabilities of topological defects. In this chapter we will investigate another instability due to the presence of topological defects. We describe a charge instability in Alice electrodynamics in (2+1)-dimensions due to the possible creation of a pair of Alice fluxes out of the vacuum following [95]. In a sense it is the two dimensional dual analog of the monopole core instability we investigated in the previous chapter. The final state is one in which the electric charge is completely delocalized, i.e., it is carried as Cheshire charge by the flux pair, which gets infinitely separated. We determine the decay rate in terms of the parameters of the model. The relation of this phenomenon with other salient features of 2-dimensional compact QED, such as linear confinement due to instantons/monopoles, and the introduction of a so called Cheshire current is discussed in the appendix.

### 6.1 Introduction

As we saw before AED contains magnetic monopoles, just as compact  $U(1)$  gauge theory. As is well known the monopoles become instantons in two dimensional electrodynamics and lead to confinement of charge, see [58] and [59]. The potential between two static charges becomes linear and the string tension due to the instantons was determined by Polyakov in [59] and is given by:

$$T \propto g^2 \exp\left(-\frac{S_{inst}}{2g^2}\right) \quad , \quad (6.1)$$

with  $S_{inst}$  the action of the instanton in (2+1)-dimensions, or the mass of a monopole in (3+1)-dimensions, and  $g$  the (dimension-full) coupling constant. In compact Alice

electrodynamics there are instantons as well. One therefore in principle expects the same confining potential between charges. However, as we will see, whether this confinement will be realized physically depends on the parameters in the model.

With respect to the monopoles/instantons in AED we have, see chapter 5, made another observation, namely that the core structure of a magnetic monopole may be unstable and deform into a ring of Alice flux carrying a Cheshire magnetic charge. This feature, however is not expected to bear on the confinement mechanism as such, because the core structure does not affect the long range behavior of the fields. We return to this point towards the end of the chapter.

We saw before that the topological structure of AED is richer than the topology of ordinary electrodynamics, as it supports topologically stable Alice fluxes. In this chapter we will show that these fluxes may have a dramatic influence on the infrared behavior of the potential between two static charges. In the infrared region the potential will not grow linearly as in ordinary compact electrodynamics, but the potential will saturate and become constant at a scale set by the mass of the Alice flux. This follows from the fact that a static charge will be unstable under the creation of two Alice fluxes and the possibility of (induced) Cheshire charges carried by such a pair. We calculate the decay rate of a charge due to this instability, into a state where the charge is completely delocalized, i.e., virtually disappeared.

Before turning to a detailed treatment of this remarkable charge instability, it is useful to briefly discuss some generic features of the parameter space we are considering. To be as flexible as possible in separating the various dynamical aspects of the theory, we like to think of a lattice version of the theory (as discussed in chapter 3), because in that setting one can introduce different mass scales for the fluxes ( $m_f$ ), for the monopoles ( $m_m$ ), and possibly also for dynamical, charged degrees of freedom ( $m_q$ ) by hand. Of course in continuum versions of the model, see chapter 2, one often finds that these physical scales may be linked and one is forced to restrict oneself to a smaller region of the parameter space than the one we explore in the remainder of this chapter.

The chapter is organized as follows. In section 6.2 we examine the classical configuration of a pair of Alice fluxes in the presence of a charge. We determine the field line pattern of such a configuration and the energy gain due to the introduction of flux pair. In section 6.3 we analyze the resulting charge instability in a semi-classical approximation and determine the action of the bounce solution for some specific decay channels. In the concluding section we discuss the relevance of our results in the broader context where one also takes the instantons into account. In the appendix we introduce the notion of a so called magnetic Cheshire current and point out its relation with electric Cheshire charge.

## 6.2 Alice fluxes in the presence of a charge

In this section we examine the classical field configuration of a pair of Alice fluxes in the presence of a charge. We first analyze this situation qualitatively which leads to

the conclusion that the pair of Alice fluxes will carry an induced (Cheshire) dipole charge. Here we will also examine some specific configurations in LAED in (3+1)-dimensions, see chapter 3, on the dipole behavior of an Alice loop and the effect this has on the dynamical response of the vacuum to the presence of an external charge. Then to see what the dipole behavior looks like, in (2+1)-dimensions, we determine the configuration of electric field lines generated by a conducting needle between two oppositely charged point charges. The conducting needle represents a pair of Alice fluxes (one at either end) with their core structure ignored. Finally, we will determine the energy gain due to the introduction of the needle/flux pair.

### 6.2.1 The induced Cheshire dipole

Let us now study the field configuration of a charge in the presence of an Alice loop (i.e., a pair in two dimensions). Due to conservation and quantization of charge, field lines cannot cross an Alice flux, a situation reminiscent to that of the Meissner effect in a super conductor. In fact, at first sight one would be tempted to interpret the whole collection of Cheshire phenomena as a manifestation of some exotic form of electric and/or magnetic super conductivity in the core of an Alice loop. However, this is not possible because the flux tube itself cannot carry electric/magnetic charge or current, see chapter 1. Let us now consider what happens if we create an Alice loop in the neighborhood of a charge.

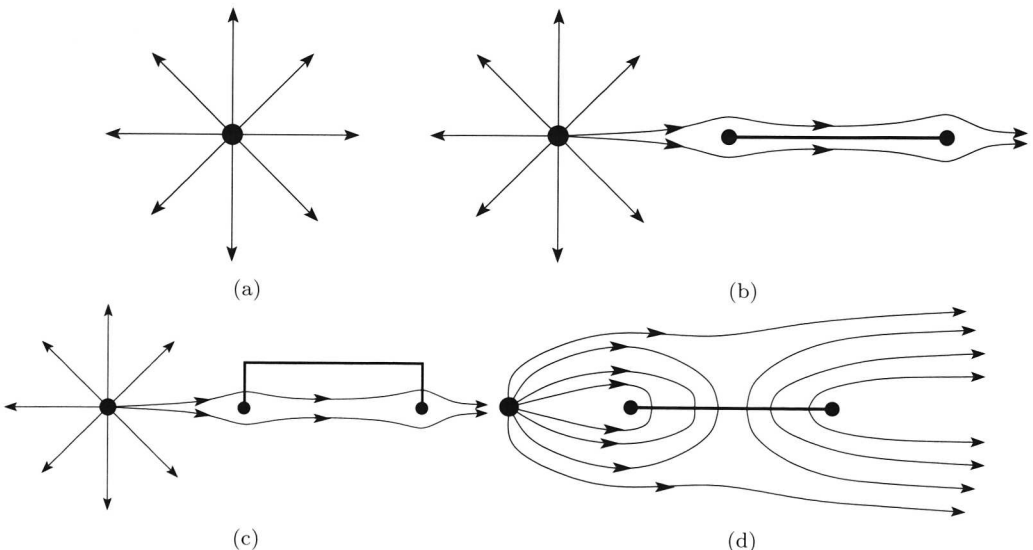


Figure 6.1:

A sequence of figures that leads to the correct field line configuration for two Alice fluxes in the presence of a charge. Figure (a) shows a single charge in figure (b) a pair of fluxes is created in the vicinity of the charge but with the wrong field line pattern as follows from deforming  $\mathbb{Z}_2$ -gauge sheet, figure (c). The correct field line pattern is given in figure (d).

A first guess of how a radial field would be affected due to the creation of the Alice loop might be the same as for the case of a super conducting loop, i.e.. the field lines would be pushed away by the loop. However the analysis performed in figure 6.1 yields a very different picture<sup>1</sup>. Some of the field lines close around the first flux while an equal number emanates from the sheet to close around the second flux and go off to infinity, see figure 6.1. Thus the total charge carried by the Alice flux configuration stays zero, as it should, but the flux configuration acquires an induced electric (Cheshire) dipole moment. For convenience we only examine cases where the flux pair lies on the line connecting the charges. The electric field lines have to be perpendicular to the line segment between the two fluxes, because (i) the electric field lines need to change sign when going around a single flux and (ii) the reflection symmetry through the horizontal axis of the configuration.

In certain symmetric configurations the  $\mathbb{Z}_2$ -sheet may be considered to act like a conducting plate from which follows that the charge is pulled towards the Alice loop. However, one should be careful with this analogy because the conducting plate boundary condition of the  $\mathbb{Z}_2$ -sheet only holds in the particular gauge that satisfies the obvious symmetry condition. In a general gauge the  $\mathbb{Z}_2$ -sheet has an arbitrary shape and cannot be interpreted as a conducting plate. On the other hand, the field line pattern closing partially around the first and the second flux is gauge invariant. We conclude that the charge induces a dipolar Cheshire charge on the Alice loop (or in 2 dimensions, on the pair of fluxes). This is a natural generalization of the result obtained in [5], but, straightforward as the generalization may be, there is an important aspect to it. As we mentioned before, a system of two fluxes or an Alice loop can be in the topologically trivial sector of the theory and thus may play a role in the dynamical response of the vacuum to an external charge.

As an inter-mezzo that provides extra support to these findings we will briefly investigate two specific configurations in LAED in (3+1)-dimensions, see chapter 3. First we will show that an Alice loop can carry a (magnetic) dipole Cheshire charge in LAED. Then we will look at the dynamical response of the vacuum to an external magnetic monopole pair.

To investigate the possibility of a dipole Cheshire charge in LAED we will examine a configuration with a fixed monopole, anti-monopole and Alice loop. All objects are in one plane and the Alice loop lies in the middle of the two monopoles<sup>2</sup>. We will examine this configuration in the limit of  $g \rightarrow 0$ , the naive classical limit, and  $m_{flux} \rightarrow \infty$ . In this limit no extra Alice fluxes appear and we will work in the  $\mathbb{Z}_2$  gauge where the only  $\mathbb{Z}_2$  sheet is the minimal surface spanned by the Alice loop. In this limit there appear to be two possibilities: either there are no extra monopoles and the Alice loop will presumably behave as a (magnetic) dipole configuration or there is a compensating monopole stuck to each fixed monopole<sup>3</sup>. Which of the two configurations has the

---

<sup>1</sup>Thus first one assumes the naively expected configuration to be formed in analogy with a pair of superconducting wires. However, if one deforms the  $\mathbb{Z}_2$ -sheet (which is just a gauge artifact) bounded by the fluxes one sees that that must be wrong, suggesting the correct and consistent configuration.

<sup>2</sup>On a periodic lattice 'in the middle' is of course not possible, but we mean that the distance the other way around is larger.

<sup>3</sup>If we had an extra bare mass term for the monopole we could simply send it to infinity to force

## 6.2. Alice fluxes in the presence of a charge

lowest energy depends on the different length scales in the configuration. Now we will consider a configuration where there are no extra monopoles present.

In this configuration the monopole, the anti-monopole and the Alice loop lie in the  $xy$  plane. In figure 6.2 we plotted the  $z$  component of the magnetic field just above and below the plane in the dual lattice in which the configuration of the monopole, the anti-monopole and the Alice loop lies. The monopole, the anti-monopole and the Alice loop have not been plotted, but it should be clear where they are. In this figure we see that the  $z$  component of the magnetic field just above the plane in which the objects lie is, going from the left to the right, positive above the first monopole, becomes negative above the Alice loop then it becomes positive on the other end of the Alice loop and finally is negative above the last monopole. This shows that the Alice loop gets an induced (magnetic) dipole moment, as if the Alice loop is a conducting plate, in the presence of charges, just as we expected.

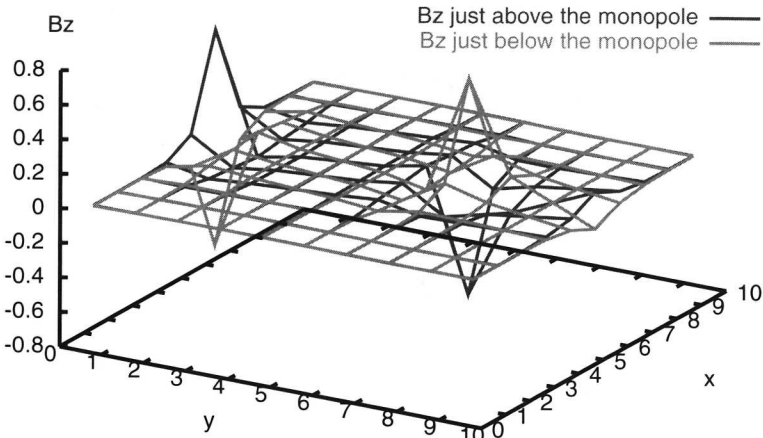


Figure 6.2: This plot shows the  $z$  component of the magnetic field just above and just below the plane in which the monopoles and the Alice loop lie. It shows the induced dipole behavior of the Alice loop in the presence of a charge.

So an Alice loop can act as an induced dipole in the presence of charges. This implies that dynamical Alice loops can screen a charge as they can help to polarize the vacuum. Now we will look at a configuration of a fixed monopole and anti-monopole in the background of dynamical Alice fluxes, i.e., we are not in the limit of  $m_{flux} \rightarrow \infty$ . So dynamical Alice loops can form and can possibly screen the monopoles. We take a small value of  $g$  to make sure that no other monopoles form and we take  $m_{flux}$  such that the background flux density is around 0.03. Thus there are some fluxes around, but they are not condensed in the bulk.

In figure 6.3 we plotted some specific height lines of the flux density in the  $x-t$ ,  $y-$

the extra monopole pair to disappear and only the desired configuration is left.

$t$  and  $z$ - $t$  directions and the positions of the monopoles. The monopole is fixed at  $(5\frac{1}{2}, 2\frac{1}{2}, 4\frac{1}{2})$  and the anti-monopole at  $(5\frac{1}{2}, 6\frac{1}{2}, 4\frac{1}{2})$ . The flux density peaks around the two monopoles, i.e., screening the two monopoles. From this and the fact that an Alice loop in the presence of a charge gets a dipole moment we conclude that in LAED Alice loops do screen charges.

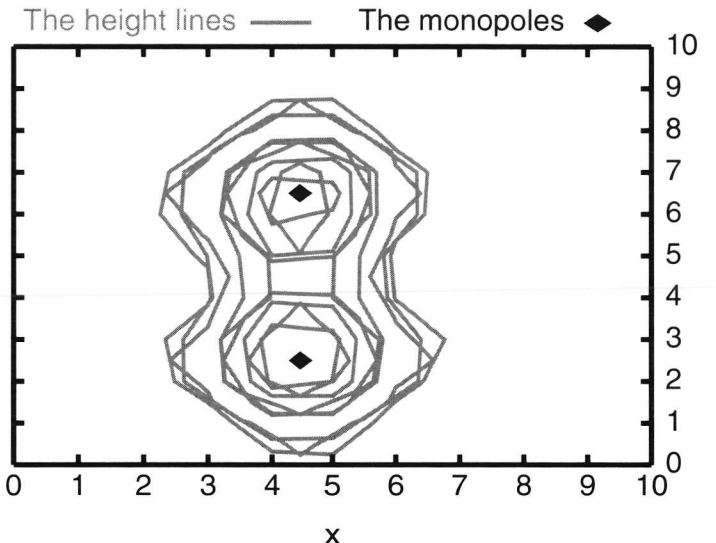


Figure 6.3: This plot shows some specific height lines for the flux density in the  $x$ - $t$ ,  $y$ - $t$  and  $z$ - $t$  directions and the positions of the monopoles.

After this brief digression into the screening effects of Alice loops in (3+1)-dimensions we now return to the discussion in (2+1)-dimensions. The dipolar behavior of an Alice flux pair in the presence of a charge can have important consequences. Just like a particle anti-particle pair, these pairs may contribute to the screening of a bare charge, but an even more drastic consequence is possible. The scenario runs as follows. One of the fluxes can absorb the point charge, after which the charge would be carried as a Cheshire charge by the flux pair. This Cheshire charge acts like a fictitious charge distribution along the line connecting the fluxes, generating a repulsive force between the two fluxes<sup>4</sup> causing the fluxes to move away from each other. This would mean that the Cheshire charge would increasingly spread and weaken, put more bluntly, it effectively just disappears. The fluxes would cause an extreme case of charge delocalization. So, in two dimensions it therefore appears that in these type of theories, charge leaks away, implying the absence of any (static) charge.

<sup>4</sup>We assume for simplicity that a priori there is no flux-flux interaction. This is not true in general, in the case of Nielsen-Olesen fluxes it depends on the value of the Landau parameter, but if the static forces are zero or repulsive, then the result obviously holds.

### 6.2.2 The field configuration

We now turn to the determination of the field configuration of a flux pair located between two oppositely charged point particles. We use the boundary conditions imposed by the fluxes but neglect the core structure of the fluxes. This boils down to calculating the electric field configuration of a conducting needle located between two oppositely charged point particles, where the needle lies on the line connecting the charges.

Two-dimensional electrostatics (i.e., potential theory) has the convenient property that it is conformally invariant. Exploiting this conformal invariance one can construct explicit solutions satisfying the boundary conditions imposed by the geometry we are interested in. We start with determining the solution of a charge in the presence of a conducting disc with the help of the method of images. Then we use a conformal transformation which maps this conducting disc into a conducting needle/flux pair, see figure 6.4. Since a conformal transformation is angle preserving, a conductor gets mapped to a conductor.

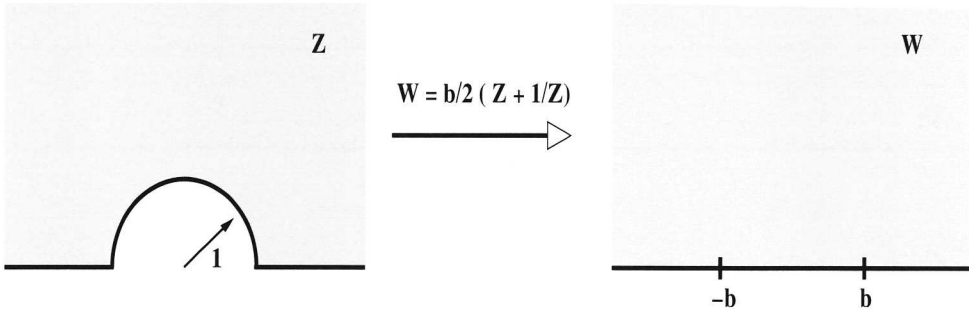


Figure 6.4: The conformal transformation,  $w = \frac{b}{2} (z + \frac{1}{z})$ , which maps the conducting disc of radius one into a conducting needle of length  $2b$ .

To construct the configuration of two charges with a flux pair in between, we first determine the single charge case and then superpose two of these configurations. We determine the potential of a charge in the presence of a conducting disc with the help of the method of images. It is similar to the textbook example of the charge in the presence of a conducting ball in three dimensions, but for the case at hand the charge of the image charges does not depend on the distance of the charge to the conducting disc. Making use of the identity,  $|\vec{n}_1 + a\vec{n}_2| = |a\vec{n}_1 + \vec{n}_2|$  with  $|\vec{n}_1| = |\vec{n}_2| = 1$ , one easily finds the potential  $\Phi(z)$ ,  $z = x + iy$ . The potential is given by:

$$\Phi(z) = \frac{Q}{2\pi} \left\{ \log |z - z_0| - \log \left| z - \frac{R^2}{|z_0|^2} z_0 \right| + \log |z| \right\} , \quad (6.2)$$

with  $R$  the radius of the conducting disc, whose center is located in the origin and  $z_0$  denotes the location of the charge. The field lines correspond with the height lines of

the function:

$$\Psi(z) = \frac{Q}{2\pi} \left\{ \arg(z - z_0) - \arg \left( z - \frac{R^2}{|z_0|^2} z_0 \right) + \arg(z) \right\} . \quad (6.3)$$

The results are plotted in figures 6.5a and 6.5b for the equipotential lines and the electric field lines respectively.

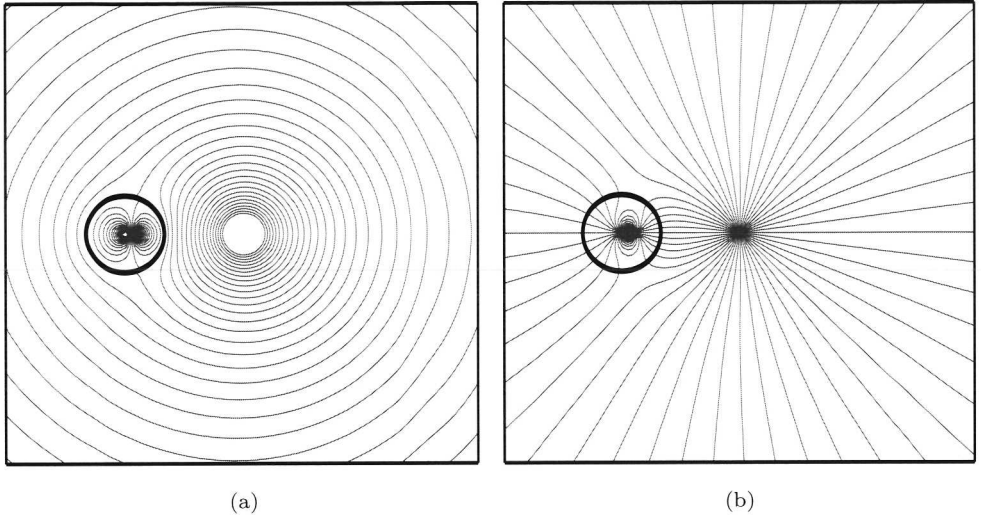


Figure 6.5: These figures show some of the equipotential lines, figure (a), and field lines, figure (b), of a charge in the presence of a conducting disc. The thick dark circle is the boundary of the conducting disc. The configuration inside this circle represents the 'image' charges.

We can use this solution to find the solution of a charge in the presence of a flux pair with the help of the conformal transformation given in figure 6.4. To be more general we first determine the configuration of two charges in the presence of a disc. This is straightforward since electrodynamics is linear in the sense that potentials just add. Thus for the situation of two (oppositely charged) charges we get the following potential:

$$\begin{aligned} \Phi(z) = & \frac{Q}{2\pi} \left\{ \log |z - z_1| - \log \left| z - \frac{R^2}{|z_1|^2} z_1 \right| - \log |z - z_2| \right. \\ & \left. + \log \left| z - \frac{R^2}{|z_2|^2} z_2 \right| \right\} . \end{aligned} \quad (6.4)$$

The field lines are now given by the height lines of the function:

$$\begin{aligned} \Psi(z) = & \frac{Q}{2\pi} \left\{ \arg(z - z_1) - \arg \left( z - \frac{R^2}{|z_1|^2} z_1 \right) - \arg(z - z_2) \right. \\ & \left. + \arg \left( z - \frac{R^2}{|z_2|^2} z_2 \right) \right\} . \end{aligned} \quad (6.5)$$

Let us now use the conformal transformation to map this solution to the solution of two charges in the presence of a flux pair located on the line connecting the charges. To be able to use the conformal map, of figure 6.4,  $R$  needs to be unity. We can get the desired configuration if the two charges and the disc also lie on one line and the disc is between the two charges. We rotate the system such that  $z_1$  and  $z_2$  are real. After this we can use the conformal map to map this solution to the solution of the flux pair between two oppositely charged point charges. This is done by replacing  $z$  by the corresponding function of  $w$ , which is given by:  $z = x + \sqrt{x^2 - 1}$  where we have defined  $x = \frac{w}{b}$  and will use corresponding definitions for  $x_1$  and  $x_2$ . This gives the following potential:

$$\begin{aligned} \Phi(x) = & \frac{Q}{2\pi} \left\{ \log \left| x + \sqrt{x^2 - 1} - x_1 - \sqrt{x_1^2 - 1} \right| \right. \\ & - \log \left| x + \sqrt{x^2 - 1} - \frac{x_1 + \sqrt{x_1^2 - 1}}{\left| x_1 + \sqrt{x_1^2 - 1} \right|^2} \right| \\ & - \log \left| x + \sqrt{x^2 - 1} - x_2 - \sqrt{x_2^2 - 1} \right| \\ & \left. + \log \left| x + \sqrt{x^2 - 1} - \frac{x_2 + \sqrt{x_2^2 - 1}}{\left| x_2 + \sqrt{x_2^2 - 1} \right|^2} \right| \right\} \end{aligned} \quad (6.6)$$

and the field lines follow from:

$$\begin{aligned} \Psi(x) = & \frac{Q}{2\pi} \left\{ \arg \left( x + \sqrt{x^2 - 1} - x_1 - \sqrt{x_1^2 - 1} \right) \right. \\ & - \arg \left( x + \sqrt{x^2 - 1} - \frac{x_1 + \sqrt{x_1^2 - 1}}{\left| x_1 + \sqrt{x_1^2 - 1} \right|^2} \right) \\ & - \arg \left( x + \sqrt{x^2 - 1} - x_2 - \sqrt{x_2^2 - 1} \right) \\ & \left. + \arg \left( x + \sqrt{x^2 - 1} - \frac{x_2 + \sqrt{x_2^2 - 1}}{\left| x_2 + \sqrt{x_2^2 - 1} \right|^2} \right) \right\} . \end{aligned} \quad (6.7)$$

The conformal transformation only correctly generates the solution in the upper half plane,  $Re(x) > 0$ . The solution in the lower half plane follows by the obvious symmetry of the problem. In figure 6.6(a) and 6.6(b) we plotted the resulting equipotential and field lines for the configuration.

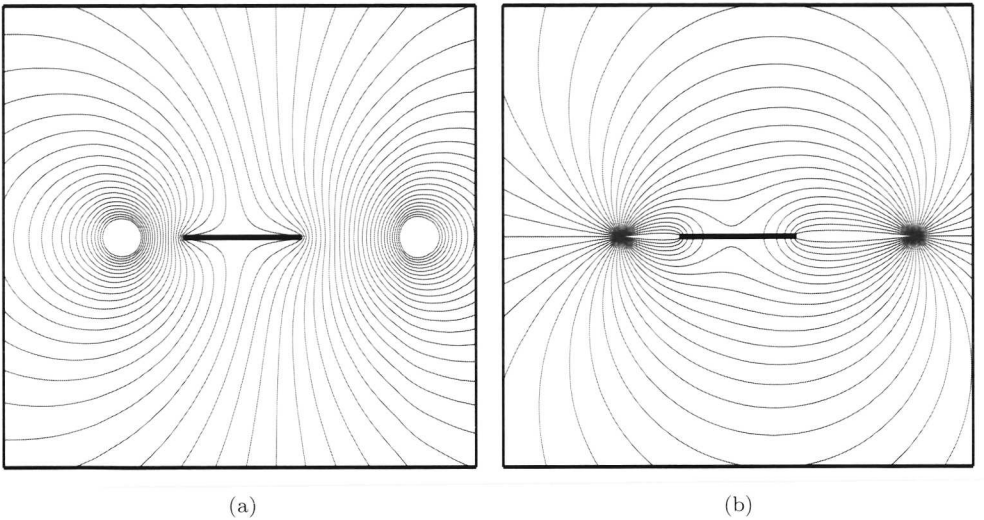


Figure 6.6: These figures show some of the equipotential lines, figure (a), and field lines, figure (b), of two oppositely charged charges in the presence of the Cheshire dipole carried by a pair of fluxes located at the endpoints of the black line segment.

### 6.2.3 The energy gain

In the previous subsection we determined the potential and the field configuration of a flux pair between two point charges. In this subsection we calculate the energy difference of this configuration with the (coulomb type) field configuration without the flux pair. To be able to determine the energy difference we have to regularize the expression, i.e., we introduce a UV cut off which will be removed later. With this cutoff the total energy difference is equal to the integrated energy density difference. Written in this form, the cutoff can be removed leaving the energy difference finite, and this is how we calculate the energy gain due to the presence of the flux pair. To simplify life the calculation is performed in  $z$  space, not in  $w$  space. So we use the conformal transformation, which is also just a convenient change of variables, to transform the solution back into  $z$  space and as an intermediate step, determine the energy gain due to the presence of a conducting disc and the energy cost due to the presence of a magnetic super conducting disc. The energy gain due to the presence of a flux pair is determined from these two results. The relation between these energy differences is given by:

$$\begin{aligned} \int \{E_{dipole} - E_{fpair}\} dw &= \int \{E_{mscdisc} - E_{disc}\} dz \\ &= \int \{E_{dipole} - E_{disc}\} dz - \int \{E_{dipole} - E_{mscdisc}\} dz , \end{aligned} \quad (6.8)$$

## 6.2. Alice fluxes in the presence of a charge

where  $E_{mscdisc}$  is the energy density of two opposite charges with a disc in the middle, which we identify as a magnetic super conductor (msc) as the electric field lines are parallel to it. This configuration is the configuration that one obtains after applying the inverse conformal transformation, thus from  $w$ -space to  $z$ -space, to the dipole configuration in  $w$ -space. First we will determine the energy gain due to the presence of a conducting disc. This yields the expression:

$$\begin{aligned}\Delta E_{disc} = & 2 \int_0^\pi \int_R^\infty \left\{ (\partial_r \Phi_2(r, \theta))^2 + \left( \frac{1}{r} \partial_\theta \Phi_2(r, \theta) \right)^2 \right. \\ & \left. - (\partial_r \Phi_1(r, \theta))^2 - \left( \frac{1}{r} \partial_\theta \Phi_1(r, \theta) \right)^2 \right\} r \ dr d\theta \\ & + 2 \int_0^\pi \int_0^R \left\{ (\partial_r \Phi_2(r, \theta))^2 + \left( \frac{1}{r} \partial_\theta \Phi_2(r, \theta) \right)^2 \right\} r \ dr d\theta \quad , \quad (6.9)\end{aligned}$$

with  $\Phi_1(r, \theta)$  given by formula 6.4 and  $\Phi_2(r, \theta)$  is given by formula 6.4 with  $R = 0$ . This gives:

$$\Delta E_{disc} = -\frac{Q^2}{2\pi} \log \left( \frac{(z_1^2 - R^2)(z_2^2 - R^2)}{(z_1 z_2 + R^2)^2} \right) \quad . \quad (6.10)$$

The energy gain due to the presence of a magnetically super conducting (msc) disc is determined by:

$$\begin{aligned}\Delta E_{mscdisc} = & 2 \int_0^\pi \int_R^\infty \left\{ (\partial_r \Phi_2(r, \theta))^2 + \left( \frac{1}{r} \partial_\theta \Phi_2(r, \theta) \right)^2 \right. \\ & \left. - (\partial_r \Phi_3(r, \theta))^2 - \left( \frac{1}{r} \partial_\theta \Phi_3(r, \theta) \right)^2 \right\} r \ dr d\theta \\ & + 2 \int_0^\pi \int_0^R \left\{ (\partial_r \Phi_2(r, \theta))^2 + \left( \frac{1}{r} \partial_\theta \Phi_2(r, \theta) \right)^2 \right\} r \ dr d\theta \quad , \quad (6.11)\end{aligned}$$

with  $\Phi_1(r, \theta)$  given by formula 6.4 and  $\Phi_3(r, \theta)$  by:

$$\Phi_3(z) = \frac{Q}{2\pi} \left\{ \log \left| \left( z + \frac{1}{z} \right) - \left( z_1 + \frac{1}{z_1} \right) \right| - \log \left| \left( z + \frac{1}{z} \right) - \left( z_2 + \frac{1}{z_2} \right) \right| \right\} \quad . \quad (6.12)$$

One obtains:

$$\Delta E_{mscdisc} = \frac{Q^2}{2\pi} \log \left( \frac{(z_1^2 - R^2)(z_2^2 - R^2)}{(z_1 z_2 + R^2)^2} \right) \quad . \quad (6.13)$$

For the case of  $R = 1$  we have  $E_{fpair} = \Delta E_{disc} - \Delta E_{mscdisc}$ . Thus we get:

$$E_{fpair} = -\frac{Q^2}{\pi} \log \left( \frac{(z_1^2 - 1)(z_2^2 - 1)}{(z_1 z_2 + 1)^2} \right) \quad . \quad (6.14)$$

This result is still in  $z$  language, i.e.,  $z_1$  and  $z_2$  need to be written in terms of  $w_1$  and  $w_2$ . This is done with the help of the conformal transformation,  $z = x + \sqrt{x^2 - 1}$ , and leads to the following expression for the energy gain:

$$E_{f\text{pair}} = \frac{Q^2}{\pi} \log \left( \frac{1}{2} \left( 1 + \frac{1 + x_1 x_2}{\sqrt{x_1^2 - 1} \sqrt{x_2^2 - 1}} \right) \right) . \quad (6.15)$$

We see that the energy gain due to creating a flux pair between two charges is basically unbounded. Moving the flux pair closer to one or both of the charges increases the energy gain. One expects that due to the renormalization of the charge this would not go on for ever, effectively one expects a UV cutoff.

Let us now investigate the single charge configuration, i.e., we send one of the charges to infinity. In this case the energy gain is given by:

$$E_{f\text{pair}} = -\frac{Q^2}{\pi} \log \left( \frac{4\sqrt{d}}{\left( 1 + \sqrt{d} \right)^2} \right) . \quad (6.16)$$

where  $d$  is the ratio of the distance of the two fluxes to the charge.

We find that the energy gain due to the presence of the flux pair only depends on the ratio of the distance of the two edges to the charge. Thus no matter what the size is of the UV cutoff, the flux radius or in fact any other length scale, the energy gain can always be as large as one wants in a region where all length scales are insignificant with respect to the distances of the fluxes to the charge and between the fluxes. This shows that in two dimensions a single charge is always unstable (or meta-stable) with respect to a decay into a flux pair with a Cheshire charge no matter what the length scales are. However, the length scales of course drastically change the decay time of a charge.

## 6.3 The charge instability

In this section we analyze a novel type of instability in the electric field of a charge. We pointed out before, that a pair of Alice fluxes in the presence of a charge acquires an induced dipole, subsequently we determined the energy gain due to the creation of such pair. This raises the question to what extend the electric field configuration of a pair of static localized charges remains stable with respect to flux pair creation. We study this question in a lattice version of AED (LAED). The reason is, as mentioned in the introduction, that LAED allows us to introduce independent parameters, a mass  $m_f$  for the Alice flux and a mass/action  $m_m$  for the monopole/instanton. First we analyze the charge instability, then we will determine what the decay time is and compare it with the instability under the creation of a pair of charged point particles (with mass  $m_q$ ), assuming that these are present in the theory. To what extend these results can be carried over to a continuum version of the theory will be discussed in the concluding section.

Before turning to the the detailed calculations, let us make some general observations concerning the role of the various mass scales in the model. If both  $m_m$  and  $m_f$  are very large, a charge in two dimensions generates the well known logarithmic potential in the classical (small  $g^2$ ) limit.:

$$V(r) = \frac{Q^2}{\pi} \log\left(\frac{r}{r_0}\right) \quad , \quad (6.17)$$

with  $r_0$  some UV cutoff. Needless to say that the presence of dynamical charges in the model would (a) give rise to the standard (short distance) renormalization of the charge and (b) provide a cutoff to the potential at an energy of the order of mass of the charged particles  $m_q$ . If the monopole mass  $m_m$  comes down and  $m_f$  remains very large we get that the monopoles cause confinement, i.e., a linearly rising potential and the role of dynamical charges would be very much the same as for the logarithmic case. For the moment however, we will assume that no charged dynamical particles are present in the model (i.e., we assume them to be very massive). If now the flux mass comes down as well, then of course we get the possibility to dynamically create flux pairs out of the vacuum and these will cause the decay of the electric fields generated by the external charges. One expects a situation to arise where the potential (irrespective of its character) basically saturates and turns into a constant at a distance  $(r/r_0)$  where field energy becomes comparable to the value  $2m_f$ .

### 6.3.1 The life time of charge

Let us now compute the decay time of a system of two charges by performing an instanton calculation in the spirit of the “false vacuum” as described by Coleman and Callan [96], [97]. To lowest order in  $\hbar$  one only needs to determine the bounce solution with lowest action. The bounce is a classical solution of the Euclidean system, i.e., with the original potential inverted. In the mechanical analogue a classical particle moves from the meta stable point to the corresponding point at the other side of the barrier and back again. The instability, i.e., the tunneling through the barrier corresponds to half the Euclidean bounce solution, after which a real Minkovski time evolution takes over. At this point the system is not yet in its final state, but one expects that the new lowest energy state will be reached by emitting/dissipating energy through conventional (in this model presumably primarily electromagnetic) radiation processes. In the mechanical system with the inverted potential one should then find the particle trajectory with minimal action  $S_b$ . In the semi-classical domain the decay time is given by:

$$\tau \propto e^{\frac{S_b}{\hbar}} \quad . \quad (6.18)$$

In our system we find two extremal paths. We expect one of these two to have the lowest action, independent of the distance  $2w$  between the two external charges. In the following we analyze the situation for two cases, firstly we will determine the action for the instability due to the creation of a flux pair, then we do the same for the creation of a pair of point charges and finally we compare both mechanisms.

We first consider the case where the pair of fluxes or of charges are created in the most symmetric way. This means that they start out exactly between the external charges. The other decay channel we investigate corresponds to the most asymmetric configuration, where the fluxes or charges are created in the vicinity of one of the external charges and only one flux or charge will move. The other flux or charge remains with the charge at a fixed minimal distance  $R_0$ , which represents the UV cutoff of the bare charge. We will also determine the action of the bounce - the pair creation rate - in a constant electric field.

So the calculations we are about to make for the various cases are very similar, so let us, before providing the specific details for each case, give the general structure of the results.

In the previous sections we have calculated the energy gain  $E$  in the electric field due to the pair creation. From that we can determine the potential  $V_{pair}$  for the creation of a pair as a function of their separation  $2b$  and of course also dependent on the other fixed parameters that characterize the configuration, such as the external charges  $Q$ , their separation  $w$ , the masses  $m_f$  (or  $m_q$ ) and sometimes a core size  $R_0$ .

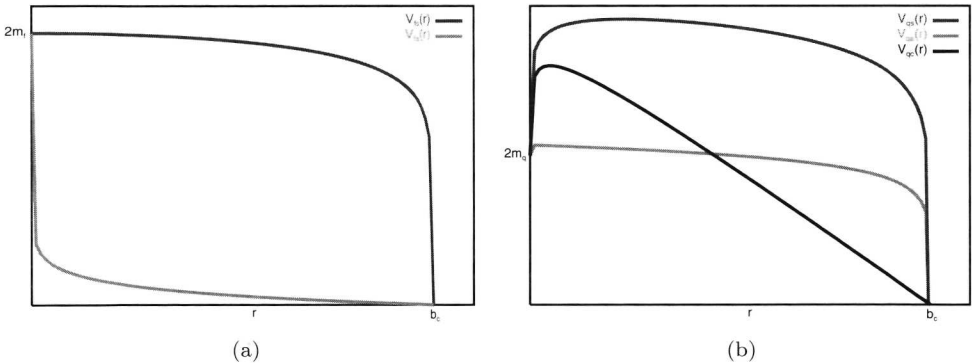


Figure 6.7: In figure (a) we plotted two typical potentials for the bounce of two Alice fluxes in the symmetric and asymmetric channel respectively. In figure (b) we plotted two typical potentials for the bounce of two dynamical charges in the symmetric and asymmetric channel respectively and the potential for the bounce of two dynamical charges in a constant field.

We have indicated the generic shape of the potentials in figures 6.7(a) and 6.7(b) for the pair creation of fluxes and dynamical charges respectively. For the fluxes we have assumed there to be no flux-flux interactions so that only the mass  $2m_f$  comes in. For the charged pair, however one expects the potential to grow with separation which means that the maximum of the potential is shifted towards larger separation. As is well known in one dimensional physics, the action of the extremal path generically is given by:

$$S^{pair} = 2 \int_{b=0}^{b=b_c} \sqrt{4mV_{pair}} db . \quad (6.19)$$

We can bring this expression in a more or less canonical form. One first introduces

a dimensionless separation variable  $y$  obtained by conveniently scaling  $b$  with some relevant length scale, for example the critical separation  $b_c$  labeling the turning point, this brings out a factor of the relevant length scale out in front. Next one scales the potential by its maximal value:  $V = V_{max}\hat{V}$ .  $V_{max}$  may conveniently be written as  $V_{max} = 2m\gamma^2$  where  $\gamma$  is a dimensionless quantity satisfying  $\gamma \geq 1$  and the equal sign applies to the flux pair creation (see figures). Putting the scaling factors in front of the integral the expression for the action takes the general form,

$$S^{pair} = \text{const.} \times b_c m \gamma F(w, m, Q, R_0) , \quad (6.20)$$

where the dimensionless function  $F$  may depend on all the parameters but because of the rescalings takes on only values between zero and one.

$$F = \int_{y=0}^{y=1} \sqrt{\hat{V}_{pair}} dy . \quad (6.21)$$

We see that the action is typically of the order (mass of pair)x(critical separation), as one would expect naively. Yet, we will study the various cases separately in more detail, because it turns out that there are interesting differences in the functional dependence of  $S^{pair}$  on for example the distance  $w$  of the external charges, which are important physically.

### 6.3.2 Charge decay due to creation of an Alice flux pair

We compute the action for a bounce corresponding with the creation of a flux pair in the presence of two external charges. First we consider the symmetric channel, then the asymmetric channel and finally the case of a constant electric field.

#### The symmetric channel:

In the symmetric channel we may use formula 6.15 with  $x_1 = x_2 = x$ , which gives the energy gain:

$$E_{fpair} = -\frac{Q^2}{\pi} \log \left( 1 - \frac{1}{x^2} \right) . \quad (6.22)$$

During the bounce the external charges remain fixed while the distance between the fluxes increases. The suitably scaled variable for this situation is  $y \equiv \frac{1}{x} = \frac{b}{w}$ . So far we only determined the energy gain due to the boundary conditions created by the Alice fluxes, but the potential in which the fluxes move is not only given by the energy gain, we also should include the energy cost which equals the mass of the flux pair,  $2m_f$ . The potential for the pair is therefore given by:

$$V_{fpair} = 2m_f \left( \Theta(|y|) + \frac{1}{\mu} \log(1 - y^2) \right) . \quad (6.23)$$

where  $\Theta(0) = 0$  and equals one otherwise. The constant  $\mu$  is defined as  $\mu = \frac{2\pi m_f}{Q^2}$ . We should note that keeping  $y_1 = y_2 = y$  for all times is in fact a solution to the

equations of motion for the system with the inverted potential. The action of this solution is simply given by:

$$S_{sym}^f = 4\sqrt{2} b_c m_f F_{sym}^f(\mu) . \quad (6.24)$$

where the turning points are given by the zeros of the potential, i.e.,

$$b_c = w \sqrt{1 - e^{-\mu}} \quad (6.25)$$

and where  $F_{sym}^f(\mu)$  is given by:

$$F_{sym}^f(\mu) = \int_0^1 \sqrt{1 + \frac{1}{\mu} \log(1 - y'^2(1 - e^{-\mu}))} dy' . \quad (6.26)$$

Note that the function  $F_{sym}^f$  depends in this case only on one particular combination of parameters  $\mu$ . The integrand varies from one at  $y = 0$ , to zero at  $y = 1$ . Although the integral cannot be done analytically, a little analysis shows that the function always lies between the functions  $f(y) = \sqrt{1 - y^2}$  and  $f(y) = 1$ . The integrals of these functions are easily determined to be  $\frac{\pi}{4} \approx 0.8$  and one. So we have that  $\frac{\pi}{4} \approx 0.8 \leq F_{sym}^f(\mu) \leq 1$  which is indeed correct as one can see from the numerical evaluation of  $F_{sym}^f(\mu)$  plotted in figure 6.8.

As mentioned before we need to introduce a UV cutoff for the bare charges, allowing the fluxes to approach a charge only up to a minimal distance  $R_0$ . One way to put this is that for the symmetrical process to be able to take place, or for that matter any decay mode using fluxes,  $w$  needs to exceed a minimal value depending on  $R_0$  and  $\mu$ . This constraint on  $w$  is easily determined with the help of formula 6.23 by putting  $b = w - R_0$  in other words  $y = 1 - r_0$  with  $r_0 = R_0/w$ . Determining the zero of the potential than gives the minimal value of  $w$ , yielding:

$$\frac{1}{r_0} = \frac{w}{R_0} \geq 2e^{\mu/2} \left( e^{\mu/2} + \sqrt{e^{\mu} - 1} \right) . \quad (6.27)$$

### The asymmetric channel:

The asymmetric channel is the channel where one of the fluxes stays close to one of the charges and the other flux moves away. An interesting fact about this decay channel is, that in the limit of widely separated charges,  $w \rightarrow \infty$ , this channel will still give a finite decay time, whereas the symmetric channel would not. The energy gain due to the presence of a flux pair in this system again follows from formula 6.15. We fix one of the fluxes at the minimal cut-off distance  $R_0$  from one of the charges. The other flux is pushed away from this charge. In this case it is natural to scale the variables by the core size  $R_0$  as this is the only length scale in the limit of  $w \rightarrow \infty$ , so we define  $\tilde{w} = \frac{w}{R_0}$  and  $\tilde{y} = \frac{b}{R_0}$ . The energy gain of this configuration is given by:

$$E_{fpair} = \frac{2m_f}{\mu} \log \left( \frac{1}{2} \left( 1 + \frac{2\tilde{w}(1 + \tilde{y}) - 1 - 2\tilde{y}}{\sqrt{(2\tilde{w} - 1)(2\tilde{w} - 2\tilde{y} - 1)(2\tilde{y} + 1)}} \right) \right) . \quad (6.28)$$

The potential is obtained by adding the mass term for the creation of the two Alice fluxes out of the vacuum. The action of the bounce is determined in the same manner as we did in formula 6.19. not only do we have a different potential, we also need to change a factor 4 into 2, because only one flux is moving in this decay channel. For the action we obtain the following expression:

$$S_{asym}^f = 4 m_f b_c F_{asym}^f(\mu, \tilde{w}) \quad , \quad (6.29)$$

where the critical separation  $b_c$  is given by:

$$b_c = \frac{(2\tilde{w} - 1)R_0}{2 - 2\tilde{w} + \frac{\tilde{w}(\cosh(\frac{\mu}{2}) + 3\sinh(\frac{\mu}{2}))}{\sqrt{e^\mu - 1}}} \quad . \quad (6.30)$$

The function  $F_{asym}^f(\mu, \tilde{w})$  is defined by:

$$F_{asym}^f(\mu, \tilde{w}) = \sqrt{\int_0^1 \left( 1 - \frac{1}{\mu} \log \left( \frac{1}{2} \left( 1 + \frac{2\tilde{w}(1 + \tilde{y}'\tilde{y}_c) - 1 - 2\tilde{y}'\tilde{y}_c}{\sqrt{(2\tilde{w} - 1)(2\tilde{w} - 2\tilde{y}'\tilde{y}_c - 1)(2\tilde{y}'\tilde{y}_c + 1)}} \right) \right) d\tilde{y}' \quad , \quad (6.31)}$$

and depends also on the separation of the external charges  $2\tilde{w}$ . Although we do get a similar expression as in the symmetric case the integral in the asymmetric case is not that easily estimated, see figure 6.9 for a plot of  $F_{asym}^f(\mu, \tilde{w})$  and figure 6.8 for the value this integral takes in the limit of  $\tilde{w} \rightarrow \infty$ .

The remarkable fact is that this action remains finite in the limit of  $\tilde{w} \rightarrow \infty$ . Thus the decay time of a single charge (i.e., of charge itself) is finite in two dimensional Alice electrodynamics.

#### The constant field:

Next we investigate the decay width per volume of a constant electric field. The energy gain due to the presence of a flux pair in line with the electric field strength can be found from formula 6.22. We move the charges to infinity and increase  $Q$  such that the ratio  $Q/w$  is kept fixed and we define the electric field as  $\mathcal{E} \equiv \frac{Q}{\pi w}$ . The resulting energy gain due to the presence of a flux pair then equals:

$$E_{fpair} = \pi \mathcal{E}^2 b^2 \quad . \quad (6.32)$$

The action is easily determined to be:

$$S_{const}^f = \sqrt{2\pi} m_f b_c \quad , \quad (6.33)$$

where the critical separation is.

$$b_c = \sqrt{\frac{2m_f}{\mathcal{E}^2 \pi}} \quad . \quad (6.34)$$

The result is of course independent of position as it determines the decay rate per unit volume of a constant electric field.

### 6.3.3 Charge decay time due to creation of point charges

Let us now investigate the field instability of a pair of external charges under the creation of two dynamical charges. Since point charges have a singularity in the field energy at the core we introduce again a cutoff  $R_0$  to regulate some of the infinities in our calculations. First we will determine the energy gain due to the presence of two point charges. We denote the two initial charges as  $C_1$  and  $C_2$ , the created charges as  $D_1$  and  $D_2$ . We put the four charges on one line and obviously assume the charges to be alternating. Symbolically the energy gain can be written as:

$$\begin{aligned} E_{gain}^q &= (C_1 + C_2)^2 - (C_1 + C_2 + D_1 + D_2)^2 \\ &= -(D_1^2 + D_2^2 + 2D_1D_2) - 2(C_1 + C_2)(D_1 + D_2) \quad . \end{aligned} \quad (6.35)$$

The first part,  $D_1^2 + D_2^2$ , has an infinite contribution at the cores of the charges and only these infinities will be removed, i.e., only in this term we cut away a disc with radius  $R_0$  around the charges. Taking the origin halfway between the two created charges and denoting the distances of the charges with respect to this origin  $w_1$ ,  $w_2$  and  $b$ , the energy difference  $E_{gain}^q$  is given by:

$$E_{gain}^q = -\frac{Q^2}{\pi} \log \left( \frac{2(x_1 - 1)(x_2 - 1)}{(x_1 + 1)(x_2 + 1)\tilde{r}_0} \right) \quad . \quad (6.36)$$

with  $x = \frac{w}{b}$  and  $\tilde{r}_0 = \frac{R_0}{b}$ .

This is the change in energy due to the electrical field configuration. We still need to take the mass of the point charges into account. We assume that the point charges are created a distance  $2R_0$  away from each other and the energy cost of this process we call  $2m_q$ . Thus the total energy gain is given by:

$$V_{qpair} = 2m_q \left( 1 + \frac{1}{\nu} \log \left( \frac{(x_1 - 1)(x_2 - 1)(x_1 + \tilde{r}_0)(x_2 + \tilde{r}_0)}{(x_1 - \tilde{r}_0)(x_2 - \tilde{r}_0)(x_1 + 1)(x_2 + 1)\tilde{r}_0} \right) \right) \quad . \quad (6.37)$$

with  $\nu = \frac{2\pi m_q}{Q^2}$ .

Next we will use this energy gain to determine the action of the bounce in different channels of the decay process.

#### The symmetric channel:

In the symmetric channel the potential is given by:

$$V_{qpair} = 2m_q \left( 1 + \frac{1}{\nu} \log \left( \frac{(y - 1)^2(r_0 + 1)^2y}{(r_0 - 1)^2(y + 1)^2r_0} \right) \right) \quad . \quad (6.38)$$

where we still use  $y = \frac{1}{x} = \frac{b}{w}$  and  $r_0 = \frac{R_0}{w}$ .

To determine the action of the bounce we need to determine:

$$S_{qpair} = 2w \int_{y=r_0}^{y=y_c} \sqrt{4m_q V_{qpair}} \, dy \quad . \quad (6.39)$$

This is a quite non-trivial integral. We will estimate this integral by slightly changing the boundary conditions. As the lower boundary condition we will not take  $r_0$ , but the point between  $r_0$  and zero where  $V_{qpair} = 0$ . Later we will estimate the part we add to the action by this change in the boundary conditions.

So first we will determine the integral:

$$S_{sym}^{q,1} = 2w \int_{y=y_-}^{y=y_c} \sqrt{4m_q V_{qpair}} dy , \quad (6.40)$$

with  $y_c$  and  $y_-$  the two values of  $y$  where  $V_{qpair}$  is equal to zero and with  $0 < y_- < y_c < 1$ . This integral is still quite difficult. We can determine it up to a part that we evaluate numerically and understand quite well. The action can be written as:

$$S_{sym}^{q,1} = 4\sqrt{2}m_q(b_c - b_-)\gamma_{sym}^q F_{sym}^q(\lambda) , \quad (6.41)$$

with  $\gamma_{sym}^q = \sqrt{\frac{\lambda - \lambda_{min}}{\nu}}$ ,  $\lambda = \nu + \log\left(\frac{(r_0+1)^2}{(r_0-1)^2 r_0}\right)$ ,  $\lambda_{min} = \log\left(\frac{1}{2}(11 + 5\sqrt{5})\right)$  and  $F_{sym}^q(\lambda)$  given by:

$$F_{sym}^q(\lambda) = \int_0^1 \sqrt{\frac{1 + \lambda^{-1} \log\left(\frac{(1 - ((y_c - y_-)y' + y_-))^2}{(1 + ((y_c - y_-)y' + y_-))^2}((y_c - y_-)y' + y_-)\right)}{1 - \frac{\lambda_{min}}{\lambda}}} dy' , \quad (6.42)$$

with  $y_c = b_c/w$  and  $y_- = b_-/w$ .

In figure 6.8 we have plotted a numerical evaluation of the function  $(y_c - y_-)F_{sym}^q(\lambda)$ . We still need to estimate the part introduced by taking different boundary values. This may be estimated by the maximum of the integrand in the region between  $y_-$  and  $r_0$  times  $r_0$ . If  $(-2 + \sqrt{5}) > r_0$   $V_{qpair,max} = 2m_q$  else  $V_{qpair,max} = 2m_q\sqrt{\frac{\lambda - \lambda_{min}}{\nu}}$ . Thus we estimate this part of the action to be  $S_{sym}^{q,2}$ , which is typically much smaller than  $S_{sym}^{q,1}$ , as follows:

$$S_{sym}^{q,2} \leq 4\sqrt{2}m_q R_0 \quad \text{if } (-2 + \sqrt{5}) > r_0 \quad (6.43)$$

and else

$$S_{sym}^{q,2} \leq 4\sqrt{2}m_q R_0 \sqrt{\frac{\lambda - \lambda_{min}}{\nu}} . \quad (6.44)$$

### The asymmetric channel:

In the asymmetric channel the potential is given by:

$$V_{qpair} = 2m_q \left( 1 + \frac{1}{\nu} \log\left(\frac{2\tilde{y}(\tilde{w} - \tilde{y} - 1)}{(\tilde{y} + 1)(\tilde{w} - 2)}\right) \right) . \quad (6.45)$$

The action of the bounce is given by:

$$S_{asym}^q = 4m_q b_c \gamma_{asym}^q F_{asym}^q(\nu, \tilde{w}) . \quad (6.46)$$

with  $\gamma_{asym}^q = \sqrt{1 + \frac{1}{\nu} \log \left( \frac{2(1-\sqrt{\tilde{w}})^2}{\tilde{w}-2} \right)}$  and

$$b_c = R_0 \left( \frac{1}{4} e^{-\nu} (2 + 2e^\nu (\tilde{w} - 3) - \tilde{w} + \sqrt{-8e^\nu (\tilde{w} - 2) + (-2 - 2e^\nu (\tilde{w} - 1) + \tilde{w})^2}) \right) \quad (6.47)$$

and  $F_{asym}^q(\nu, \tilde{w})$  is given by:

$$F_{asym}^q(\nu, \tilde{w}) = \int_0^1 \sqrt{\frac{1 + \frac{1}{\nu} \log \left( \frac{2(\tilde{y}'\tilde{y}_c+1)(\tilde{w}-\tilde{y}'\tilde{y}_c-2)}{(\tilde{y}'\tilde{y}_c+2)(\tilde{w}-2)} \right)}{1 + \frac{1}{\nu} \log \left( \frac{2(1-\sqrt{\tilde{w}})^2}{\tilde{w}-2} \right)}} d\tilde{y}' . \quad (6.48)$$

In the limit  $\tilde{w} \rightarrow \infty$  we can determine the integral exactly, yielding:

$$F_{asym}^q(\nu, \infty) = \frac{4e^\nu - \frac{\sqrt{\pi} \operatorname{Erfi}[\sqrt{\nu+\log(2)}]}{\sqrt{\nu+\log(2)}}}{4e^\nu - 2} . \quad (6.49)$$

Plots of  $F_{asym}^q(\nu, \tilde{w})$  and  $F_{asym}^q(\nu, \infty)$  are given in figures 6.9 and 6.8.

We recall that in the asymmetric channel for the creation of Alice fluxes the result remains finite in the limit of widely separated external charges, obviously this is not the case for the action of the bounce corresponding to the creation of a pair of point charges.

### The constant field:

Finally we will consider the case of a constant electric field and examine the action of the bounce if two point charges are created. To determine the energy gain in the field configuration we can use formula (6.37). However we cannot take the charge of the initial charges equal to the charge of the created point charges. To get the configuration in a finite electric field we take the distance between the initial charges to infinity while keeping the charge over the distance ratio fixed. Again we take the electric field  $\mathcal{E} = \frac{Q_{initial}}{w\pi}$ . The potential for the creation of two point charges in a constant electric field is given by:

$$V_{qpair} = 2m_q \left( 1 + \frac{1}{\nu} (\log(\tilde{y}) - u(\tilde{y} - 1)) \right) , \quad (6.50)$$

with  $u = \frac{4\pi\mathcal{E}R_0}{Q^2}$ .

The action of the bounce is given by:

$$S_{const}^q = 2R_0 \int_{\tilde{y}=1}^{\tilde{y}=\tilde{y}_c} \sqrt{4m_q V_{qpair}} d\tilde{y} . \quad (6.51)$$

Just as in the symmetric channel we take slightly different boundary conditions and estimate the difference later on. We will use the two values of  $\tilde{y}$  where  $V_{qpair} = 0$  and

we get:

$$S_{const}^{q,1} = 2R_0 \int_{\tilde{y}=\tilde{y}_-}^{\tilde{y}=\tilde{y}_c} \sqrt{4m_q V_{qpair}} d\tilde{y} . \quad (6.52)$$

This leads us to:

$$S_{const}^{q,1} = 4m_q (b_c - b_-) \gamma_{const}^q F_{const}^q(\kappa) , \quad (6.53)$$

with  $\gamma_{const}^q = \sqrt{\frac{\kappa-1}{\nu}}$ ,  $\kappa = \nu - \log(u) + u$ ,  $b_c \frac{u}{R_0} = (\tilde{y}'_c) = \kappa + \log(\kappa + \log(\kappa + \dots))$  and  $b_- \frac{u}{R_0} = (\tilde{y}'_-) = \exp(-\kappa + \exp(-\kappa + \exp(-\kappa + \dots)))$ , where  $\tilde{y}'_c$  and  $\tilde{y}'_-$  are the two real solutions of  $\kappa + \log(\tilde{y}') - \tilde{y}' = 0$ .  $F_{const}^q(\kappa)$  is a function which varies only from  $\frac{\pi}{4}$  at  $\kappa \rightarrow 1$  to  $\frac{2}{3}$  at  $\kappa \rightarrow \infty$  and is given by:

$$F_{const}^q(\kappa) = \int_0^1 \sqrt{\frac{\kappa + \log((\tilde{y}'_c - \tilde{y}'_-)\tilde{y}' + \tilde{y}'_-) - ((\tilde{y}'_c - \tilde{y}'_-)\tilde{y}' + \tilde{y}'_-)}{\kappa - 1}} d\tilde{y}' . \quad (6.54)$$

see figure 6.8 for a plot of  $F_{const}^q(\kappa)$ .

We still need to estimate the part we introduced by taking different boundary values. We approximate that part by the maximum of the integrand in the region between  $\tilde{y}_-$  and 1 times  $R_0$ . If  $u < 1$  then  $V_{qpair,max} = 2m_q$  and otherwise  $V_{qpair,max} = 2m_q \left(\frac{\kappa-1}{\nu}\right)$ . Thus the upperbound for this part of the action,  $S_{const}^{q,2}$ , is typically much smaller than  $S_{const}^{q,1}$ , to be explicit:

$$S_{const}^{q,2} \leq 4\sqrt{2}m_q R_0 \quad \text{if } u < 1 \\ \text{else} \quad (6.55)$$

$$S_{const}^{q,2} \leq 4\sqrt{2}m_q R_0 \sqrt{\frac{\kappa-1}{\nu}} . \quad (6.56)$$

### 6.3.4 Comparing the decay channels

We just determined the actions of bounce solutions corresponding to some decay channels of two static point charges. As expected the action depends strongly on the parameters of the model. LAED allows for the different parameters to be independent of each other, so there are many possibilities for the preferred decay channel. Although the LAED model we described before does not require dynamical charges we did determine the action of some decay channels for the creation of pairs of such charges. Both dynamical charges and Alice fluxes can render the static point charge configuration unstable. However, the decay time will typically depend exponentially on the distance between the two static charges except for one possible mode: the asymmetric decay channel of the two static charges under the creation of two Alice fluxes. The action of this channel saturates. This means that even the decay width of a single point charge is finite in AED, in contrast to ordinary ED. This instability is the process mentioned at the end of section 6.2.1, which may be considered as the

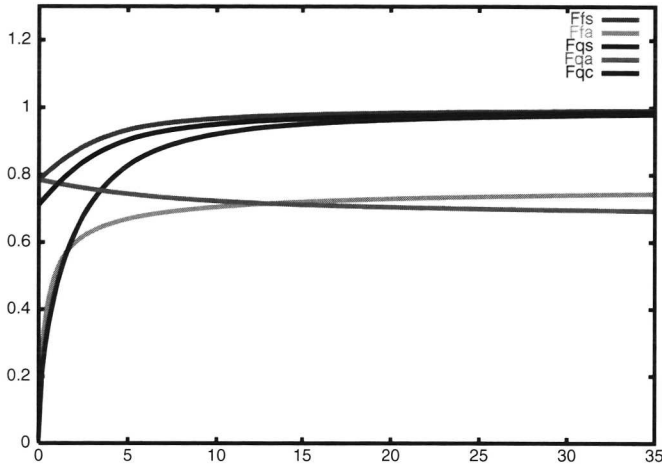


Figure 6.8:

This figure shows the five functions  $Ffs = F_{sym}^f(\mu)$ ,  $Ffa = F_{asym}^f(1/\mu)$ ,  $Fqs = (y_c - y_-)F_{sym}^q(\lambda - \lambda_{min})$ ,  $Fqa = F_{asym}^q(\nu)$  and  $Fqc = F_{const}^q(\kappa - 1)$  numerically, with  $\lambda_{min} = \log\left(\frac{1}{2}(11 + 5\sqrt{5})\right)$ ,  $F_{asym}^q(\nu) = F_{asym}^q(\nu, \infty)$  and  $F_{asym}^f(1/\mu) = F_{asym}^f(1/\mu, \infty)$

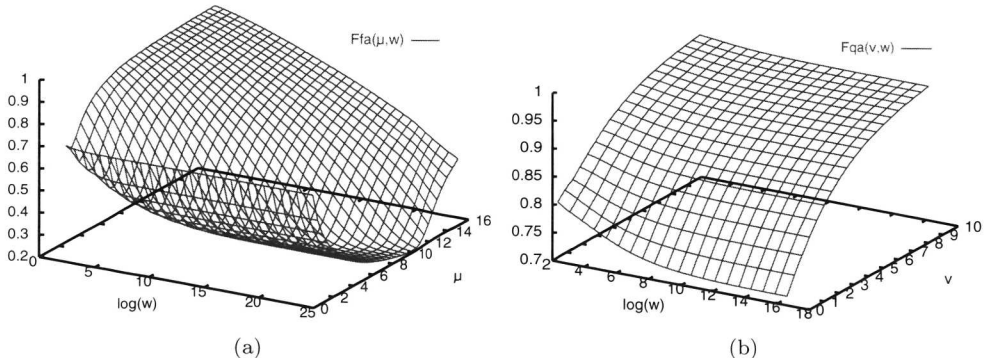


Figure 6.9:

Figure (a) shows a plot of  $F_{asym}^f(\mu, \tilde{w})$ . The figure shows that the limit of the integral at  $\tilde{w} \rightarrow \infty$  is reached only very slowly. The minimum value of the integral only moves slowly to large  $\mu$  as  $\tilde{w}$  grows exponentially. Figure (b) shows a plot of  $F_{asym}^q(\nu, \tilde{w})$ . The figure shows that the limit of the integral at  $\tilde{w} \rightarrow \infty$  is reached very fast. In the limit of  $\tilde{w} \rightarrow \infty$  we know the integral exactly.

two dimensional dual analog of the monopole core instability described in chapter 5. This implies basically the nonexistence of static charges in the theory, and that is the main observation we make in this chapter.

We already mentioned that a pair of Alice fluxes can be represented by a conducting

needle in our configurations. On a conductor charges are free to move and one can for example have an induced dipole moment. In this picture the creation of two point charges is just a highly singular charge distribution on this line segment and it is obvious that the action of the bounce for Alice fluxes can always be made lower because the charge distribution can still be varied. A simple and extreme example is the asymmetric channel in the limit of  $\tilde{w} \rightarrow \infty$ . Here the action of the bounce for the point charges is infinite while the action of the bounce for the Alice fluxes remains finite.

## 6.4 Conclusions and outlook

In this chapter we have extensively analyzed the behavior of Alice fluxes in the presence of electric charges in (2+1)-dimensions. We showed that a pair of Alice fluxes in the presence of an electric charge develops an induced electric dipole moment. This dipole moment is of the Cheshire type which means that it is carried by the flux pair, and that the would-be charges making up the dipole are strictly nonlocalizable and thus remain elusive. Exploiting conformal invariance we determined the resulting field configurations exactly which in turn allowed us to calculate the energy gain due to the introduction of a pair of Alice fluxes between two external charges. Subsequently we considered the stability using semi-classical methods, using a Euclidean bounce solution.

We used a lattice model of AED, see chapter 3, to investigate the effects of Alice fluxes on a configuration of static point charges, because it allowed us to investigate the effects of the different topological defects separately. In the case of heavy monopoles we found an instability in the charge configuration due to the creation of a pair of Alice fluxes. Although this instability looks quite similar to the instability due to the creation of two dynamical point charges there is a crucial difference. In the limit of increasing separation between the static charges the decay time due to the creation of dynamical point charges diverges, while for the creation of two Alice fluxes it saturates and remains finite. To reach this conclusion we did not have to calculate the fluctuation determinant in detail, assuming that it is finite. Consequently in (L)AED a single bare charge is unstable under the creation of two Alice fluxes, which can be seen as the (2+1)-dimensional dual analog of the monopole core instability, see chapter 5. If the monopole mass moves down, i.e., the confinement scale comes into play, the instabilities due to a flux pair and a charge anti-charge pair become very similar. In figure 6.10 we have sketched the potential for a typical situation.

Let us now give some comments on the continuum theory. We expect the situation to be not so much different. The topological defects arise as a consequence of spontaneous symmetry breaking, which means that the mass scales for the fluxes and monopoles might be much more constrained. In chapter 5 we showed that if the flux mass gets much less than the monopole mass, one may well get that the monopole decays in a flux ring carrying a Cheshire magnetic charge. This suggests that the confinement scale and the instability scale (due to flux creation) cannot be too much different. As

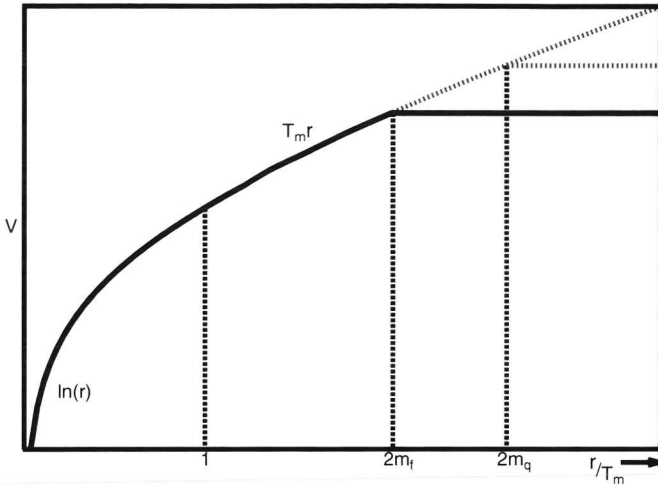


Figure 6.10: The effective potential for a pair of external charges. The figure represents the case where the mass of the Alice flux pair is larger than the confinement scale, but smaller than the mass of dynamical charges. It is possible to lower  $m_f$  below the confinement scale.

we explained, if the monopole and Alice flux mass are comparable the potential still saturates due to the instability under the creation of two Alice fluxes.

In this chapter we showed that the possibility of Cheshire charge in a theory has serious consequences for the stability of charge in the theory in two dimensions. It is usually a question of energetics what the stable configuration is, but for theories which allow for Cheshire charges, a Cheshire charge configuration is the natural second candidate to carry the charge. This suggests that any theory which breaks to a subgroup which contains a discrete and continuous component that do not mutually commute the gauge charges may well become unstable due to the Cheshire phenomenon. An other interesting class of theories which typically contain Cheshire charged configurations are the theories with non-abelian discrete gauge symmetries, which are best described with the help of a spontaneously broken Hopf symmetry [8, 9].

In the appendix of this chapter we introduce an object called the (magnetic) Cheshire current and we discuss its relation with (electric) Cheshire charges. We will also discuss its relation with the closed electric field lines that occur if one interprets the occurrence of an instanton as an event in the (2+1)-dimensional (Alice) electrodynamic setting. From this picture the confinement mechanism can be understood quite easily.

Acknowledgment: We thank Jan Smit for very useful discussions on the topics discussed in this chapter.

## Appendix

### 6.5 Cheshire current and confinement

In this appendix we will discuss the notion of a (magnetic) Cheshire current in AED and the confinement of charges in (2+1)-dimensional (Alice) electrodynamics [59]. We'll introduce a configuration in AED named (magnetic) Cheshire current and explain its relation with (electrical) Cheshire charges and confinement in two dimensions. We'll introduce a picture of two dimensional confinement from which qualitatively the confinement of the electrical flux into a flux tube comes apparent.

#### 6.5.1 The Cheshire current

Neither electric nor magnetic field lines are allowed to cross an Alice flux, suggesting some exotic type of super conductivity through the core of the flux tube. In this part of the appendix we return to this analogy and find an interesting gauge complementarity between electric Cheshire charges and a magnetic Cheshire currents. Let us introduce the latter first.

Let us consider the following “gedanken” experiment. We create two charged particles from the vacuum and take one of the two particles around two spatially separated fluxes and then annihilate the two particles again. If the flux tubes are magnetic super-conductors this would have resulted in two magnetic current carrying fluxes, each with closed electric field lines around them. In the case of two Alice fluxes a different picture emerges. Since the field lines cannot close around a single Alice flux, one needs to take an even number of fluxes to be able to annihilate the particles again. This means that if one pulls the two fluxes apart one cannot be left with two fluxes which each carry a current. The field lines need to stay around both fluxes. A situation very different from the super conductors indeed. The system as a whole carries the current and just as in the case of a Cheshire charge the current is non-localizable; we should call this object a Cheshire current.

The resulting field line configuration, depicted in figure 6.11, implies an attractive interaction between the two fluxes, on top of the normal flux interactions. It has the opposite effect of a Cheshire charge, which leads to a repulsive force between the two fluxes.

Upon closer inspection we will see that there is a certain *gauge complementarity*, reconciling the two different pictures, describing non-localizable Alice effects. At first sight electric Cheshire charge and a magnetic Cheshire current appear to be very different entities. Let us now point out that there is actually a close relation between them. Imagine we repeat the gedanken experiment we just performed, but now we move in two more Alice fluxes from infinity in such a way that all four of them are on one single line. As we know, on each flux one  $\mathbb{Z}_2$  line should end. For convenience we put these half lines on top of the line on which we put the fluxes. For every flux we then still have the freedom to let the line go to the left or to the right. The result

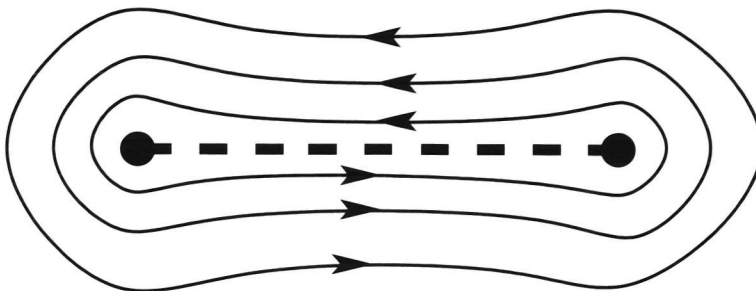


Figure 6.11: Closed electric field lines of a (magnetic) Cheshire current configuration.

just yields two different, but gauge equivalent, configurations, as is illustrated by the top and bottom pictures in figure 6.12.

As we argued before, one can deform the  $\mathbb{Z}_2$  lines in any way one wants by gauge transformations. From figure 6.12 it is clear that we can gauge transform the first configuration into the last one. This means that they both describe the same physics, although their interpretation appears to be quite different. In one case, see the bottom picture of figure 6.12, one would argue that two Cheshire charges are the source of the field lines, but in the other situation, see the top picture of figure 6.12, one would argue that three Cheshire currents are the source of the field lines. Apparently there are two different ways of looking at this configuration. As was explained before [4] one needs to cut away some region(s) of space-time if one wants to consider field strengths which are not single valued in the presence of an Alice flux. However, there is of course not a unique choice to do this. This freedom of choice corresponds exactly to the gauge complementarity of Cheshire charge and Cheshire current.

We do note that although they are related by a gauge transformations it does not mean that all configurations can be thought of as consisting only of Cheshire charges or only of Cheshire currents. A simple example is a pair of Alice fluxes carrying a Cheshire charge and a Cheshire current. This object may in fact be a stable configuration in two dimensions, since the electric Cheshire charge results in a repulsive force between the two fluxes whereas the magnetic Cheshire current results in a attractive force between the two fluxes. These could be made to cancel leading to a stationary configuration.

### 6.5.2 Confinement in a two dimensional picture

In this subsection we will consider the confinement of (2+1)-dimensional electrodynamics. This problem was already solved in [59]. For any non-zero value of the gauge coupling constant (2+1)-dimensional electrodynamics is confining (in the quenched approximation). It is well known that the instanton density increases and polarizes around the minimal sheet bounded by a closed Wilson loop. In a three dimensional Euclidean space the instanton configuration is in fact just a magnetic monopole. After

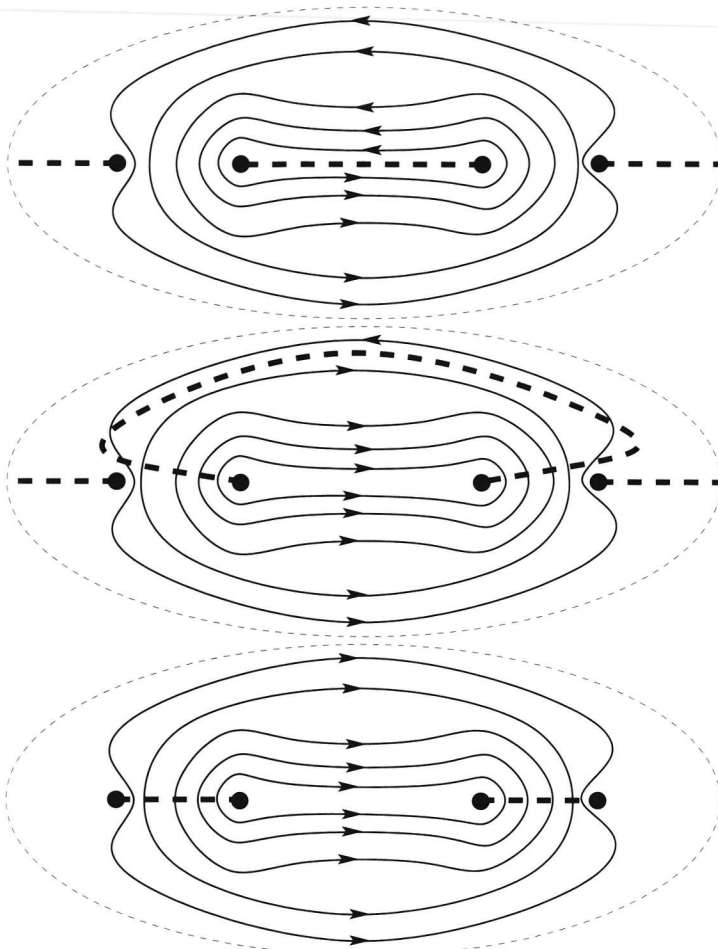


Figure 6.12: The 'duality' transformation from three magnetic Cheshire currents into two electric Cheshire charges.

translating the instanton configuration to Minkovski space it is easy to understand that the polarization of the instanton density results in the confinement of the electrical flux into a flux tube.

By going to Minkovski space the interpretation of the fields change. The  $z$ -component of the magnetic field becomes the pseudo scalar magnetic field in the (2+1) dimensional Minkovski space, while the  $\theta$  and  $\rho$  components of the magnetic field get translated into the  $\rho$  and  $\theta$  components of the electric field respectively. For the moment we will ignore the factors of  $i$  as they will have no influence on the picture we use, although they do play an important role in the dynamics and the polarization of the instanton density.

Changing from Euclidean to Minkovski space allows us to interpret the instanton density as a magnetic current density in Minkovski space. The nice thing of this two dimensional interpretation is that the confinement of the electrical flux into a flux tube easily follows from the superposition of the field lines of the pair of charges and the magnetic currents. In figure 6.13 we see that superimposing a magnetic current to the electric dipole configuration moves the field lines inwards. Indicating that a (polarized) magnetic current density would confine the electric flux into a flux tube.

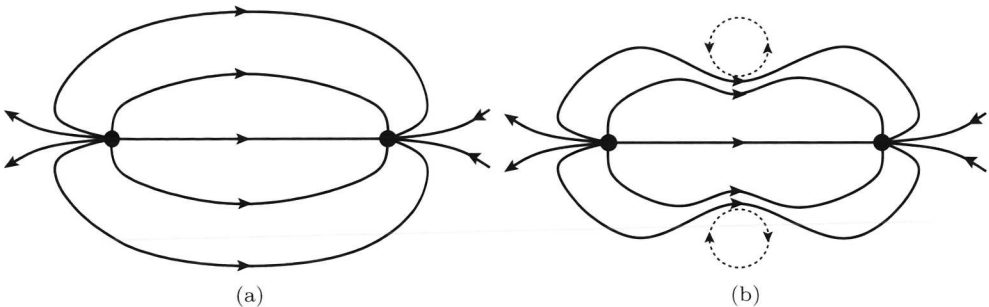


Figure 6.13: In figure (a) we plotted the field configuration of two opposite charges in the absence of instantons. In figure (b) we see that the introduction of magnetic currents, representing the instantons in Minkovski space, pushes the field lines inwards explaining the fact that the electric flux gets confined in a flux tube in the presence of a (polarized) instanton density.

In the previous section of this appendix we introduced an object in AED which can also be identified as a magnetic (Cheshire) current. However the dynamics, due to the factors of  $i$ , is very different.

# Epilogue

In this thesis we investigated physical effects that occur if simple gauge theories get broken to models with a non-abelian residual symmetry group. As a specific example we have investigated Alice Electrodynamics with gauge group  $U(1) \ltimes \mathbb{Z}_2$  in quite some detail. This is a theory in which charge conjugation symmetry is gauged, which leads to a number of remarkable physical properties. We started by the construction and comparison of different types of (L)AED models, for example models which allowed for first order Bogomolny type equations. Exact numerical solutions for the Alice fluxes in the continuum models were obtained. The phase structure of (L)AED in three and four dimensions was determined using a lattice formulation of the theory. We measured quantities rather precisely, such as the Alice flux density and the monopole/instanton density in different parts of the parameter space. After having investigated these lattice models we turned to stability questions related to topological defects. We first noted that in a theory with a topological degeneracy dynamics may well select a particular lowest energy state or asymptotic vacuum. This mechanism was shown to hold for the situation of kinks and fluxes in a certain class of models as a consequence of the fact that not all topologically non-trivial boundary conditions allowed for static solutions. These features are in particular relevant for (1+1)- and (2+1)-dimensional models with flat directions in their potential. In a following chapter we turned to the question whether a spherically symmetric magnetic monopole could decay into a magnetically Cheshire charged Alice loop. With the help of a variational method we demonstrated that this is indeed the case in some part of the parameter space of the model. Although these magnetic Cheshire rings were not necessarily exact solutions to the equations of motion, they did provide an upper bound for the energy of the configuration from which instability could be concluded. Finally we looked at the fate of electric charge in (2+1)-dimensional AED. There we basically established that a pair of static external charges is unstable under the creation of a pair of Alice fluxes if they are separated far enough. This is in fact a novel kind of screening in which binding of an electric charge to one of the fluxes implies that its charge gets converted in a totally delocalized Cheshire charge. So in (2+1)-dimensional AED the potential between two charges saturates around twice the mass of an Alice flux. It would be interesting to determine the effective potential between two external charges by a quantum Monte Carlo computation. However as is well known from QCD such a saturation of the potential is notoriously hard to detect

## Epilogue

---

[98, 99]. and we considered this problem beyond the scope of this thesis.

The main ingredient in the monopole instability and the charge instability in (2+1)-dimensions is the possibility of an Alice loop or a pair of Alice fluxes to carry a Cheshire charge. This possibility is a general feature of Alice models. In all Alice models there is a natural second candidate to carry the magnetic and/or electric charge. So one would expect such instabilities to appear in other Alice models as well.

Although AED might not be the phenomenologically most favored model for electrodynamics, its physical properties are striking if one realizes how modest the change in the theory in fact is. As we mentioned in the first chapter of this thesis there are several places in high energy physics and condensed matter physics where Alice effects may turn out to be relevant.

**Acknowledgments.** We would like to thank Jan Smit and Jeroen Vink for valuable advice and support related to lattice gauge theories, M.M.H.Postma for his contributions in the early stages of the project and A. Achúcarro, L. Pogosian and T. Vachaspati for discussions on dynamical vacuum selection. Furthermore we would like to thank COSLAB and especially FOM (NWO) for their financial support.

# Bibliography

- [1] Joe E. Kiskis. Disconnected gauge groups and the global violation of charge conservation. *Phys. Rev.*, D17:3196, 1978.
- [2] Mark de Wild Propitius and F. Alexander Bais. Discrete gauge theories, in *Particles and Fields*, edited by G.W. Semenoff, CRM Series in Math. Phys., Springer Verlag, pp. 353-440, 1998. (hep-th/9511201)
- [3] John Preskill and Lawrence M. Krauss Local discrete symmetry and quantum mechanical hair. *Nucl. Phys.*, B 341:50-100, 1990.
- [4] A. S. Schwarz. Field theories with no local conservation of the electric charge. *Nucl. Phys.*, B 208:141, 1982.
- [5] Mark Alford, Katherine Benson, Sidney Coleman, John March-Russell, and Frank Wilczek. Zero modes of nonabelian vortices. *Nucl. Phys.*, B 349:414–438, 1991.
- [6] F. Alexander Bais, Peter van Driel, and Mark de Wild Propitius. Quantum symmetries in discrete gauge theories. *Phys. Lett.*, B280:63–70, 1992.
- [7] F. Alexander Bais, Peter van Driel, and Mark de Wild Propitius. Anyons in discrete gauge theories with chern-simons terms. *Nucl. Phys.*, B393:547–570, 1993.
- [8] F. A. Bais, B. J. Schroers, and J. K. Slingerland. Hopf symmetry breaking and confinement in (2+1)-dimensional gauge theory. *JHEP*, 05:068, 2003.
- [9] F. A. Bais, B. J. Schroers, and J. K. Slingerland. Broken quantum symmetry and confinement phases in planar physics. *Phys. Rev. Lett.*, 89:181601, 2002.
- [10] Edward Witten. Quantum field theory and the jones polynomial. *Commun. Math. Phys.*, 121:351, 1989.
- [11] N. Reshetikhin and V. G. Turaev. Invariants of three manifolds via link polynomials and quantum groups. *Invent. Math.*, 103:547–597, 1991.
- [12] E. Guadagnini, M. Martellini, and M. Mintchev. Braids and quantum group symmetry in chern-simons theory. *Nucl. Phys.*, B336:581, 1990.

## Bibliography

---

- [13] Edward Witten. (2+1)-dimensional gravity as an exactly soluble system. *Nucl. Phys.*, B311:46, 1988.
- [14] F.A. Bais, N. Muller and B.J. Schroers. Quantum group symmetry and particle scattering in (2+1)-dimensional quantum gravity. *Nucl. Phys.*, B640:3-45, 2002.
- [15] Chung-Pei Ma.  $SO(10)$  cosmic strings and baryon number violation. *Phys. Rev.*, D48:530–542, 1993.
- [16] Martin Bucher and Alfred Goldhaber.  $SO(10)$  cosmic strings and  $SU(3)$ -color cheshire charge. *Phys. Rev.*, D49:4167–4181, 1994.
- [17] Anne-Christine Davis and Stephen C. Davis. Microphysics of  $SO(10)$  cosmic strings. *Phys. Rev.*, D55:1879–1895, 1997.
- [18] Katherine M. Benson and Tom Imbo. A topological criterion for Alice strings. [hep-th/0304161](#), 2003.
- [19] Katherine Benson and Tom Imbo. Twisted Alice loops as monopoles. [hep-th/0304162](#), 2003.
- [20] S. Ben-Menahem and A. R. Cooper. Baryogenesis from unstable domain walls. *Nucl. Phys.*, B388:409–434, 1992.
- [21] Leandros Perivolaropoulos, Andrew Matheson, Anne-Christine Davis, and Robert H. Brandenberger. Nonabelian Aharonov-Bohm baryon decay catalysis. *Phys. Lett.*, B245:556–560, 1990.
- [22] Brett T. McInnes. Alice universes. *Class. Quant. Grav.*, 14:2527–2538, 1997.
- [23] Brett T. McInnes. Methods of Alice physics. *J. Phys.*, A31:3607–3623, 1998.
- [24] S. Deser, R. Jackiw, and Gerard 't Hooft. Three-dimensional Einstein gravity: Dynamics of flat space. *Ann. Phys.*, 152:220, 1984.
- [25] J. Richard Gott and Mark Alpert. General relativity in a (2+1)-dimensional space-time. *Gen. Rel. Grav.*, 16:243–247, 1984.
- [26] Gerard 't Hooft. Nonperturbative two particle scattering amplitudes in (2+1)-dimensional quantum gravity. *Commun. Math. Phys.*, 117:685, 1988.
- [27] Katherine M. Benson and Maha Saadi. QCD flux tubes in a current algebra approach. *Phys. Rev.*, D51:3096–3107, 1995.
- [28] Katherine M. Benson, Aneesh V. Manohar, and Maha Saadi. QCD flux tubes as sigma model relics. *Phys. Rev. Lett.*, 74:1932–1935, 1995.
- [29] G. R. Dvali, Ian I. Kogan, and Mikhail A. Shifman. Topological effects in our brane world from extra dimensions. *Phys. Rev.*, D62:106001, 2000.

- [30] Ki-woon Choi, David B. Kaplan, and Ann E. Nelson. Is cp a gauge symmetry? *Nucl. Phys.*, B391:515–530, 1993.
- [31] Brett T. McInnes. Gauging discrete symmetries. *J. Math. Phys.*, 36:5414–5430, 1995.
- [32] A.P. Balachandran, F. Lizzi, and V.G.J. Rodgers. Topological symmetry breakdown in cholesterics, nematics, and  $^3\text{He}$ . *Phys. Rev. Lett.*, 52:1818, 1984.
- [33] U. Leonhardt and G.E. Volovik. How to create Alice string (half-quantum vortex) in a vector Bose-Einstein condensate. *JETP Lett.*, 72:46, 2000.
- [34] Fei Zhou. Quantum spin nematic states in Bose-Einstein condensates. *cond-mat/0108473*, 2001.
- [35] Grigori Volovik. The universe in a helium droplet. *Oxford University Press*, 2003.
- [36] G. Volovik and V. Mineev. *JETP Lett.*, 24:561, 1976.
- [37] Hae-Young Kee, Yong Baek Kim, and Kazumi Maki. Half-quantum vortex and  $\hat{d}$ -soliton in  $\text{Sr}_2\text{RuO}_4$ . *Phys. Rev. B* 62:R9275, 2000.
- [38] T.M. Rice and M. Sigrist.  $\text{Sr}_2\text{RuO}_4$ : an electronic analogue of  $^3\text{He}$ ? *J. Phys. Cond. Matter*, 7:L643, 1995.
- [39] M. Sigrist et al. Phenomenology of the superconducting state in  $\text{Sr}_2\text{RuO}_4$ . *Physica C*, 317–318:134, 1999.
- [40] Mikio Nakahara. Geometry, topology and physics. *Adam Hilger*, 1990.
- [41] V.P. Mineev. *Sov.Sci.Rev. A*:173. 1980.
- [42] J. Prost and P.G. de Gennes. The physics of liquid crystals. *Oxford University Press*, 1995.
- [43] Lewis Carroll. Alice's adventures in wonderland. *Macmillan, London*, 1865.
- [44] Lewis Carroll. Through the looking glass, and what Alice found there. *Macmillan, London*, 1871.
- [45] Martin Bucher, Hoi-Kwong Lo, and John Preskill. Topological approach to Alice electrodynamics. *Nucl. Phys.*, B386:3–26, 1992.
- [46] P.G. de Gennes. The physics of liquid crystal. *Clarendon Press*, 1974.
- [47] P.G. de Gennes. *Mol.Cryst.Liq.Cryst.*, 12:193, 1971.
- [48] F.C. Frank. *Disc. Faraday Soc.*, 25:19, 1958.
- [49] N. Schopohl and T.J. Slukin. Defect core structure in nematic liquid crystals. *Phys. Rev. Lett.*, 59:2582, 1987.

## Bibliography

---

- [50] Howard Georgi and Sheldon L. Glashow. Spontaneously broken gauge symmetry and elemenatry particle masses. *Phys. Rev.*, D 6:2977–2982, 1972.
- [51] J. Smit. Introduction to quantum fields on a lattice: A robust mate. *Cambridge Lect. Notes Phys.*, 15:1–271, 2002.
- [52] H. J. Rothe. Lattice gauge theories: An introduction. *World Sci. Lect. Notes Phys.*, 59:1–512, 1997.
- [53] Kenneth G. Wilson. Confinement of quarks. *Phys. Rev.*, D10:2445–2459, 1974.
- [54] Edward Witten. Phases of  $N = 2$  theories in two dimensions. *Nucl. Phys.*, B403:159–222, 1993.
- [55] A. A. Penin, V. A. Rubakov, P. G. Tinyakov, and S. V. Troitsky. What becomes of vortices in theories with flat directions. *Phys. Lett.*, B389:13–17, 1996.
- [56] A. Achucarro, A. C. Davis, M. Pickles, and J. Urrestilla. Vortices in theories with flat directions. 2001.
- [57] E. Lubkin. Geometric definition of gauge invariance. *Ann. Phys.*, 23:233–283, 1963.
- [58] A. A. Belavin, Alexander M. Polyakov, A. S. Shvarts, and Yu. S. Tyupkin. Pseudoparticle solutions of the Yang-Mills equations. *Phys. Lett.*, B59:85–87, 1975.
- [59] Alexander M. Polyakov. Compact gauge fields and the infrared catastrophe. *Phys. Lett.*, B59:82–84, 1975.
- [60] H. B. Nielsen and P. Olesen. Vortex line models for dual strings. *Nucl. Phys.*, B 61:45–61, 1973.
- [61] J. Striet and F. A. Bais. Simple models with Alice fluxes. *Phys. Lett.*, B497:172–180, 2000.
- [62] R. Shankar. More  $SO(3)$  monopoles. *Phys. Rev.*, D 14:1107, 1976.
- [63] M.M.H. Postma. Alice electrodynamics. Master’s thesis, University of Amsterdam, [1997].
- [64] Edward Witten. Superconducting strings. *Nucl. Phys.*, B 249:557–592, 1985.
- [65] H. J. de Vega and F. A. Schaposnik. A classical vortex solution of the abelian Higgs model. *Phys. Rev.*, D 14:1100–1106, 1976.
- [66] E. B. Bogomolny. Stability of classical solutions. *Sov. J. Nucl. Phys.*, 24:449, 1976.
- [67] Zvonimir Hlousek and Donald Spector. Bogomolny explained. *Nucl. Phys.*, B 397:173–194, 1993.

- [68] Jose Edelstein, Carlos Nunez, and Fidel Schaposnik. Supersymmetry and Bogomolny equations in the abelian Higgs model. *Phys. Lett.*, B 329:39–45, 1994.
- [69] F. A. Bais and R. Laterveer. Exact  $\mathbb{Z}_n$  monopole solutions in gauge theories with nonadjoint higgs representations. *Nucl. Phys.*, B 307:487, 1988.
- [70] Erick J. Weinberg. Multivortex solutions of the Ginzburg-Landau equations. *Phys. Rev.*, D 19:3008, 1979.
- [71] J. Striet and F. A. Bais. Simulations of Alice electrodynamics on a lattice. *Nucl. Phys.*, B647:215–234, 2002.
- [72] C. B. Lang and T. Neuhaus. Compact  $U(1)$  gauge theory on lattices with trivial homotopy group. *Nucl. Phys.*, B431:119–130, 1994.
- [73] I.J.R. Aitchison and C.D. Fosco. On the chiral and deconfinement phase transitions in parity-conserving  $QED(3)$  at finite temperature. *Nucl. Phys.*, B578:199–214, 2000.
- [74] Pieter Maris and Dean Lee. Chiral symmetry breaking in (2+1) dimensional QED. *hep-lat/0209052*, 2002.
- [75] S.J. Hands, J.B. Kogut, L. Scorzato and C.G. Strouthos. The chiral limit of non-compact  $QED(3)$ . *Nucl. Phys. Proc. Suppl.*, 119:974-976, 2003.
- [76] Gyan Bhanot. The nature of the phase transition in compact qed. *Phys. Rev.*, D24:461, 1981.
- [77] Michael Creutz, Laurence Jacobs, and Claudio Rebbi. Experiments with a gauge invariant Ising system. *Phys. Rev. Lett.*, 42:1390, 1979.
- [78] R. Balian, J. M. Drouffe, and C. Itzykson. Gauge fields on a lattice. II. strong coupling expansions and transition points. *Phys. Rev.*, D11:2104, 1975.
- [79] Gyan Bhanot and Michael Creutz. The phase diagram of  $\mathbb{Z}_n$  and  $U(1)$  gauge theories in three- dimensions. *Phys. Rev.*, D21:2892, 1980.
- [80] Michael Creutz, Laurence Jacobs, and Claudio Rebbi. Monte Carlo study of abelian lattice gauge theories. *Phys. Rev.*, D20:1915, 1979.
- [81] T. A. DeGrand and Doug Toussaint. Topological excitations and Monte Carlo simulation of abelian gauge theory. *Phys. Rev.*, D22:2478, 1980.
- [82] Burkard Klaus and Claude Roiesnel. High-statistics finite size scaling analysis of  $U(1)$  lattice gauge theory with a Wilson action. *Phys. Rev.*, D58:114509, 1998.
- [83] J. Striet and F. A. Bais. Dynamical vacuum selection in field theories with flat directions in their potential. *JHEP*, 01:032, 2003.
- [84] Ian Affleck. On constrained instantons. *Nucl. Phys.*, B191:429, 1981.

## Bibliography

---

- [85] Levon Pogosian and Tanmay Vachaspati. Space of kink solutions in  $SU(N) \times \mathbb{Z}_2$ . *Phys. Rev.*, D64:105023, 2001.
- [86] F. A. Bais and J. Striet. On a core instability of 't Hooft Polyakov type monopoles. *Phys. Lett.*, B540:319–323, 2002.
- [87] J. Striet and F. A. Bais. More on core instabilities of magnetic monopoles. *JHEP*, 06:022, 2003.
- [88] G. 't Hooft. Magnetic monopoles in unified gauge theories. *Nucl. Phys.*, B79:276–284, 1974.
- [89] A. M. Polyakov. Particle spectrum in quantum field theory. *JETP Lett.*, 20:194–195, 1974.
- [90] F. Alexander Bais and Per John. Core deformations of topological defects. *Int. J. Mod. Phys.*, A10:3241–3258, 1995.
- [91] R. Rosso and E.G. Virga. Metastable nematic hedgehogs. *J. Phys. A*, 29:4247–4264, 1996.
- [92] Jr. E.C. Gartland and S. Mkaddem. Instability of radial hedgehog configurations in nematic liquid crystals under Landau-de Gennes free energy models. *Phys. Rev. E*, 59:563–567, 1999.
- [93] S. Mkaddem and Jr. E.C. Gartland. Fine structure of defects in radial nematic droplets. *Phys. Rev. E*, 62:6694–6705, 2000.
- [94] S. Kralj and E.G. Virga. Universal fine structure of nematic hedgehogs. *J. Phys. A*, 34:829–838, 2001.
- [95] F. A. Bais and J. Striet. Charge instabilities due to local charge conjugation symmetry in (2+1)-dimensions. *Nucl. Phys.*, B666:243–268, 2003.
- [96] Sidney R. Coleman. The fate of the false vacuum. I. Semiclassical theory. *Phys. Rev.*, D15:2929–2936, 1977.
- [97] Jr. Callan, Curtis G. and Sidney R. Coleman. The fate of the false vacuum. II. First quantum corrections. *Phys. Rev.*, D16:1762–1768, 1977.
- [98] Tsuneo Suzuki and M. N. Chernodub. Screening and confinement in  $(U(1))^{n-1}$  abelian effective theories. *Phys. Lett.*, B563:183–190, 2003.
- [99] M. N. Chernodub and T. Suzuki. String breaking and monopoles. [hep-lat/0211026](#), 2002.

# Samenvatting

*Experience is a comb which nature gives to men when they are bald.*

(A Chinese Proverb)

Het is de taak van de natuurkundigen om te proberen de wetten van de natuur te achterhalen en om te voorspellen wat daaruit volgt. In analogie zouden natuurkundigen proberen te achterhalen wat de Nederlandse wetten zijn en te voorspellen wat de uitkomsten van rechtszaken zijn. Het belangrijkste gereedschap voor het achterhalen van de natuurwetten is het doen van experimenten. In vergelijking kijken natuurkundigen naar wat mensen voor en na een rechtszaak doen om aan de hand daarvan de Nederlandse wetten te achterhalen. Dat lijkt een haast onmogelijke taak, maar hier komt het uiteindelijk wel op neer.

Er zijn verschillende soorten natuurkundigen. Zo zijn er bijvoorbeeld de experimenteel natuurkundigen. Door het doen van experimenten proberen ze eigenschappen van de natuurwetten bloot te leggen. De theoretisch natuurkundigen proberen deze eigenschappen op hun beurt te verklaren. Onder theoretici heb je ook weer verschillende soorten. Er zijn mensen die de gevonden eigenschappen met behulp van bestaande en bekende natuurwetten proberen te verklaren. In analogie proberen deze theoretici de uitkomst van complexe rechtszaken te voorspellen aan de hand van bestaande en bekende wetten, ze zitten als het ware op de stoel van de rechter. Dit kan misschien triviaal lijken, maar menig advocaat kan beamen dat de uitkomst van een complexe rechtszaak lang niet altijd zo voorspelbaar is. Er is ook nog een ander soort theoretisch natuurkundigen, waartoe ik behoor. Deze theoretici proberen onbekende natuurwetten te achterhalen. Ze nemen als het ware de plaats in van de politiek. Simpel gezegd verzinnen ze een aantal wetten en proberen aan de hand van (verzonnen) simpele rechtszaken te achterhalen of deze wetten mogelijk de Nederlandse wetten zijn. Belangrijke richtlijnen in dit werk zijn de bekende natuurwetten. Aangezien deze tot op zekere hoogte bevestigd zijn door de experimenteel natuurkundigen.

Een belangrijk ingrediënt van de natuurwetten is symmetrie. Hiermee wordt niet de symmetrie van een voorwerp bedoeld, maar de symmetrie van de natuurwetten (de theorieën die de voorwerpen beschrijven) zelf. Een voordeel van een symmetrie is dat het aangeeft wat niet belangrijk is. In de natuurkunde is translatiesymmetrie een belangrijk voorbeeld van zo'n soort symmetrie. Zo denken we in de natuurkunde dat

de natuurwetten translatie-invariant zijn. Dit betekent dat de natuurwetten op elke plek in het heelal hetzelfde zijn. Dit lijkt redelijk normaal, maar is tegelijkertijd ook erg tegen intuïtief. Zijn bijvoorbeeld de natuurwetten op de Maan niet heel anders dan die op de Aarde? Het is bijvoorbeeld waar dat de aantrekkracht op de Maan veel kleiner is dan op de Aarde. Dit betekent echter niet dat de natuurwetten ook anders zijn op de Maan. Wat wel anders is, is de situatie en die zorgt ervoor dat de *effectieve* natuurwetten op de Maan anders zijn dan op de Aarde. In analogie met de Nederlandse rechtspraak zijn alle Nederlanders in beginsel gelijk voor de wet. Dat is ook wel zo fijn, anders zou er voor elke Nederlander een nieuwe set wetten moeten worden gemaakt. Dit betekent echter niet dat ook elke rechtszaak gelijk is. Situaties kunnen namelijk verschillen. Dus, ook al hebben de natuurwetten een hoge mate van symmetrie, dan betekent dat nog niet dat die symmetrie manifest is voor elke situatie. Dit zorgt ervoor dat het heel moeilijk kan zijn om de symmetrieën waar de natuurwetten aan voldoen te vinden. Probeer bijvoorbeeld maar eens het principe dat alle Nederlanders in beginsel gelijk zijn voor de Nederlandse wet te achterhalen, door alleen te kijken naar de situatie waarin iemand zich bevindt voordat de rechtszaal wordt betreden en wat de situatie is als deze persoon er weer uitkomt. Een ander mooi voorbeeld dat aangeeft dat de symmetrie van een theorie niet manifest hoeft te zijn, is een diner aan een ronde tafel. Op de tafel staan borden en tussen de borden staan glazen. Alles ziet er heel mooi en symmetrisch uit, totdat de mensen wat gaan drinken. Links en rechts van elk bord staat een glas. Iedereen heeft nu nog de keuze om het linker of het rechter glas te pakken. Duidelijk is dat de keuze van één iemand de keuze van één van zijn buren beperkt. Om boze gezichten aan tafel te voorkomen, is het van belang dat iedereen dezelfde keuze maakt: of iedereen pakt het rechter glas of iedereen pakt het linker glas. Als niet iedereen het rechter (of het linker) glas pakt, ontstaan er problemen. Er zullen mensen aan de ronde tafel zitten zonder glas en er zullen elders op de tafel glazen over zijn. Als er eenmaal gegeten en gedronken wordt, is het erg moeilijk om de links/rechts symmetrie weer terug te vinden. Dit is een voorbeeld van een spontane symmetriebreking. Dit betekent dat de natuurwetten wel een bepaalde symmetrie hebben, maar dat deze niet manifest is voor de zogenaamde grondtoestand. Eén van de mogelijke gevolgen van een symmetriebreking is het ontstaan van topologische defecten. Het diner aan de ronde tafel is ook nu een mooi voorbeeld. Zoals we al eerder opmerkten, ontstaan er problemen als niet iedereen het rechter (of linker) glas pakt. In zo'n situatie zijn er mensen die geen glas hebben en zijn er glazen die los op de tafel staan. Deze 'frustraties' noemen we topologische defecten. In 1-dimensionale natuurkunde kunnen ze ontstaan op plekken waar verschillende vacua met elkaar botsen. In de situatie van het diner aan de ronde tafel zijn er twee vacua, namelijk links en rechts. Een persoon zonder glas heeft links van hem/haar iemand zitten die zijn/haar rechter glas heeft gepakt en heeft rechts van hem/haar iemand zitten die zijn/haar linker glas heeft gepakt. Deze botsing van de verschillende vacua zorgt voor de vorming van een topologisch defect, een persoon zonder glas. Bij een vrij glas is er ook een botsing van vacua, maar dan net andersom. De begrippen symmetrie, symmetriebreking en topologische defecten komen in dit proefschrift veelvuldig aan de orde.

In dit proefschrift hebben we grotendeels één bepaalde theorie onderzocht: Alice elektrodynamica (AED). AED is een simpel voorbeeld uit een hele klasse van theorieën. Al deze theorieën hebben een bepaalde symmetriestructuur. De symmetriestructuur van het model dat we bekeken hebben, lijkt heel erg op die van elektromagnetisme. Heel veel eigenschappen van de natuurkunde van AED zijn gelijk aan de eigenschappen van de natuurkunde van elektromagnetisme. Het interessante gedeelte is het verschil tussen beide modellen. Het zijn juist deze verschillen waar we voornamelijk naar gezocht hebben en die we onderzocht hebben met behulp van verschillende methoden. De verschillen komen alleen voor in bepaalde situaties waar de zogenaamde topologische defecten in voorkomen. Bijna alle verschillen zijn gebaseerd op het zogenaamde Alice-effect van een Alice-flux (een topologisch defect). In AED zorgt het Alice-effect ervoor dat een elektrische lading van teken verandert als het om een Alice-flux heen beweegt. Het punt waarop dit gebeurt is fysisch niet belangrijk, maar dat het gebeurt heeft wel een fysische betekenis. Dit soort interacties worden topologische interacties genoemd. De interactie hangt namelijk alleen af van de topologie, hoe vaak het deeltje om de flux heen draait, en niet van de afstand tussen de flux en de lading.

In het begin van hoofdstuk één van dit proefschrift geven we een inleiding van Alice elektrodynamica. We leggen uit wat de symmetriestructuur is en welke topologische defecten er kunnen voorkomen in AED. Verder proberen we een beeld van AED te geven aan de hand van gewone elektrodynamica. In het tweede deel van het eerste hoofdstuk verklappen we alvast de belangrijkste resultaten van de andere hoofdstukken zonder al te veel op de details in te gaan.

In hoofdstuk twee wordt een oplossing voor de Alice-flux, een topologisch defect, in het originele model voor AED gepresenteerd. Verder worden er ook twee alternatieve modellen voor AED gepresenteerd, die als voordeel hebben dat ze in bepaalde situaties af te beelden zijn op bekende modellen. Deze bekende modellen hebben eigenschappen die ervoor zorgen dat de oplossingen van de topologische defecten makkelijk te vinden zijn.

In hoofdstuk drie construeren we een roostermodel (lattice model) van AED (LAED). Het voordeel van een roostermodel is dat je het goed met behulp van een computer kunt onderzoeken. Ook LAED heeft topologische defecten. Alleen zijn ze bij dit model niet aanwezig als gevolg van een symmetriebreking, maar omdat het model op een rooster leeft. De gaatjes in het rooster kunnen zich namelijk gaan gedragen alsof ze een topologische defect bevatten. Met behulp van de computer hebben we het LAED-model in drie en vier dimensies kunnen bestuderen. We hebben bijvoorbeeld de waarden van een aantal meetbare grootheden als functie van de modelparameters analytisch voorspeld. Deze uitkomsten hebben we met behulp van computerresultaten gecontroleerd.

In hoofdstuk vier bestuderen we een specifiek dynamisch gedrag dat generiek is voor een bepaalde klasse van veldentheorieën. We laten zien dat een zogenaamde vlakke richting in de potentiaal van een veldentheorie ervoor zorgt dat sommige topologische defecten niet statisch kunnen zijn. De manier waarop deze topologische defecten veranderen is heel goed voorspelbaar. We laten zien dat een systeem met zo'n topologisch defect een voorkeur heeft voor een speciaal vacuüm en dat dit systeem dit vacuüm in

## Samenvatting

---

de loop der tijd selecteert. Dit proces noemen we dynamische vacuümselectie. In hoofdstuk vijf bestuderen we een instabiliteit van de sferisch symmetrische magnetische monopooloplossing in AED. We laten eerst zien dat een ring van Alice-flux ook een magnetische lading kan dragen. Daarna laten we met behulp van het zogenaamde variationele principe en de computer zien dat de sferisch symmetrische magnetische monopooloplossing niet altijd de laagste hoeveelheid energie heeft voor een configuratie met een magnetische lading. In de delen van de parameterruimte van het model waar dit het geval is, vinden we een configuratie met minder energie, die heel erg veel lijkt op wat je zou verwachten voor een magnetisch geladen Alice-ringoplossing. We laten dus zien dat een sferisch symmetrische magnetische monopooloplossing kan vervallen in een magnetisch geladen Alice-ring.

In het laatste hoofdstuk van dit proefschrift, hoofdstuk zes, bestuderen we een ladingsinstabiliteit in AED in (2+1)-dimensies. De belangrijkste twee ingrediënten hiervoor zijn: (1) het feit dat twee Alice-fluxen uit het vacuüm gecreëerd kunnen worden, wat niet mogelijk is voor een enkele Alice-flux, en (2) dat klassiek gezien de potentiële energie tussen twee elektrische ladingen oneindig doorgroeit bij toenemende afstand tussen de ladingen. Als de afstand tussen de twee ladingen groot genoeg is, is het energetisch voordeliger om een paar Alice-fluxen te creëren en elk aan één van de ladingen te koppelen. Deze instabiliteit zorgt ervoor dat een enkele statisch elektrische lading in (2+1)-dimensies niet mogelijk is en dat de potentiaal tussen twee ladingen een maximum bereikt. Dit is het punt waarop de Alice-fluxen worden gecreëerd.

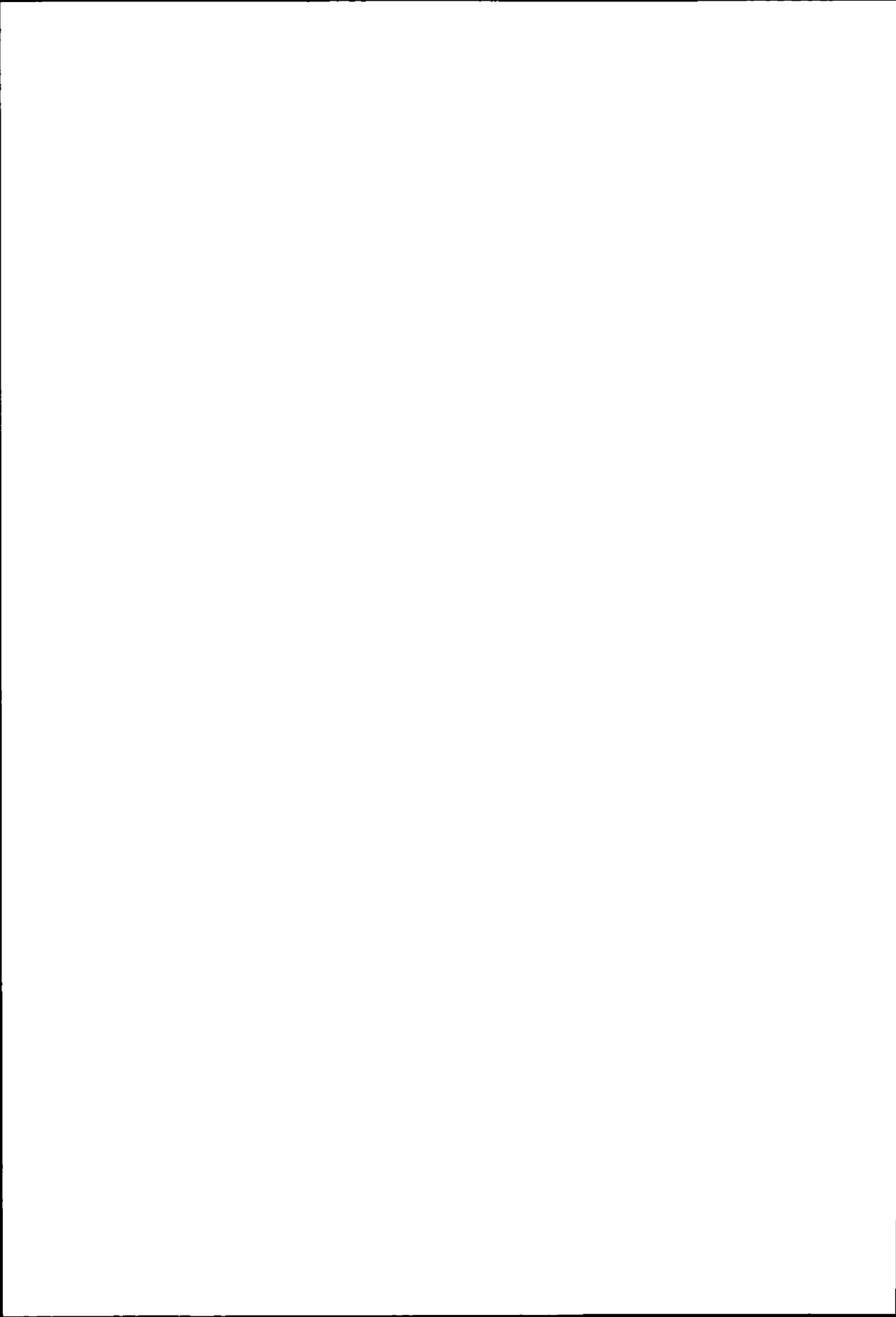
Alhoewel het grootste deel van het onderzoek zich op AED heeft gericht, verwachten we dat de resultaten ook voor andere Alice-modellen gelden aangezien deze grotendeels gebaseerd zijn op het Alice-effect van de Alice-fluxen.

# Dankwoord

Als eerste wil ik natuurlijk mijn promotor Sander Bais bedanken. Sander, heel erg bedankt voor alle samenwerking, steun, kritiek en de illusie van vrijheid in de afgelopen jaren. Ook wil ik graag Jan Smit en Jeroen Vink bedanken voor hun hulp en begeleiding in de wondere wereld van de rooster-ijktheorieën. Verder wil ik alle (oud) leden van het Instituut voor Theoretische Fysica bedanken voor de fijne en informele werksfeer. Mijn (oud) kamergenoten Joost Slingerland en Assaf Shomer wil ik bedanken. Joost je was niet alleen een hele fijne kamergenoot, maar ik heb ook erg veel van je kunnen leren. Assaf, bedankt voor de steun in deze laatste periode. Verder wil ik mijn reisleider Anders Tranberg onder andere bedanken voor zijn gezelschap op onze tochtjes door Europa, waar ik erg van genoten heb. Voor het niet geheel onbelangrijke redigeren van de verschillende delen van mijn proefschrift wil ik Anders, Joost en Marloes bedanken. Hoe belangrijk jullie werk is geweest, zal voor jullie zelf het meest duidelijk zijn.

Buiten mijn directe natuurkundewereld zijn er natuurlijk nog genoeg mensen die te lijden hebben gehad onder mijn promoveren. De leden van mijn voetbalteam zullen dit op de trainingen wel gemerkt hebben, al konden ze op zondag ook weer profiteren van het overschot aan fysieke energie. Ook wil ik in het algemeen al mijn vrienden en vriendinnen bedanken voor hun steun, afleiding en gezelschap in de afgelopen jaren. Niet te vergeten, bedank ik ook mijn (schoon)familie. Papa, mama, zus en schoonbroer, bedankt voor alle steun. Daarnaast wil ik bak-ker-tje Deeg bedanken voor zijn ongekende hoeveelheid geduld. Verder wil ik Fred Laar heel erg bedanken. Zonder jou was dit proefschrift duidelijk nooit tot stand gekomen.

Nu mist er nog één heel belangrijk persoon, Marloes. Natuurlijk mag jij al jaren genieten van mijn stuiterende aanwezigheid (en ik van die van jouw), maar je zal blij zijn dat mijn proefschrift nu bijna klaar is. Als er iemand onder geleden heeft dan ben jij dat, maar hopelijk wel met veel plezier



...

*Ik word meester later.*

